

Advanced Soft Materials, Sensor Integrations, and Applications of Wearable Flexible Hybrid Electronics in Healthcare, Energy, and Environment

Hyo-Ryoung Lim, Hee Seok Kim, Raza Qazi, Young-Tae Kwon, Jae-Woong Jeong, and Woon-Hong Yeo*

Recent advances in soft materials and system integration technologies have provided a unique opportunity to design various types of wearable flexible hybrid electronics (WFHE) for advanced human healthcare and human-machine interfaces. The hybrid integration of soft and biocompatible materials with miniaturized wireless wearable systems is undoubtedly an attractive prospect in the sense that the successful device performance requires high degrees of mechanical flexibility, sensing capability, and user-friendly simplicity. Here, the most up-to-date materials, sensors, and system-packaging technologies to develop advanced WFHE are provided. Details of mechanical, electrical, physicochemical, and biocompatible properties are discussed with integrated sensor applications in healthcare, energy, and environment. In addition, limitations of the current materials are discussed, as well as key challenges and the future direction of WFHE. Collectively, an all-inclusive review of the newly developed WFHE along with a summary of imperative requirements of material properties, sensor capabilities, electronics performance, and skin integrations is provided.

glasses, watches, wristbands, or belts, are either fully or partially composed of planar and rigid materials, which require the use of obtrusive, hard supports or additional bendable strips to be mounted on the human body. Therefore, clinical devices that use the existing wearables cause discomfort and limit monitoring of human physiological data in the laboratory. This is the big limitation factor to overcome despite the ever-growing market for wearables in broader screenings outside of the clinic. By this account, it is necessary to replace the bulky and rigid plastics and metal components in the sensors and electronics with skin-like materials for enhanced wearability and functionality.

The concept of WFHE poses a possible solution to address the aforementioned difficulties by providing user comfort, compliant mechanics, soft integration, multifunctionality, and smart diagnostics

with embedded machine learning algorithms. Specifically, such electronics would provide stable and intimate contact to the soft human skin without adding any mechanical and thermal loadings or causing skin breakdown. Current development strategies and approaches for advanced WFHE focus on soft, flexible form factors, nonirritating and nontoxic characteristics, fully autonomous energy components, seamless wireless communications,

1. Introduction

Wearable flexible hybrid electronics (WFHE) with characteristics that correspond to the human body represent a paradigm shift in wearables from loosely to tightly coupled interfaces for enhanced health monitoring, diagnostics, and human-machine interfaces. Commercial wearables, mostly in the form of

Dr. H.-R. Lim, Dr. Y.-T. Kwon
George W. Woodruff School of Mechanical Engineering
Institute for Electronics and Nanotechnology
Georgia Institute of Technology
Atlanta, GA 30332, USA

Prof. H. S. Kim
Department of Mechanical Engineering
University of South Alabama
Mobile, AL 36608, USA

Dr. R. Qazi
Department of Electrical
Computer & Energy Engineering
University of Colorado Boulder
Boulder, CO 80309, USA

 The ORCID identification number(s) for the author(s) of this article can be found under <https://doi.org/10.1002/adma.201901924>.

DOI: 10.1002/adma.201901924

Dr. R. Qazi, Prof. J.-W. Jeong
School of Electrical Engineering
Korea Advanced Institute of Science and Technology
Daejeon 34141, South Korea
Prof. W.-H. Yeo
George W. Woodruff School of Mechanical Engineering
Wallace H. Coulter Department of Biomedical Engineering
Institute for Electronics and Nanotechnology
Parker H. Petit Institute for Bioengineering and Biosciences
Center for Flexible and Wearable Electronics Advanced Research
Neural Engineering Center
Institute for Materials
Institute for Robotics and Intelligent Machines
Georgia Institute of Technology
Atlanta, GA 30332, USA
E-mail: whyeo@gatech.edu

and cost-effective processes. Note that these sophisticated properties should be tailored to meet the stringent requirements of enhanced physiological recording from the human body. The suitability of the consequent device performance is estimated and quantified in terms of mechanical, physicochemical, biocompatible, electrical, and device-level properties.^[1,2] The practical implementation of these properties, however, is limited by the narrow range of acceptable values under which they can function.^[3–5] One such example is gauge factor (GF) that represents the relevance between electrical signals and applied strains, which is analyzed under conditions where the humidity is relatively high,^[6] biodegradability is required,^[7] or transparent operation is expected maintaining a certain level of accuracy.^[8] Indeed, taking into account such multicharacteristics and their correlation plays a pivotal role in designing a high-performance and reliable WFHE. Recent reviews in wearable electronics cover high levels of functionality, individually focusing on strategies that drive huge progress: general advantages,^[9–11] materials (carbon,^[12] paper,^[13] ionics,^[14] enzyme^[15]), functions (soft,^[16] stretchability,^[17,18] bioresorbability,^[19] autonomous^[20,21]), structures and processes (nanostructure,^[22,23] printed electronics^[24,25]), sensors (physiological,^[26,27] chemical,^[28,29] electrochemical,^[30] tactile^[31] sweat,^[32] pressure^[33]), and their applications (diagnosis,^[34,35] healthcare,^[36–38] medicine,^[39] display,^[40] energy^[41–44]). These works, however, have focused on limited scopes of the wearable electronics and relevant materials.

Here, we focus on an all-inclusive review of multimodal characteristics of hybrid materials (such as nanostuctured and patterned electrodes),^[45,46] and integrated systems,^[47] for advanced WFHE and their unique applications in healthcare, energy, and environment (**Figure 1**). We summarize a comprehensive list of classification rules in mechanical, physicochemical, biocompatible, electrical, and device-level properties that are required for the design of WFHE. In addition, unique strategies and methods of developing hybrid structures and electronic systems are described in views of materials engineering, flexible mechanics, enhanced sensing, and targeted applications. Finally, we discuss future directions of next-generation WFHE, which will catalyze the continued progress.

2. Overview of Wearable Flexible Hybrid Electronics

2.1. Definition

Here, we focus on WFHE, summarizing recently published works regarding flexible hybrid devices and systems, directly attached to the surface of the human body. **Figure 2** provides the classification of wearable devices and compares several terms, including wearable technology, epidermal electronic systems, implantable devices, and systems on fabrics. Wearable technology is defined as “hybrid, network-enabled devices that can be worn on or in the body, which are integrated with the user’s everyday life and movements.”^[48] Wearable devices, in this manner, closely monitor human data without limiting their motions, enabled by integration with lightweight, flexible, mechanically robust, and human-friendly components.^[12,49,50] The researchers place no restriction on the location where such devices are positioned or materials and configurations that have



Hyo-Ryoung Lim is currently a postdoctoral research fellow in the George W. Woodruff School of Mechanical Engineering at Georgia Institute of Technology, Atlanta, GA, USA. She received her B.S. degree in materials science and engineering from the Seoul National University of Technology (South Korea) in 2012, and Ph.D. degree

in fusion chemical engineering from Hanyang University (South Korea) in 2018. Her research interests include wearable flexible sensors, electrochemical sensors, biosensors, and nanomaterials interfaces.



Woon-Hong Yeo is an Assistant Professor in the George W. Woodruff School of Mechanical Engineering and the Wallace H. Coulter Department of Biomedical Engineering at Georgia Institute of Technology. He received his B.S. degree in mechanical engineering from Inha University (South Korea) in 2003 and his Ph.D. degree

in mechanical engineering at the University of Washington, Seattle, WA, USA in 2011. From 2011 to 2013, he worked as a postdoctoral research fellow at the Beckman Institute and Frederick Seitz Materials Research Center at the University of Illinois at Urbana-Champaign. His research areas include soft electronics, human-machine interfaces, nano-biosensors, and soft robotics.

to be used as long as they are wearable. When the wearable devices are combined with flexible technology, a simple classification regarding the location where they are worn on the body has already proved its usefulness for focusing on the two different fields: epidermal electronics (in case they are worn onto the skin)^[51] and implantable devices (in case they are positioned on or at the inner organs).^[52] All have one thing in common, devices or systems should yield the desired properties that approximate those of the surface of tissues, thereby enabling compliant and robust contact.^[11]

In previous reports, the electronic systems that adhere directly to the skin, enabled by their physical properties that are well matched to the epidermis, have been referred to as “epidermal electronic systems.”^[53,54] Therefore, the term “epidermal” is sometimes interchangeable with “skin-like.” In this work, the term WFHE does not necessarily refer to the electronics that should be attached to the epidermis. For instance, as shown in **Figure 2a**, the examples to acquaint with the wearable and flexible sensors even working in the intraoral



Figure 1. Summarized key properties of advanced WFHE. Temperature sensor image: Reproduced with permission.^[136] Copyright 2018, Nature Publishing Group. Strain and pressure sensor image: Reproduced with permission.^[45] Copyright 2018, Wiley-VCH. Electrophysiological sensor image: Reproduced with permission.^[131] Copyright 2018, Nature Publishing Group. Optical sensor image: Reproduced with permission.^[144] Copyright 2017, American Chemical Society. Electrochemical sensor image: Reproduced with permission.^[55] Copyright 2018, National Academy of Sciences. Nanostructured materials image: Reproduced with permission.^[46] Copyright 2015, American Chemical Society. Gel-based ionic conductor image: Reproduced with permission.^[14] Copyright 2018, Wiley-VCH. Printed electronics image: Reproduced with permission.^[24] Copyright 2018, Wiley-VCH. Stretchable electrodes. Left image: Reproduced with permission.^[54] Copyright 2013, Wiley-VCH. Right image: Reproduced with permission.^[47] Copyright 2008, National Academy of Sciences. Bioresorbable electronics image: Reproduced with permission.^[263] Copyright 2017, National Academy of Sciences. Detection of environmental exposure image: Reproduced with permission.^[337] Copyright 2018, American Chemical Society. Detection of health factors image: Reproduced with permission.^[50] Copyright 2016, Nature Publishing Group. Development of self-powered systems image: Reproduced with permission.^[341] Copyright 2018, Nature Publishing Group.

space or onto the eyeball are given.^[55,56] Wearable electronics are defined as implantable, if they are either partly or entirely interacted with internal tissues.^[57–59] In these cases, polymer- or

ceramic-based encapsulation works as barriers to protect the electronic circuits and batteries from body fluid penetration and tissue invasion to the system. It also requires strong mechanical

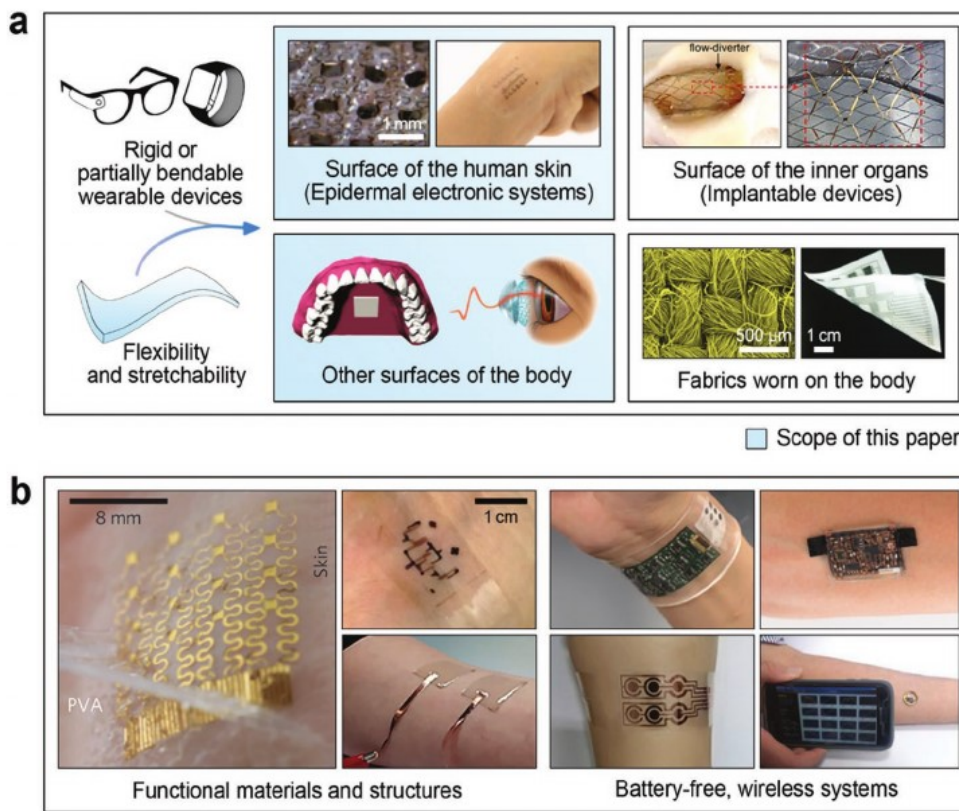


Figure 2. Types of wearable electronics and focused areas of WFHE. a) Classification of wearable electronics in terms of the location where they are integrated, including: 1) human skin (left image: reproduced with permission.^[51] Copyright 2017, Elsevier; right image: reproduced with permission.^[10] Copyright 2018, Nature Publishing Group), 2) other surfaces of the body such as palate and eyeball (left image: reproduced with permission.^[55] Copyright 2018, National Academy of Sciences; right image: reproduced with permission.^[56] Copyright 2018, Nature Publishing Group), 3) surface of the inner organs (reproduced with permission.^[52] Copyright 2018, American Chemical Society), and 4) surface of fabrics (reproduced with permission^[60] Copyright 2017, Wiley-VCH). b) Various types of WFHE, including: 1) functional materials and structures: (left) temperature heater and sensor based on patterned Au electrode (reproduced with permission.^[62] Copyright 2013, Nature Publishing Group), (top right) temperature sensor using intrinsically stretchable materials including SWCNT, PEDOT:PSS, and ionic liquid encapsulated with SEBS (reproduced with permission.^[136] Copyright 2018, Nature Publishing Group), and (bottom right) ECG sensor using transparent AgNW-embedded a-PDMS matrix (reproduced with permission.^[191] Copyright 2018, American Chemical Society); and 2) battery-free, wireless systems: (top-left) multiplexed sweat sensor integrated with flexible printed circuit board (reproduced with permission.^[50] Copyright 2016, Nature Publishing Group), (top right) self-powered capacitance-type sweat monitoring system (reproduced with permission.^[66] Copyright 2019, Nature Publishing Group), (bottom left) four-layer stretchable system integrated EMG sensor (reproduced with permission.^[148] Copyright 2018, Nature Publishing Group), and (bottom right) wireless battery-free thermal sensor using near-field communication protocols (reproduced with permission.^[70] Copyright 2018, Nature Publishing Group).

Printed by [Georgia Institute Of Technology - 069.180.027.108 - doi/pdf/10.1002/adma.201901924] at [19/10/2020].

hardness, extreme resistance to corrosion, biocompatibility, durability, and hermeticity. A more comprehensive system that is focused on internal organs is beyond the scope of this paper. WFHE are also grouped by configuration into a thin electrode and soft substrate with lab-on-a-chip devices, or textile-based electronics.^[60] Textile demands characteristics including natural warmth and style/fashion-related features as well as flexibility, which are sometimes entirely different from skin-attachable soft electronics. As a result, we refer to WFHE as mechanically soft, flexible, and stretchable electronic devices that can be tightly attached to the surface of the body, thereby providing a user-oriented monitoring system without distracting the users.

2.2. Classification

A rapid advancement of WFHE allows continuous measurements of personalized biological signals from the body. The

combination of functional nanomaterials and soft structures has accelerated the improvement of WFHE, which can be further developed by integrating battery-free, wireless systems (Figure 2b). A variety of metal electrodes that are sufficiently thin and precisely patterned play a critical role in every given type of electronics with flexible and stretchable form factors. The surface of thin electrodes is encapsulated with a polymeric layer to avoid electrical leakage, prevent the delamination, and impede the diffusion of moisture and molecules.^[61,62] In the wearable electronic system, the electrode and even stretchable transistors minimize any motion artifacts while being protected from electrical and chemical disturbance. Functional substrates that are transparent, electrically conductive, waterproof, and gas-permeable, mostly created by compositing with functional nanomaterials or using materials that exhibit such characteristics intrinsically, have broadened the field of WFHE. Layouts that involve some combination of those features render the electronics

nonobtrusive, comfortable for wearing, and more adoptable to everyday life, while maintaining the benefits of soft and flexible polymeric surfaces. Examples of such functional substrates^[63] include band-like patches, microfluidic membrane, and wearable lens. By further integrating with flexible batteries and wireless systems, the wearable electronics have benefits of low power consumption and high accessibility without the need for in-hospital care.^[64,65] Flexible batteries, such as micro-supercapacitors, can realize the practical application of WFHE while offsetting the inconvenience of charging.^[66] Furthermore, the self-powered autonomous systems utilizing energies received from the body or from outside can likely reduce or even get rid of the inconvenience of charging.^[41,67,68] The approach for a battery-free wireless system that uses a variety of communication methods can allow the devices to be used more conveniently by eliminating the huge instruments nearby and electronic wires.^[13,69,70]

2.3. Human Skin

Human skin is the largest organ of the integumentary system in our body and it offers diagnostic interface that is rich with vital biological signals from the inner organs, blood vessels, muscles, and dermis/epidermis.^[11] Figure 3a shows the major biological signal sources in the skin anatomy along with the relevant physiological information. For instance, biopotentials that emanate from major nerves in the muscle layer, brain activity, or eye motion can be recorded by WFHE. The skin also functions as a platform for understanding the underlying vascular structure and organ systems (Figure 3b).^[19] For instance, functional near-infrared spectroscopy allows the investigation of oxygenation changes in the brain, and optical tomography is also effective for detecting breast cancer.^[9,71] In this case, such optical characteristics are associated with transmission, absorption, and scattering properties occurring within human skin, which are divided into three layers of stratum corneum, underlying epidermis, and dermis. Given that motion artifacts are induced by the continuous body motion, conformal contact of WFHE with the skin enables more accurate detection, such as mapping oxygenation of skin grafts even in sleep and multipoint measurement of the concentration of oxygen from the body.^[72] As shown in Figure 3c, a wearable sensor system can even monitor the sweat, one of the most accessible biofluids, as a window to a deeper body's information.^[32] The sweat contains ions such as Na^+ , Cl^- , Ca^{2+} , and K^+ , metabolites, acids, hormones, and small proteins and peptides, which are portioned from nearby blood or interstitial fluid (ISF), and the dermal duct carries sweat to the skin surface. Its composition is correlated to that of blood and is dependent on the metabolic activities such as exercise, stress, and heat, thus providing highly acceptable physiological insight and fast detection before biodegradation. The use of skin-like WFHE with Young's modulus from 2–80 kPa (in dermis) to 140–600 kPa (in epidermis) and stretchability as high as 100% can obtain such signals and important health metrics from the skin.^[53,54,62] Given that such electronics are susceptible to constant movements of body, the properties of both skin and electronics may be altered over time. For high-fidelity signal recording, it is

essential for wearable devices to be less affected by motion-induced artifacts. At the same time, they should be airy, permeable to vapor/sweat, stickable yet detachable without pain/residue, and comfortable enough to users.

3. Required Properties of WFHE

A deep understanding of essential properties for wearable devices can largely promote further advancement in the field of WFHE. Figure 4 illustrates key material properties of advanced WFHE based on many prior works. Given that the first priority to establish wearable system is to achieve flexibility and stretchability, Young's modulus should be carefully considered along with nonobtrusive form factors. The comprehensive list also includes various physicochemical aspects, including transparency, adhesion property, gas/vapor permeability, and water repellency. When it comes to considering any harmful effects from the device on the human body, the use of materials with biocompatibility and further bioresorbability allows for them to be used safely and over long periods of time. Furthermore, multiple sensory systems that are cost-effective and nonobtrusive have already been made available through the integration of adjustable conductivity, high-power system, and scalable process, as well as coupling wireless networks with WFHE. Overall, this section provides a checklist of required characteristics along with current strategies in five main categories: mechanical, physicochemical, biocompatible, electrical, and device-level properties. The summarized strategies for enhancing each feature are also presented in Table 1.

3.1. Mechanical Properties

For better understanding of how mechanical factors are associated with soft WFHE, Figure 5a provides several mechanical terms and definitions. Brittle materials eventually result in fractures without plastic deformation or in accommodating a small amount of imposed strain after the elastic limit. They are not ductile, which is inappropriate for fully stretchable devices. Figure 5b,c illustrates the range of Young's modulus and strain limit of some conventional and newly developed materials for WFHE.^[73] Making stretchable carbon, metal, ceramics, and oxides that were originally rigid, brittle, and linearly elastic allows these materials to be used in a wearable platform. A variety of structure-modifying methodologies are effective to reduce motion artifacts of the devices attached on the surface of the body. Soft elastomers show intrinsically ductile-plastic behavior, which avoids mechanical fracture beyond the elastic limit, and the mechanism generally referred to as strain hardening is involved with the reversible (or sometimes irreversible) plastic deformation. In other words, a highly ductile substrate is elongated above the value required for bonding onto the skin, enabling out-of-plane deformation. Various elastomers, gels, and liquid metals (LMs) are inherently stretchable due to their low elastic modulus and high strain limit, which are already two most common pathways to promote the development of wearable device in mechanical aspects. Collectively, meeting a combination of key mechanical requirements

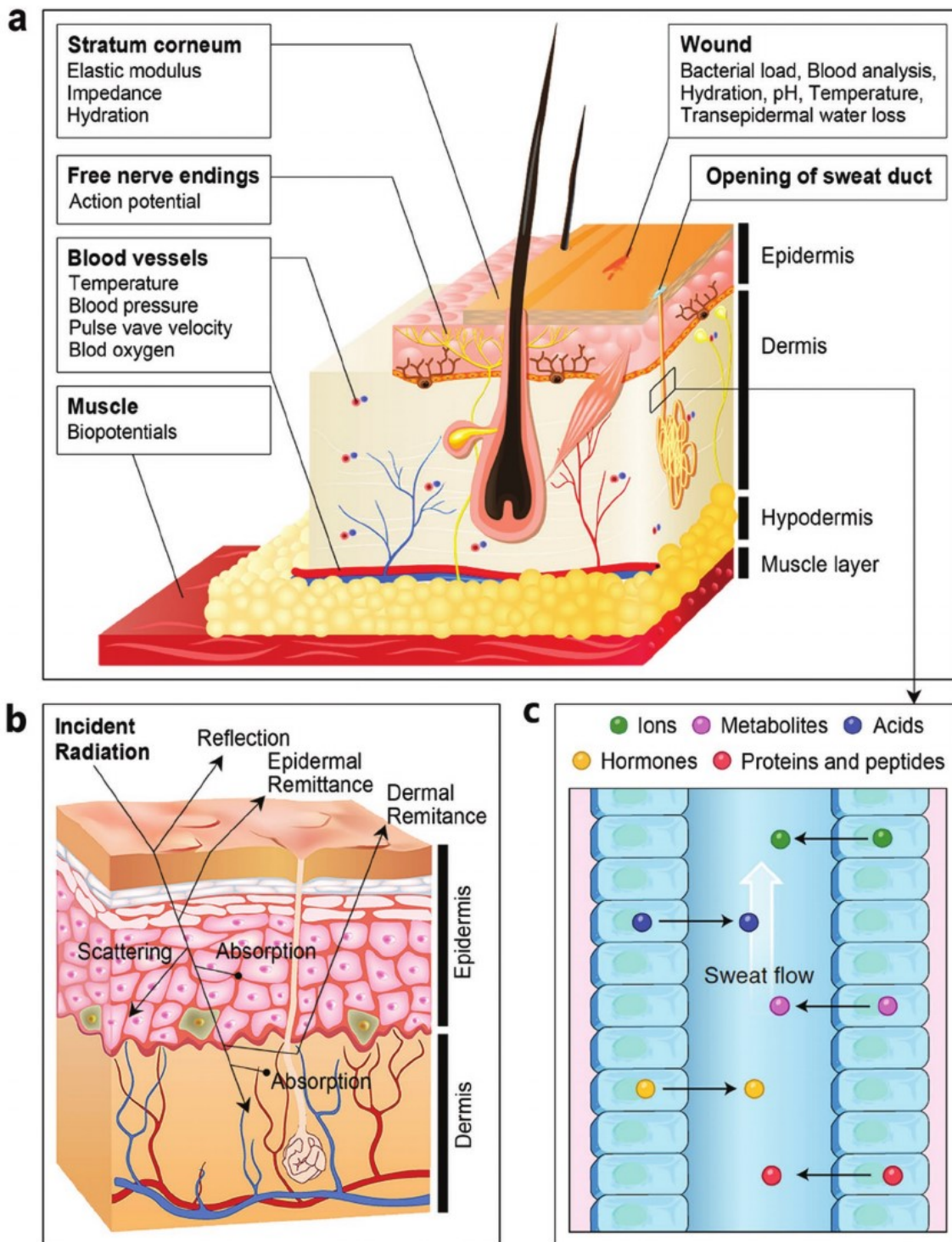


Figure 3. Description of a human skin that is used for integration of WFHE. a) Skin as a sensing platform for detecting various physiological signals. Reproduced with permission.^[1] Copyright 2017, American Chemical Society. b) Optical properties of the skin. Reproduced with permission.^[2] Copyright 2018, Royal Society of Chemistry. c) Multiple analytes in a sweat duct from (a). Reproduced with permission.^[3] Copyright 2018, Nature Publishing Group.

including low Young's modulus, high elastic limit, and high strain limit (strain value at fracture) can render the devices fully stretchable.^[24] The high diversity of materials, structures, and processes represented by the recent papers is given in the following sections.

3.1.1. Young's Modulus

Young's modulus, a measure of material's stiffness, is defined as the ratio of strain (ϵ) responses of the stress (σ) in the linear elasticity regime of a uniaxial deformation (unit: Pa). The

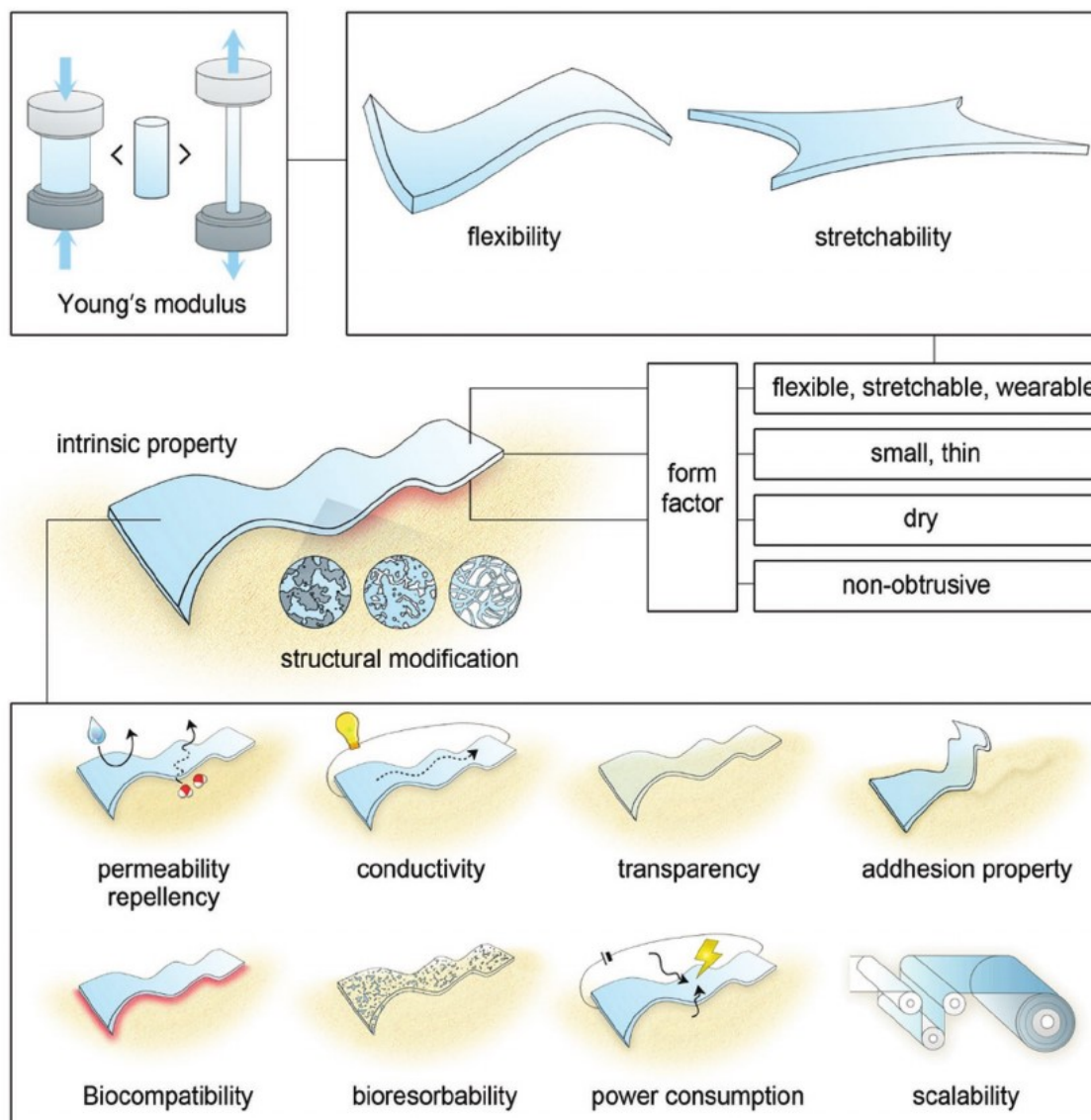


Figure 4. Schematic illustration of essential material properties for WFHE.

elastic modulus, where its value is fundamentally based on the atomic structure and bonding energy,^[75,76] determines not only mechanical but also electronic properties of the various materials that comprise integrated devices.^[77] When the modulus is small enough (corresponding value 2–600 kPa of the skin)^[53,78] in a broad stress range (up to the high failure strain), WFHE on the skin exhibit the desired characteristics without compromising the mechanical and electrical properties. To decrease the modulus of conventional materials in a wearable form factor, several researchers have downscaled the film thickness whose value is below a certain threshold. The background of this concept focused on silicon (Si) wafer, which is readily applicable to conventional devices and processes. With the thinning approach, the modulus of strained films is inversely proportional to the thickness when lower than 80 nm, given by the following equation:

$$E = 54.872 \times h^{0.226} \quad (1)$$

where h is the film thickness, which is well verified both theoretically and experimentally.^[77] Such a simple concept as downscaling the thickness addresses this problem by enabling rigid materials in their bulkiness to gain low Young's modulus.^[53] Unlike Si wafers, typical metal possesses malleability that makes it easy to deform; however, it is hard to retain conductivity to higher elongations.^[30,79,80] Thin-film electrodes with a careful control over strain-tolerant layouts can exert a remarkable improvement in retaining their conductivity, preventing any delamination, thus rendering the whole part stretchable in device scale. Nawrocki et al. demonstrated a wearable physiological sensor using sub-300 nm thin and dry gold (Au) film as an electrode (Figure 6a).^[81] The bending stiffness, a quantitative metric determining the comfort that a user experiences, is calculated to be 0.33 pN m². It is over two orders of magnitude lower than that of 3 μm sensor (75.85 pN m²) and thus is comparable to the uppermost layer of human skin. In the case of copper (Cu), the changes in film thickness of 200 nm to 1 μm do

Table 1. Important mechanical, physicochemical, biocompatible, and electrical properties for advanced WFHE.

Category	Remarks	Typical strategies	Refs.
Young's modulus	Low value is required for direct contact due to a low mechanical interfacial stress between the human skin and the device	Thinning of the inorganics or organics Creating a porous substrate Making filamentary serpentine structures of metals Embedding inorganics in/onto the organic substrate Adding plasticizer into the polymer Combining with liquid metal or ionic liquid	[83,96] [85] [96] [23]
Stretchability	High value is essential for intimate attachment to curved surfaces of human skin and for maintenance of mechanical robustness without device failure	Downscaling of the electrode material dimension Strain-tolerant designs of metal electrode Combination of ultrathin plastic and prestrained wavy or buckled elastic substrates Making percolating networks of hybrid materials into intrinsically stretchable composite Introducing intrinsically stretchable polymers, hydrogels, and ionic liquids	[40] [40] [40] [40] [18]
Form factor	Flexible, stretchable, wearable, small, thin, dry, and nonobtrusive form factors are required for sustaining the various properties while achieving sensing capabilities over long time frames	Miniaturizing or thinning each component including electrodes, substrates, and chips Developing soft-material-based components and effective encapsulation Band-aid patch, temporary tattoo Gel-free, dry, and reusable adhesive Transparent, lightweight, comfortable Devices integrated with microfluidics, 3D scaffold form, and devices made of fibers Integrating with wireless near-field communication protocols Flexible batteries or battery-free approaches	[83] [10] [169] [22] [275] [93] [55] [176]
Transparency	High optical transparency is required to be mounted directly on the human skin to be invisible during daily activities	Polymeric transparent films Limiting the width of metal electrode lines Transparent elastic films of carbon nanotubes, silicon nanowires, metal nanowires Reducing the thickness of layered structure based on nanopapers Use of the intrinsically transparent materials	[163] [8] [188,222] [194] [196]
Adhesion	Adequate or tunable adhesion through chemical, van der Waals, or electrostatic force guarantees proper strain transfer between two distinct surfaces	Wavy and suspended structures of electrodes and substrates Micropillar arrays with various tip geometries and aspect ratios Using dry adhesives for improving signal accuracy and quality Kirigami-inspired geometries by tuning adhesion through heterogeneous stiffness and actual contact width	[228] [202] [204] [205]
Permeability	High permeability to gas (air, oxygen) and water is required not to block sweat gland, to suppress the risks of skin inflammation even under perspiration evaporation for long-term wearing and tight adhesion	Thin silicon substrates Adding extra encapsulation layers not to degrade the device performance Inorganic nanomeshes or nanofiber-based conductors Fiber/yarn-like papers based on wood, silk, cellulose Porous graphene on elastomer sponges	[62] [215] [184] [13] [98]

Table 1. Continued.

Category	Remarks	Typical strategies	Refs.
Water repellency	Unaffected by water or resisting the ingress of water under specified conditions	Adopting polymeric substrates with intrinsically water-repellent properties Hybrid nanofiller-shaped composites	[239] [244]
		Chemical treatment with silane, carboxyl, and fluorine groups on the surfaces to generate a repellent surface	[97]
Biocompatibility	Low toxicity or nontoxicity is required for long-term retention of the wearable flexible bioelectronics on the human skin	Encapsulation or compositing with biocompatible materials Adopting intrinsically nontoxic polymers and metal oxides Biodegradable porous nanostructures Using gel-free dry adhesives	[12] [10] [262] [131]
Bioresorbability	To avoid the many long-term complications associated with detachment processes or nondegradability	Using bioresorbable materials including Si, Mg, Zn, Mo, W, SiO ₂ , MgO, PLGA, ^{a)} PI, ^{b)} etc.	[260,261]
		Using biomaterials including proteins, enzymes, and DNA	[246]
Gauge factor	High gauge factor within large strain range is required to detect the small strains induced by subtle human expressions	Using intrinsically high gauge factor materials such as semiconducting ZnO, ZnSnO ₃ , CNTs, and C-diamond Introduction of cracks in a conductive thin film Ultrathin metal foils on prestretched dielectrics for capacitive-type strain sensor Hierarchical architecture with MXene ^{c)} –AgNW as the “brick” and PDA ^{d)} /Ni ²⁺ as the “mortar” 0D–1D–2D ternary nanocomposite based on fullerene–SiNWs–graphene oxide	[278] [279] [145] [143] [139]
Scalability	Large scalability and cost effectiveness are attractive for future electronics	FET structure for thermistor-type temperature sensors Microfabrication of solderable and stretchable sensing system based on nickel–vanadium and gold pad metal layers and copper interconnection Adopting large-scale low-cost manufacturing method such as solution and printing processes	[12] [287] [289]

^{a)}PLGA = poly(lactic-co-glycolic acid); ^{b)}PI = polyimide; ^{c)}MXene = 2D titanium carbide Ni₃C₂T_x; ^{d)}PDA = polydopamine.

not affect the failure strain; however, they are associated with the weakening of yield strength.^[82] These phenomena initiate crack propagation and detachment from the substrate, decreasing reversible stretchability unless the thickness decreased close to a few hundred nanometers. Nevertheless, the reduction of Young's modulus down to the nanometer regime is regarded as difficult to achieve without the use of expensive and time-consuming processes or silicon-on-insulator wafers.^[83] Moreover, other problems arising from the poor performance, delicate handling, and uncontrolled buckling are encountered frequently.^[81,84] As an alternative, the neutral mechanical plane concept has been developed to integrate a several-hundred-nanometer Si layer into stretchable/foldable circuit systems by using polyimide (PI) as an encapsulating layer.^[61] The modulus of the other set of electrode materials, such as novel metals, incorporated into polymeric encapsulation layers or membranes has been under consideration in terms of not only the dimension scaling but also geometric patterning. Regarding the interconnection between metal electrodes, whose elastic limit is quite small ($\approx 2.0\%$), an approximate expression was proposed for the effective modulus of the entire, such as epidermal electronic system

$$E = E_{\text{int}} \left(1 + L_d / L_s \right) \quad (2)$$

where E_{int} is the effective modulus of the interconnects, L_d is the characteristic device size, and L_s is the distance between devices.^[53] As it follows from Equation (2), filamentary serpentine structures can afford an undoubtedly effective design by decreasing the E_{int} , while ultrathin devices with those patterns reduce the effective value of L_d to zero. Such configuration overcomes lowering fracture deformation involved with the partly ductile metal electrodes. Yeo et al. reported a comprehensive study regarding the thickness and geometric pattern used for the completed devices including Au electrode, silicone membranes, platinum (Pt) meander lines, and PI top and bottom layers (total thickness: <800 nm), which is more than 50 times thinner than the human epidermis (Figure 6b).^[54] The filamentary serpentine structures of such electrodes improve the bendability and degree of conformal contact combined with a thin layer (≈ 200 nm) of spray-on-bandage adhesive. This geometric approach is now widely accepted as a major strategy for minimizing strain-induced stress at the level of the overall system.^[85] On the other hand, looking into the selection of the electrode

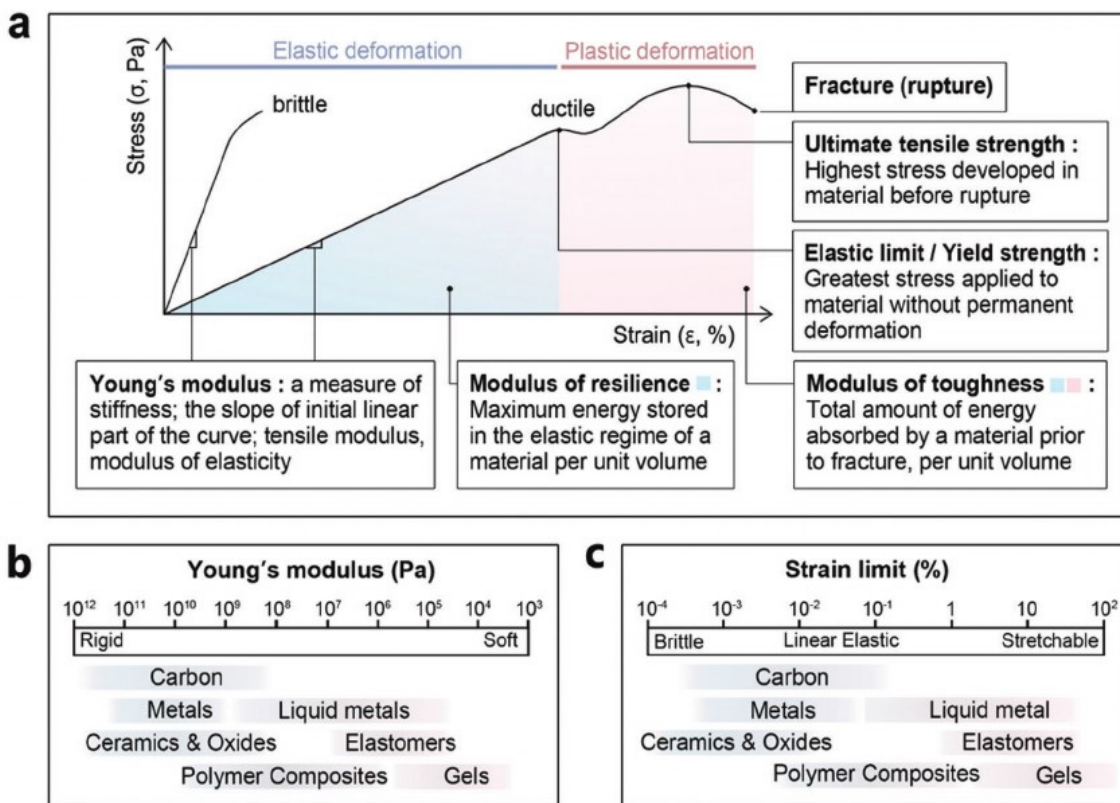


Figure 5. Summarized list of key mechanical properties of typical materials used in the development of WFHE. a) Stress–strain curves of brittle and ductile materials along with the description of important terms to describe the material's properties. b) Young's modulus (unit: Pa) and c) strain limit (unit: %) of widely used materials for WFHE. b,c) Adapted with permission.^[73] Copyright 2017, Wiley-VCH.

material, elastic stretchability of the electronics increases as the modulus of a metal layer increases with and without the existence of strain (as opposed to the trend in a substrate).^[86] Carbon-based materials, including monolayer or multilayered graphene and carbon nanotube (CNT), are promising electrode candidates; their elastic modulus is 0.5–1.8 TPa.^[87–89] Note that, in most cases, the stress experienced by electrodes that are packaged over the final platform is proportional to Young's modulus of the polymeric substrate around/underneath them, so that the whole device can be highly stretchable.^[90–93] Therefore, the most critical aspect for stretchability enhancement, particularly regarding the elastic modulus, is the selection and optimization of substrate materials, their structures, and processing methods. Such substrates should have modulus low enough to allow electrodes to deform out of plane and thus to retain high stretchability after full integration, not stirring up any detachment in the interface region.^[17] The best example is polydimethylsiloxane (PDMS) ($E = 360\text{--}870 \text{ kPa}$), whose mechanical compatibility with the skin and the electrode has enabled the contributions for the use in WFHE with various form factors: encapsulation layer, membrane film, porous platform, functional composite, microfluidic substrate, microneedle/pillar,^[94] and the like.^[95] In addition, many inherently soft materials, such as poly(vinylpyrrolidone) (PVP), ethylene–vinyl acetate, Tegaderm, Ecoflex, and Parylene, can afford significant weight/thickness reduction, improve mechanical compliance at the interface, and enhance conformability to the skin. For more

information, readers can refer to comprehensive and detailed reports with tables.^[10,96,97] Likewise, the synthetic tunability of naturally stretchable plastics, which affords easy modulation in the shape and structure, has allowed for the manipulation of Young's modulus in these devices. The latest progress made toward high-performance wearable devices relies on such organic materials tuned in effective ways to reduce the elastic modulus. Making them in porous structures is regarded as an ideal direction to achieve not only low modulus but also gas/moisture permeability. Sun et al. reported a porous silicone sponge substrate by using size-controlled sugar as a template of the final device thickness with 500 μm (Figure 6c).^[98] This randomly porous structure decreases the effective modulus of the substrate from the original value of 170 kPa (Dragon Skin; Smooth-On) to 15 kPa with the following equation:

$$E/E_s \approx (\rho/\rho_s)^n \quad (3)$$

where ρ is the density, n is the power that is dependent on the material's microarchitecture, and "s" denotes the respective bulk value of the solid constituent material property.^[99] Another report showed that hierarchical PDMS exhibits a low elastic modulus (174 kPa) and thus guarantees increased contact area with poly(vinylidene fluoride-co-trifluoroethylene) that has much higher elastic modulus ($\approx 1 \text{ GPa}$), which in turn was effectively used for triboelectric sensors with interlocked structures.^[100] However, this strategy requires sophisticated

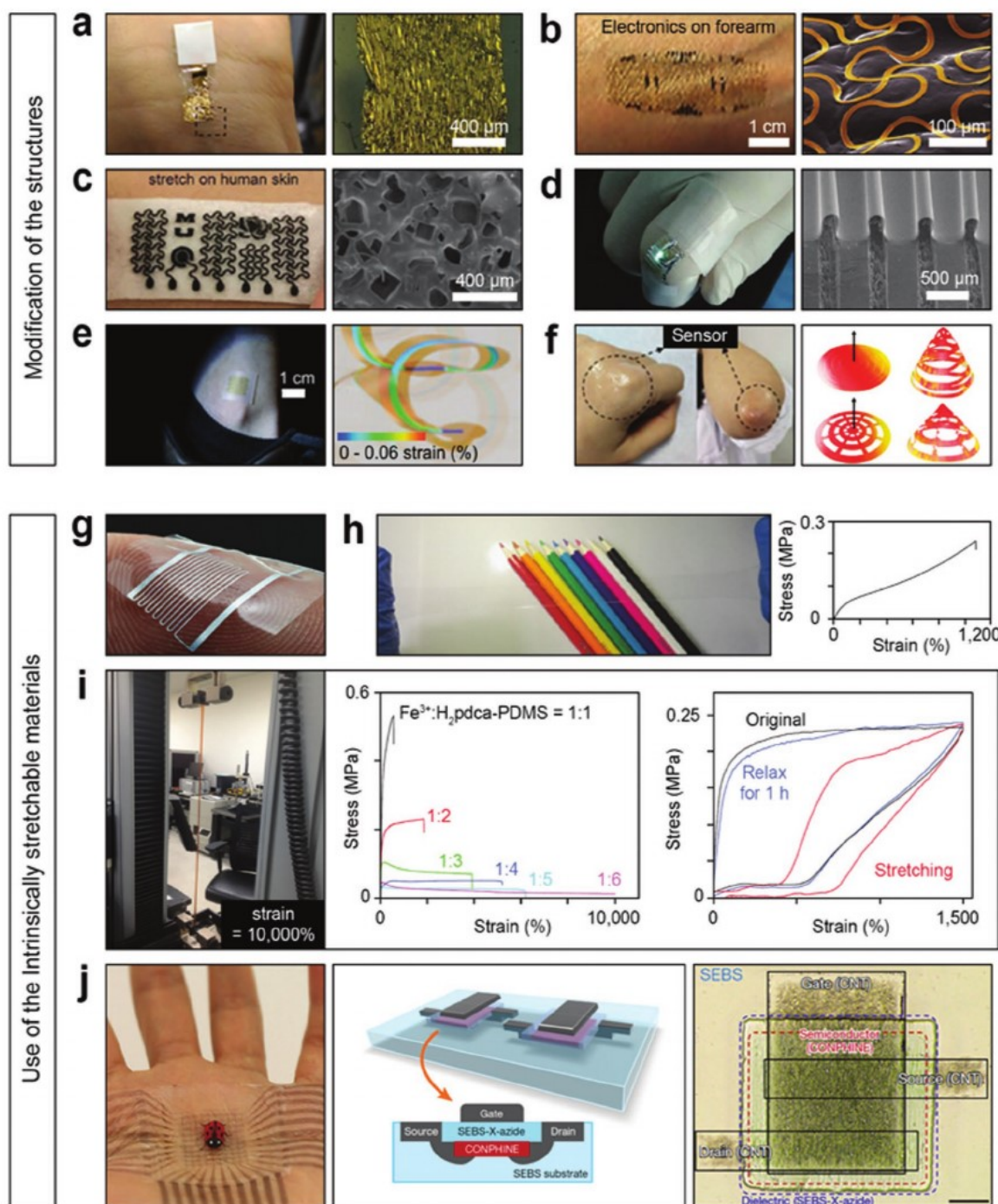


Figure 6. Strategies for enhancing mechanical stretchability. a) 300 nm thick metal electrode on the skin (left) and top of an elastomer (right). Reproduced with permission.^[81] Copyright 2018, Wiley-VCH. b) Thin, filamentary serpentine electrode mounted on the skin (left) and a skin replica (right). Reproduced with permission.^[54] Copyright 2013, Wiley-VCH. c) Porous graphene/Si sponge substrate on the skin (left) and magnified structure of the elastomer (right). Reproduced with permission.^[98] Copyright 2018, Wiley-VCH. d) Stretchable OLED (left) and structure of the OLED/polymer film on a prestretched elastomer (right). Reproduced with permission.^[84] Copyright 2016, Nature Publishing Group. e) 3D wavy structured thermoelectric coil on a flexible film for energy harvesting (left) and a magnified geometry with predicted mechanics (right). Reproduced with permission.^[130] Copyright 2018, American Association for the Advancement of Science. f) Kirigami-inspired humidity sensors attached to the finger joint and elbow (left) and schematic images recorded during pulling processes of the film (right). Reproduced with permission.^[342] Copyright 2018, Wiley-VCH. g) Biphasic gold–gallium liquid metal patterned on PDMS. Reproduced with permission.^[149] Copyright 2016, Wiley-VCH. h) Stretchable ionic conducting hydrogels. Reproduced with permission.^[157] Copyright 2018, Nature Publishing Group. i) Self-healing PDMS with tuned stretchability by metal–ligand interaction (after stretching: 10 000%). Reproduced with permission.^[155] Copyright 2016, Nature Publishing Group. j) Intrinsically stretchable transistor array adhered to a human palm, example of the configuration, and optical microscope image. Reproduced with permission.^[101] Copyright 2018, Nature Publishing Group.

fabrication techniques and also accompanies a degradation in mechanical properties that reduces relative densities of the device.^[101] The use of intrinsically ultrastretchable polymer, such as soft ionic conductors,^[14] or the adoption of the effective way of tuning its structure has addressed such problems. The elastic modulus of newly developed polymers and nanofibrils (cellulose, chitin, and silk) with distinct functionality, such as self-healing property^[102–105] and biodegradability,^[106] depends on not only chain entanglement or cross-linking, but also the ratio of units, structure, or orientation index.^[107,108] Along with their easy processability, changing the ratio of each unit in the polymer tunes Young's modulus, fracture strain, and fracture energy. Kang et al. reported a self-healing stretchable material with multistrength hydrogen bonding interaction that was rationally designed by decreasing the ratio of 4,4'-methylenebis(phenylurea) (MPU) units in the polymer.^[102] In another example for silk-based hydrogels, Young's modulus and stretchability were tuned from 5–12 GPa to 0.15 MPa and from <20% to >400%, respectively, by plasticization and control of the water content.^[109] In many cases, plasticizers are used to improve both the toughness and flexibility, and thus the formability of the polymer films that can be used in wearable form factor.^[110,111]

In the application of energy harvesting that is one of the most potent abilities of WFHE, it is significantly important to modulate the Young's modulus precisely.^[112,113] The output response of a piezoelectric material is represented by the following equation:

$$D = d\sigma = dE\varepsilon \quad (4)$$

where D is the electrical charge separation and d is the piezoelectric coefficient.^[114] Intuitively from Equation (4), high modulus can endow conventional piezoelectric materials, such as poly(vinylidene fluoride), with benefits that improve the piezoelectric generator. On the other hand, to enable the integration of piezoelectric energy into the wearable power system, it is likely to obtain the intended capabilities as well as the optimized modulus. Other than that, the realization of robotics, which is another related field of using WFHE, is also affected by modulus in various ways (see refs. [115–117]).

3.1.2. Stretchability

Stretchability, in general more than 10% while retaining their functions, has been advocated as a useful term for illustrating the distinct property of WFHE.^[74,118] To be specific, to successfully make "stretchable" electronics, it primarily requires accommodating the strain induced by the motion of the body as well as the deformation of the skin that exhibits complex topography and reversible stretchability up to 100%. As a useful instance, the use of thin electrodes that are embedded in or atop low-modulus soft substrates can render the electronics stretchable in a way that they are bent, wrinkled, or crumpled. More importantly, such devices should have high deformability without any degradation in the additional hybrid functionalities (such as electrical conductivity), while preserving such stretchability of deformed components even after applying the maximum strain

repeatedly. To date, many studies in stretchable electronics have proved that there are two ways to make stretchable electronics: 1) structural modification of electrodes, substrate, and their composites, or 2) the use of intrinsically stretchable materials. First, the deterministic patterns including fractal^[119] and serpentine^[86,120] enable the device to actuate appropriately in both the component-interconnected and the substrate-attached regions. Such stretchable metals built on a polymeric substrate then function as a highly conductive electrode without inducing significant changes in mechanical properties during the use of the device on the skin. In the other way, deterministically patterned substrates, such as mesh-type,^[121] mogul pattern,^[122,123] prestrained, helical, origami and kirigami engineered,^[124–128] or merged structures,^[129] have been created to make the whole device sufficiently stretchable. Yin et al. described a prestrained strategy that uses periodic buckles preformed on thin poly(ethylene terephthalate) (PET) foil substrate via laser ablation (Figure 6d).^[84] Notably, this buckling profile enhances the performance of organic light-emitting diode (OLED)/polymer device that exhibits a luminous efficiency of -70 cd A⁻¹ under 70% strain. Moreover, the device accommodates high strain up to 100% while retaining performance over 15 000 stretch-release cycles. With this strategy, they demonstrated the use of such stretchable OLEDs in wearable form factor by mounting them on the back of a finger joint, where the strain value changed to 55–60%. Nan et al. demonstrated that an integration of thin-film materials into open 3D helical chain can provide flexible thermoelectric energy harvester that can integrate effectively with the human body (Figure 6e).^[130] The effective integration of thermoelectric materials based on 2D thin-film serpentine-shaped p- and n-legs made of boron and phosphorus-doped Si was conducted, where silicon dioxide (SiO_2) served as mask for doping, and then they were encapsulated by PI for maintaining mechanical stability. This approach acted as a powerful tool for aligning toward the out-of-plane deformable WFHE. As a result, the open-circuit voltage of 51.3 mV at $\Delta T = 19$ K measured from 8×8 array of coils does not diminish over time, showing the steady thermal profile and the maximum power output of 2 μW from an area of a wristwatch (10 cm^2). Aside from optimal stretchability, the format in coils also allows excellent thermal contact with the heat source, which is the surface of the skin, ensuring higher maximum power. In the other report, Figure 6f shows kirigami-engineered materials, in which their stretchability rises due to the changes in the in-plane or out-of-plane geometry rather than deformation of actual material.^[124,125] Studies on such kirigami method found that, despite its poor coverage of the surface, this 2D mesh could be readily applied to wearable electronics such as electrocardiogram (ECG) recording and even implantable electronics that fit an inner organ surface.^[126,131] Moreover, by the fact that those deterministic patterns are predictable, it commonly comes with a 3D finite element method enabling a fast prediction for stretchable models on structures before real integration.^[132] Comparing those, there are other useful methods for making composites that have desired functionality and stretchability. Rather than using layered structures of electrode and substrate, filler materials are randomly or orderly incorporated within a plastic substrate. In general, it is efficient to control the required performance of the whole hybrid system,

yet among all components with certain functionality, several fillers are usually not stretchable on their own. This can be changed by the use of nanomaterials, as a strain relief approach, especially in the form of 1D^[133–137] or hybrid forms,^[138,139] rather than 0D,^[140] which ensures high conductivity even if cracks or notches appear in the structure. To enhance stretchability while improving conductivity or transparency, such hybridization combining not only 1D materials in different scales, but also diverse materials and composition into the one composite is highly effective. Moreover, ultrathin 2D materials show enhanced performance based on their intrinsic conductivity and scalability such that they can be good candidates for the future.^[141] Graphene is a great filler, on that account, and the others such as molybdenum disulfide (MoS₂)^[128] and MXene^[142,143] have been recently adopted for a wearable platform that shows high intrinsic flexibility over a large area, while allowing high optical transparency and efficient carrier transport.^[141] As an example, a strain sensor that is attached to the joint or directly mounted on the muscle can be expressed in another property gauge factor, which is the ratio of the stretchability and their conductivity during natural body activities for human motion inspection. Furthermore, in the view of process, those compositing methods can adopt restrained constructs,^[84,144,145] polymer-assisted metal deposition,^[146] 3D spalling,^[147] 3D integration,^[148] and the like. Nevertheless, the composites made with nanomaterials exhibit high tailoring capabilities, multiaxial stretchability, associated patterning processes, and adhesion problems. There are several recent concepts, such as ionic conductor and LM, which are also interesting candidates for “intrinsically stretchable” electronic materials. LM, encapsulated in soft substrates, is highly stretchable, mostly based on its liquid yet metallic conductive features (Figure 6g).^[149] Hirsch et al. formed biphasic gold–gallium (Au–Ga) LM that is patterned on a elastomer membrane by sputtering an alloying Au film followed by the thermal evaporation of liquid Ga, resulting in the solid intermetallic alloy AuGa₂. The photolithography was used for patterning electrode part with critical dimension of 100 μm on a 40 μm thick PDMS membrane. They found that the biphasic liquid films show low sheet resistance ($1 \Omega \text{ sq}^{-1}$), low gauge factor (≈ 1), and no dependence on strain history. Such great electrical constancy is maintained independently of applied elongation, enabling a cost-effective approach including printing process, and thus is used for wearables in a variety of applications for triboelectric nanogenerator,^[150] glove-type strain sensor with meander resistors,^[151] and air-quality monitoring system.^[152] The other ionic conductor, which includes hydrogels,^[14,103,105,153] plasticized silk proteins,^[109] and semiconducting polymers,^[154] is also stretchable and endows the device with additional functionality such as self-healing capabilities.^[102,132,155,156] Shi et al. fabricated ionic conducting elastomers (ICEs) by employing lithium bis(trifluoromethane sulfonimide), butyl acrylate (BA), poly(ethylene glycol) diacrylate, and 1-hydroxycyclohexyl phenyl ketone (photoinitiator 184) as an electrolyte salt, monomer, cross-linker, and photoindicator, respectively (Figure 6h).^[157] This ICE prepared by copolymerization possessed high stretchability with elongation to 1100% as well as high conductivity of $1.27 \times 10^{-7} \text{ S cm}^{-1}$ at room temperature (20 °C). Moreover, it shows high-temperature stability up to 300 °C and long-term

use by virtue of its noncorrosive and hydrophobic features as well as a full transparency of 92.4% with a 1 mm thick sample in the visible light region. Sarwar et al. disclosed a method of monitoring finger proximity by using ionically conductive hydrogel electrodes, which project electrical field above a capacitive sensor to detect the movement and location of multiple fingers.^[158] The bendability, stretchability, and transparency of the hydrogel facilitated its proximity, touch, and pressure sensors. Li et al. reported Fe–Hpdca–PDMS polymer with an iron (Fe(III)) metal and 2,6-pyridinedicarboxamide (H₂pdca)–PDMS ligand. Its metal-coordination interaction contributes to a maximum applied strain of 1500% (maximum fracture strain up to $4500 \pm 20\%$) with 90% healing efficiency after 48 h of cutting at ambient temperature (Figure 6i).^[155] Given that its high mechanical properties were fully recovered after damage (i.e., rheological features), the self-healing effect can significantly increase the operation time over biological relevant timescales.

The use of intrinsically stretchable array of transistors using cross-linked styrene–ethylene–butadiene–styrene (SEBS), conjugated polymer/elastomer phase separation induced elasticity (CONPHINE) film, CNTs as a dielectric, semiconductor, and electrodes allows the skin electronics to be semitransparent without hard–soft integration. The fabricated device includes a stretchable array of 6300 transistors in an area of around $4.4 \times 4.4 \text{ cm}^2$ (Figure 6j).^[101] These devices are fully stretchable and transparent, which would allow inkjet printing for large-scale fabrication.

3.2. Physicochemical Properties

3.2.1. Small and Thin Form Factor

Form factor is a combination of various factors of a device determined mostly by its size, shape, and other physical arrangements. Generally, in electronic packaging, consumer electronics, and nanomaterials fabrication, the term describes the physical size and shape of a material or device that represents a class of similarly sized components and prescribes a specific standard.^[159–161] Many people have adopted new lifestyles created by wearable technology in revolutionary form factors: glasses, goggles, wristwatches, bracelets, armbands, rings, gloves, necklaces, pins, headsets, and clothes. By contrast, WFHE continues to expand by adding unique characteristics and unprecedented attributes in which the value is adjusted with respect to the skin interface. According to recent studies, when functional devices are desired to be fully matched to the surface of the body, the requirements include flexible/stretchable, small, thin, dry, and nonobtrusive form factors. Throughout all this, the focus is much on implementing a variety of ideas with the goal of satisfying such physicochemical mandates and thus achieve dynamic capabilities over long time frames. Thin, small, lightweight, and bendable components are required to make direct contact with the human skin and send signals without distracting users. To fabricate such functional electronics that are so light and thin that the thickness goes down to several hundreds of nanometers, the use of transferring approaches of thin polymeric layer encapsulating a functional electrode or device allows the device to fly in the air or not to distract human from any movement.^[162–164]

To decrease the thickness of substrate, which is polymer-based material, ultrathin organic,^[165] carbon-based composite,^[166] cellular composite,^[167] and 3D monolithic types^[168] are also used. To obtain small and thin devices, the approach for thinning of conventional inorganics is also broadly used in the microelectromechanical system, not only for the electrodes and substrates, but also for ultrathin chips (<50 μm) obtained from brittle and rigid Si wafer. The above-mentioned strategies allow fabrication of patch-type WFHE, which can monitor a variety of vital signals.^[25] Recent papers have covered the examples including the electrochemical sweat sensor,^[169] ISF-based biochemical sensor,^[170] graphene-based physiological sensor,^[171] LM-based electromyogram (EMG) sensor,^[172] commonly used Au-based sensor,^[133] and even the supercapacitor.^[173] It is also possible to use it as a battery-embedded smart lens,^[174,175] or 1D flexible battery.^[176] To increase sensitivity to a small amount of chemicals from the human body, such as from sweat, microfluidic channel is also adopted, usually in the form of PDMS that is repellent to water solution.^[177,178] In this case, water permeability of microchannel can be nonnegligible, so additional treatment is required (see Section 3.2.4).^[179]

3.2.2. Transparency

High optical transparency (unit: %) is instrumental for making wearable devices and smart displays, yielding a visually perfect fit with the human body.^[40,180] The aforementioned PDMS is flexible and optically transparent, making it suitable for using in bioelectronics. However, its conductivity and functionality are worse than those of conductive electrodes, such as novel metals and carbon-based materials.^[181,182] Many efforts have been made to obtain high stretchability, transparency, and desired functionality at the same time. In this section (Figure 7), recent studies that have a focus on increasing transparency as well as adding functionality to WFHE are given. Figure 7a shows that ultrathin organic field-effect transistors (OFETs) composed of a 100 nm thick Au metal film evaporated onto the 1 μm polyethylene naphthalate (PEN) foil became lightweight and crumpled like a sheet of paper.^[163] Such ultrathin electronic film made up of PI-encapsulated Si complementary metal–oxide–semiconductor (CMOS) circuits formed onto prestretched elastomers (3M VHB) is used for a tactile sensor (total thickness: 2 μm).^[163] When the prestrained elastomer is relaxed, the ultrathin foil forms a network of out-of-plane wrinkles (thickness of folds: 100 μm) so that the device accommodates subsequent tensile strains up to 233%. Decreasing the thickness of layered structures based on micro- and nanopaper can be used as a methodology for synthesizing highly transparent as well as gas-permeable films.^[13] Wang et al. demonstrated that a triboelectric tactile sensor with patterned silver nanofiber (AgNF) electrodes on the elastomeric PDMS matrix showed high transparency as well as rapid response time of 70 ms.^[183] The diameter and transparency of AgNFs depend on the time for electrospinning and sputtering, respectively, and the results, in turn, show the high conductivity of the electrodes of 1.68–11.1 $\Omega \text{ sq}^{-1}$ at high transmittance of >70%. Fan et al. demonstrated a breathable epidermal electrode composed of a scaffold-reinforced conductive nanonetwork based on Ag nanowires (NWs) and polyamide (PA) NFs.^[184] Figure 7b shows the AgNWs–PA NFs that exhibit high transparency (84.9%)

with a low sheet resistance of 8.2 $\Omega \text{ sq}^{-1}$. In this case, PA NFs formed a scaffold-reinforced network for solution-dispersed AgNWs followed by the effective embedding via vacuum filtration afterward. Furthermore, this structure achieved excellent mechanical robustness in uniaxial strain (0–50% elongation) and high durability under 3000 bending cycles with 300 m⁻¹ curvature. In this manner, scale- or shape-controlled composites consisting of metals and polymers presented high transparency at the visible light region in Ag nanoparticles (NPs)/polyurethane (PU) (77%),^[185] AgNPs/PDMS (86%),^[186] PDMS/AuNW–AgNW (86%),^[135] AgNWs–PDMS (88.3%),^[121] and AgNF–AgNW/PI (89.05%),^[8] for the flexible strain/tactile sensors. Besides, functional inorganic materials, such as boron nitride nanosheet (BNNS), dispersed in PDMS with the controlled contents (1.0 wt%) have been proposed for transparent and flexible piezoelectric sensors.^[187] The BNNS/PDMS composite shows higher transparency than the bulk BN with the same contents, which yields 40 μW and a conversion efficiency of 12.6% from human movement in a transparent manner. Carbon-based materials, such as high-quality graphene exhibiting transparency higher than 90%, are a promising candidate for a flexible electrode.^[188] The conductivity of CNT/PDMS is 1809 S cm⁻¹ at >85% transmittance, increasing to 3316 S cm⁻¹ at 100% tensile strain.^[189] Several works reported on graphene-based (semi-)transparent substrates focusing on their use as sensors.^[190,191] Films consisting of biomimetic chitin, silk, and their hybrids are also highly transparent under visible light.^[110,192–194] Using biomimetic chitin NFs and silk fibroin (β -sheet) with conductive AgNFs, the hybrid films show high transparency of >90% (Figure 7c).^[192] The addition of a β -sheet increases the elastic modulus up to 6.5 GPa, provided by hydrogen-bonded cross-links, while reducing the defects of the chitin NFs. In this manner, such devices having high transparency were used for an intraocular lens that was able to be worn on a rabbit eye while sensing glucose concentration in tear fluids in a wireless manner. Furthermore, such a hybrid film made for film heater showed a coefficient of thermal expansion (17 ppm K⁻¹) comparable to that of PI (17.5 ppm K⁻¹). The replacement of the electrodes or substrates with ionic conductors, which are intrinsically soft and stretchable, is of particular interest (Figure 7d,e). Thanks to further investigation on electronic designs and material packaging in the iontronic field, a skin-attached pressure sensor exploiting an epidermal–iontronic interface demonstrated high optical transparency (>85%) and ultrathin construction (weight: 5 g m⁻²), along with high sensitivity (5 nF kPa⁻¹) (Figure 7d).^[195] Even though hydrogel electrolytes are susceptible to moisture, a side effect of their dehydration at a high temperature (\approx 100 °C) and their ensuing weight loss,^[157] they are still powerful enough to use in wearable platforms since the polymer network does not scatter light and shows similar optical properties of water even with increased thickness, which ensures an acceptable conductivity (Figure 7e).^[195–197] Moreover, the array of small, thin, and elastic transistors renders the skin electronics semitransparent, removing the need for the hard–soft integration (Figure 7f).^[101] The use of the intrinsically stretchable cross-linked SEBS-azide, CONPHINE film, and CNTs can make the entirety of the skin electronics transparent, even when fully patterned with 6300 transistors. For more information regarding transparent flexible electronics, one can refer to the recent review.^[198]

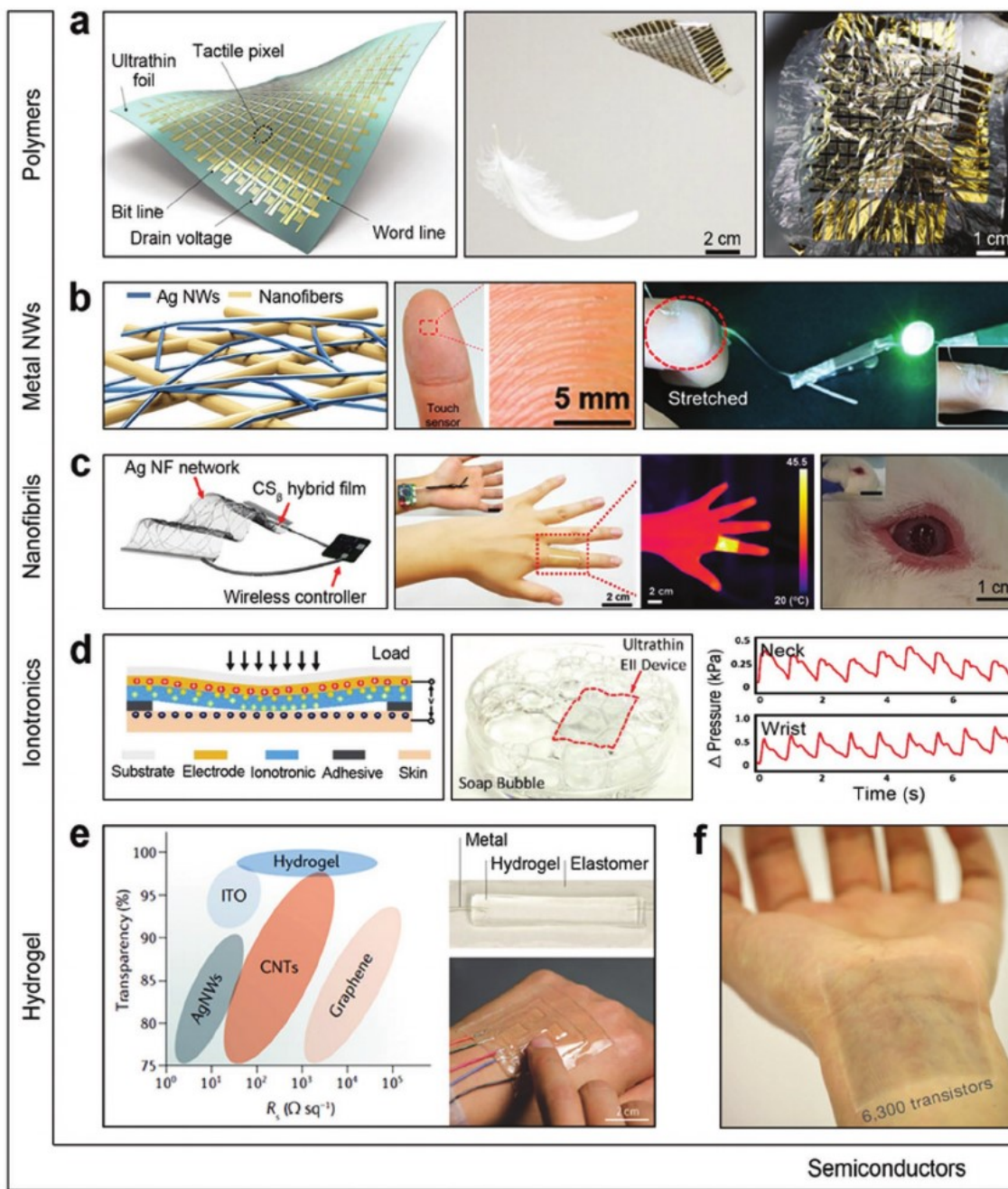


Figure 7. Strategies for enhancing transparency. a) Ultrathin plastic electronic foils (crumpled like a sheet of paper). Reproduced with permission.^[163] Copyright 2013, Nature Publishing Group. b) Scaffold-reinforced AgNWs/PA NFs attached on the fingertip, finger knuckle, and their use for powering LEDs. Reproduced with permission.^[184] Copyright 2018, American Chemical Society. c) Nanofibers and silk fibroin (β -sheet) hybrid film heater and contact lens, applied on a rabbit eye. Reproduced with permission.^[192] Copyright 2018, Wiley-VCH. d) Capacitive pressure sensor using an epidermal-iontronic interface. Reproduced with permission.^[195] Copyright 2018, Wiley-VCH. e) Transparent and conductive hydrogel-based pressure sensor attached to the back of a hand. Reproduced with permission.^[196] Copyright 2018, Nature Publishing Group. f) Fully patterned transparent electronics with 6,300 transistors using CNT, SEBS-azide, and CONPHINE. Reproduced with permission.^[101] Copyright 2018, Nature Publishing Group.

3.2.3. Adhesion

When two surfaces of differing structures come into direct contact with each other, it is inevitable that they will come apart after a certain period of time has elapsed, whether by design or by accident. While adhesion to skin can result in highly accurate signals, immediate drawbacks include the difficulty

of separating such devices from the skin. Additionally, medical adhesives, such as acrylic adhesives, which are found in commonplace tapes, dressing, ECG electrodes, and medication patches, may cause allergic contact dermatitis.^[199] Superficial layers of the skin are readily removed by patches or adhesive products when such patches are detached from the surface of the skin.^[200] The abovementioned phenomena reduce the

skin's barrier function, leading to potential toxicity and irritation from the substances, which increases the risk of infection. As a result, recent studies have focused on dry features, especially of interfacial adhesion. Instead of using sticky adhesives, forming a dry and continuous contact via the action of van der Waals forces or electrostatic forces is required.^[201] Conformal adhesion has been achieved by using extremely thin electrodes, pattern-imprinted substrates, and self-adhesive materials as the basis for a flexible stretchable form factor as well as conformal/dry contact between the skin and WFHE. As shown in Figure 8a, an ultrathin Au electrode that is partially encapsulated by Parylene improved adhesion to the skin by reducing bending stiffness (i.e., by modifying its mechanical property).^[81] Its total thickness of sensing area reduced to 200 nm ensures self-adhesion to any 3D biological surface, resulting in the development of motion artifactless ECG and EMG sensors. Hybrid approaches, whereby an adhesion area is architected with micrometer-scale pillars, get rid of the need for a glue yet maintain adhesion quality by establishing the more reliable interconnections between the soft WFHE and the skin (Figure 8b). By adopting a polymeric surface covered in micrometer-sized mushroom-shaped projections, the substrate can adhere to human skin without using glue. This negates the need for sticky residues and irritations that commonly result when using sticking plasters with acrylic adhesives. By focusing on adhesion mechanisms used in the animal kingdom, including well-known examples such as the gecko or octopus, wearable devices recorded vital signals even from wet skin while bypassing any toxicity induced by the currently used adhesives that are based on acrylic compounds.^[202–204] One example includes stretchable electronics with octopus-like patterns imprinted on a carbon-based conductive polymer composite film (Figure 8c).^[203] These bioinspired conductive suckers allow high adhesive capabilities under both dry and wet conditions on silicon (5.24 N cm^{-2}) and skin replicas (1.89 N cm^{-2}) without leaving behind residues after detachment, even with an effortless peel-off procedure. By controlling the ratio of the carbon fillers (optimum: 7 vol%) in PDMS matrix, which resulted in the successful formation of the percolation networks, vital biosignals such as ECG and the bending motions of a human wrist were detected even under water. The kirigami-inspired structure was also used for enhancing the adhesion strength (Figure 8d).^[205] PET films were patterned by laser cutting and coated with an adhesive silicon primer between the PET films and PDMS substrate. The design of the pattern, such as the number of interconnects, controlled spatial and directional adhesion strength to the skin. Other approaches include an addition of a small amount of surfactant to modify adhesion strength of the most used substrate, which is PDMS (Figure 8e).^[191] Triton X that contains polar functional groups interacted with a curing agent in the PDMS, thereby modulating its mechanical properties and enabling the use for ECG sensor embedded with AgNWs. The use of hydrogel has garnered great attention as a means of improvements in adhesion that leave no residue after detachment.^[105,206–210] Figure 8f shows one example of hydrogels that are very durable and adhesive, inspired by the delaminated structure of the skin.^[105] In situ polymerization of nucleobase-driven adhesive hydrogels on the conductive tough hydrogels resulted in robust direct adhesion to the skin as well as various

solid materials. Furthermore, effectively blocking the current from the tough conductive layer protects the skin from harm. They also exhibit high flexibility and strain sensitivity, enabling the detection of large-range human motions as well as tiny physiological signals. One example showed a high bonding capability that was mainly attributed to a high stretchability (up to 2100%) and adhesion strength even under water (10–20 kPa) allowing for the monitoring of subtle motions such as swallowing and smiling, where the relative resistance change was below 5%.^[104] Hydrogel serves as an optimal adhesive in part due to its composition. Han et al. demonstrated that programmable changes in the adhesion strength of hydrogel, which are synthesized by in situ formation of polydopamine (PDA)-doped polypyrrole nanofibrils, interwoven in an elastic and transparent polyacrylamide network, resulted in controllable values up to 30 kPa in maximum.^[211] Moreover, Oh et al. recently demonstrated a resistor-type temperature sensor exhibiting high thermal sensitivity of $2.6\% \text{ }^{\circ}\text{C}^{-1}$ ($25\text{--}40 \text{ }^{\circ}\text{C}$), enabled by the integration of the use of functional hydrogel and the aforementioned hierarchical layout of the surface (Figure 8g).^[212] They designed PDMS surfaces according to bioinspired octopus sucker-like microstructures that have a cavity ($7.5 \mu\text{m}$) and rim ($4 \mu\text{m}$). Fabricated from a mold, each surface of the microstructure was spin coated with thermoresponsive hydrogel layer, poly(*N*-isopropylacrylamide) (pNIPAM). This produced strong adhesion without the pNIPAM coating layer up to 3.78 kPa, which is greater than that when using the pNIPAM (2.28 kPa); creating rim structure achieved adhesion 14–23 times higher than the flat PDMS. Furthermore, such results were reversed when the temperature rose to $40 \text{ }^{\circ}\text{C}$ (13.4 kPa) by the deswelling of the pNIPAM, the shrinkage of the hydrogel, the increase of the internal concavity volume, and thereby the suction effect of the rim structure. These features can last at least half a day at $25\text{--}40 \text{ }^{\circ}\text{C}$ and enable easy detachment. Therefore, they were adopted for skin-attached temperature sensors with reusability and high durability.

3.2.4. Permeability

Many sensors and components that constitute a WFHE encounter complex environments that are abundant in gases, liquids, and molecules. This external circumstance may cause inevitable penetration of chemical species into the surface of wearable devices mounted on the body, and thus the sensor capabilities may deteriorate over time. This lack of environmental robustness is a major obstacle to achieving stability while exhibiting a sufficient sensing performance. Apart from that the general electronics are prone to moisture, stagnant water under the devices also damages the epidermis, causing infection, pain, and delayed healing.^[200] Therefore, WFHE should be selectively permeable or impermeable to gases such as water vapor (mostly from the external environment) and liquids that contain salts, proteins, and other molecular substances (from the biological environment).

An encapsulating layer that is low water permeable or water repellent has been applied to the surface of WFHE, providing stability to the interfaces. One of the examples is the use of PDMS that is flexible and biocompatible; however, it

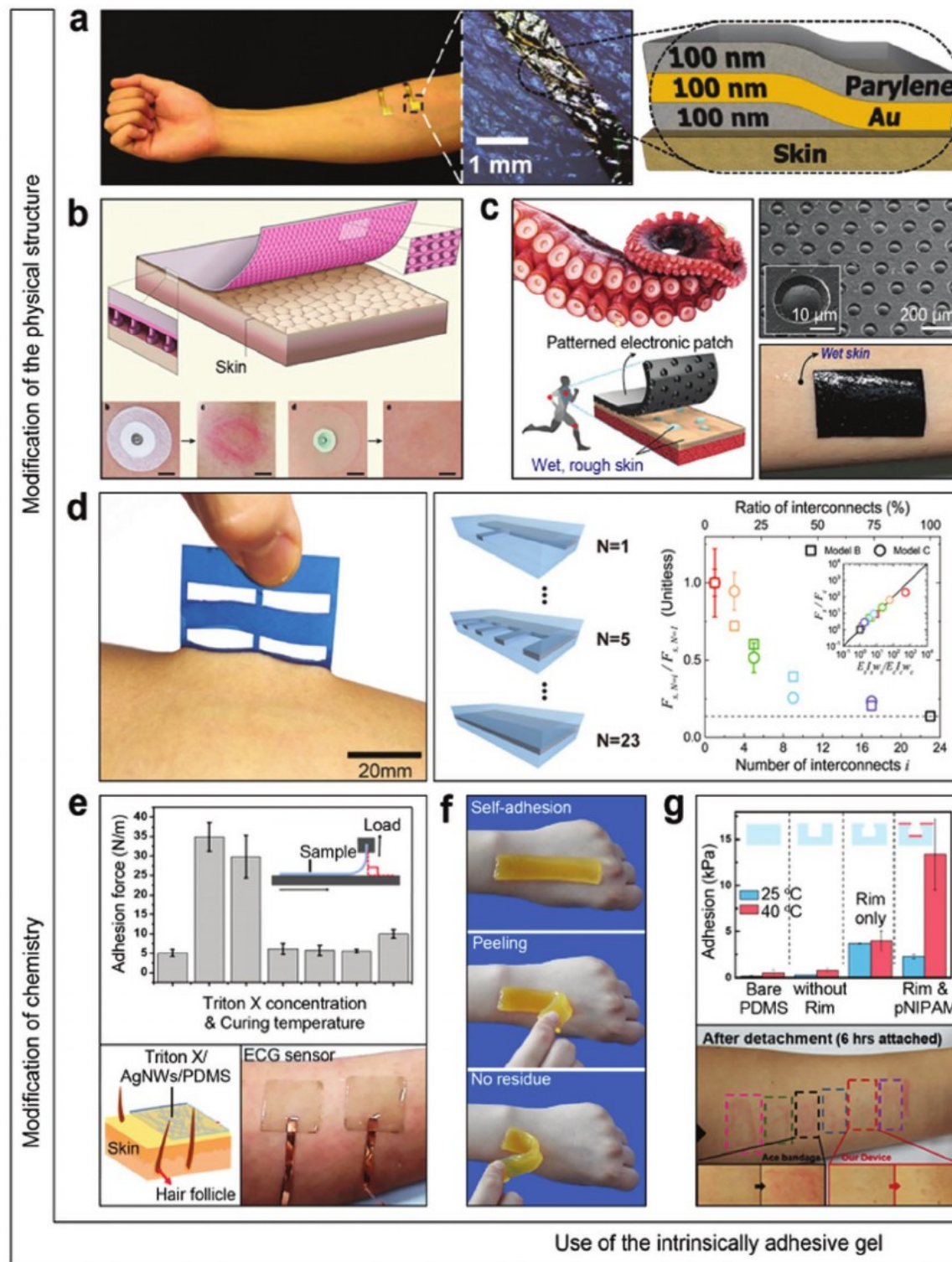


Figure 8. Strategies for enhancing adhesion. a) Downscaling of a metal thin film. Reproduced with permission.^[81] Copyright 2018, Wiley-VCH. b) Micrometer-scale structure for a dry contact onto the skin. Reproduced with permission.^[202] Copyright 2011, Nature Publishing Group. c) Octopus-like patterns imprinted on a carbon-based conductive polymer composite. Reproduced with permission.^[203] Copyright 2018, Wiley-VCH. d) Kirigami-inspired structure (left) and its adhesion force (right) with a varying number of interconnects. Reproduced with permission.^[205] Copyright 2018, American Chemical Society. e) Programmable adhesion force enabled by polar functional groups of Triton X and its use for ECG sensor. Reproduced with permission.^[191] Copyright 2018, American Chemical Society. f) Intrinsically adhesive hydrogel with no residue. Reproduced with permission.^[105] Copyright 2019, Elsevier. g) Octopus-like patterned PDMS coated with hydrogel (pNIPAM). Reproduced with permission.^[212] Copyright 2018, American Chemical Society.

is permeable to water, organic solvents, and small lipophilic molecules, preventing a hermetic seal.^[78] This shortcoming is negligible only if the operational timescale and the target analyte are rationally acceptable such as in a way that was used in a microfluidic channel.^[213] In this case, multilayer coating with an additional polymer, most prominently Parylene that has a low permeability to moisture and a long-term stability, can tune the surface permeability.^[214,215] PI that has high durability and flexibility is also a good candidate. Kim et al. verified that its lower permeability could maintain electrical properties for a longer time than a PDMS-coated electrode in water and saline solutions.^[216] Nonetheless, the synthesis of stretchable polymers that are wholly impermeable to water and oxygen is impossible because their long chains have pores much larger than such small molecules.^[196] Inorganic encapsulation layers that are thin enough to be flexible are attractive alternatives. Thermal SiO₂ (200 nm) together with silicon nitride (SiN_x) (200 nm) bilayer addressed a vulnerability of electronics discovered in harsh environments, allowing a simultaneous impermeability to water and ions.^[217] This methodology is already indispensable for serpentine-patterned electrodes or other components used in wearable devices thus far. Also, the LMs, a new vigorously growing field, also need to be encapsulated because water can change the composition of their surface oxide and weaken a mechanical strength and a breakdown voltage.^[218,219] Wang et al. developed Mg–GaIn materials by mixing Ga-based LM with magnesium (Mg) particles. They utilized the Mg–GaIn LMs in tumor therapy by patterning those electrodes on a flexible paper substrate. The results showed a superior photothermal conversion effect (61.5%).^[220] These paper-based substrates also have unique impermeability to LMs, simplifying fabrication of the fully stretchable electronics.^[13,221]

Another considerate aspect of the permeable feature of WFHE is the breathability that guarantees long-term wearing and tight adhesion of WFHE during times of perspiration. For instance, the substrate materials that have high permeability to water vapor and gas do not block sweat gland ducts, suppressing the potential risks of skin inflammation.^[222] Recent papers demonstrated a successful modulation of selective permeability by controlling the structure of the substrate materials in terms of porosity and its pore size.^[55,223–225] Electrodes made up with graphene, which is known as an impermeable nanosheet,^[226] achieved a high water vapor permeability of 18 mg cm⁻² h⁻¹ in a porous structure combined with porous elastomer sponge, indicating that dimensional pores effectively improve a gas/vapor permeability of the whole composite (Figure 9a).^[98] Those water-wicking electronics comprised of hydrophobic porous graphene/elastomer sponge expedite sweat transportation and water evaporation, thereby minimizing the risks of inflammation. Aside from the substrates, electrodes have also mimicked a porous structure of fabric/textiles by using NWs,^[222,227] vertically aligned 3D electrodes,^[41] and rugged substrates.^[228] Miyamoto et al. fabricated Au nanomesh conductor exhibiting excellent water vapor permeability, which was measured by weight loss of water when the electronics were attached to the opening of a water bottle at 25 °C temperature and 30% humidity (Figure 9b).^[222] The Au layer with a thickness of 70–100 nm deposited on top of mesh-like

electrospun poly(vinyl alcohol) (PVA) (300–500 nm in diameter) had high gas permeability, showing the same rate in the weight loss of water as the bottle without a nanomesh conductor. In the case of 1.4 µm thick PET films and 10 µm thick silicone films, the weight of the bottle barely decreased, or only 23% of the water remained in the bottles after 1 week.

Other than that, selective permeability is of the essence for the functionalization of the materials, which constitute sensing part of the WFHE. As the materials destined for sensors generally have a high surface-to-volume ratio and have a number of chemically activated sites on their surface, they are likely to be accumulated by unwanted molecules and thus turn ineffective over time. To address this problem, ion-selective permeable membranes have been incorporated onto the sensing layer, acting as a barrier as well as enabling the immobilization of essential molecules in it.^[32] Such antifouling layers can prevent the degradation of the sensing materials in high-humidity and salt environments, thereby retaining initial degree of sensing capabilities.^[229–231] As an additional consideration, transdermal drug delivery systems, equipped with therapeutic tips or layers under the WFHE, highly require the selective permeability for vital chemicals to the outer layer of skin (stratum corneum).^[25,232–234]

3.2.5. Water Repellency

WFHE ensure high-accuracy physiological signals only if the device adhered to the skin without hindrance. As mentioned earlier, a stagnant water layer between the device and the skin produces potential drift and even causes skin injury. In this case, modifying the surface energy by a structural or chemical treatment can change the water affinity of the surface of the devices, making them unaffected by water absorption or passage. This offers the possibility of a stable adhesion at the various surfaces and interfaces of WFHE by blocking the water that comes from breathing, sweating, washing, and showering.^[6,54,69,235,236] Moreover, an antifreezing effect induced by superhydrophobicity foresees the use of hydrogel-based WFHE in an extremely cold environment under 0 °C.^[206,210] In this section, we introduce some recent methods to change the water affinity of wearable substrates, along with emerging materials that contribute to the enhancement of the water repellency. Various flexible substrates used in WFHE are typically hydrophobic due to their polymeric nature, making them robustly matched to the human skin that is intrinsically hydrophobic.^[237,238] The examples include silicon rubber, Ecoflex, PDMS, and Parylene (except for PI).^[214] However, PDMS is also well known for its lack of hermeticity to water vapor over time. To address this problem, Reeder et al. reported a sweat sensor that can operate under water and during swimming by using hydrophobic block copolymer, poly(styrene-isoprene-styrene) (SIS), as a microfluidic channel (Figure 9c).^[239] The results demonstrated high-barrier properties of SIS, showing a water mass change (less than 20% for 4 h) lower than that of PDMS (100% within 3 h) at 37 °C. The other reports of the use of a patch-type sweat sensor monitoring cortisol concentrations used polyethylene-based hydrophobic polymer as an outermost waterproof layer.^[63] Li et al. introduced a spontaneous synthesis

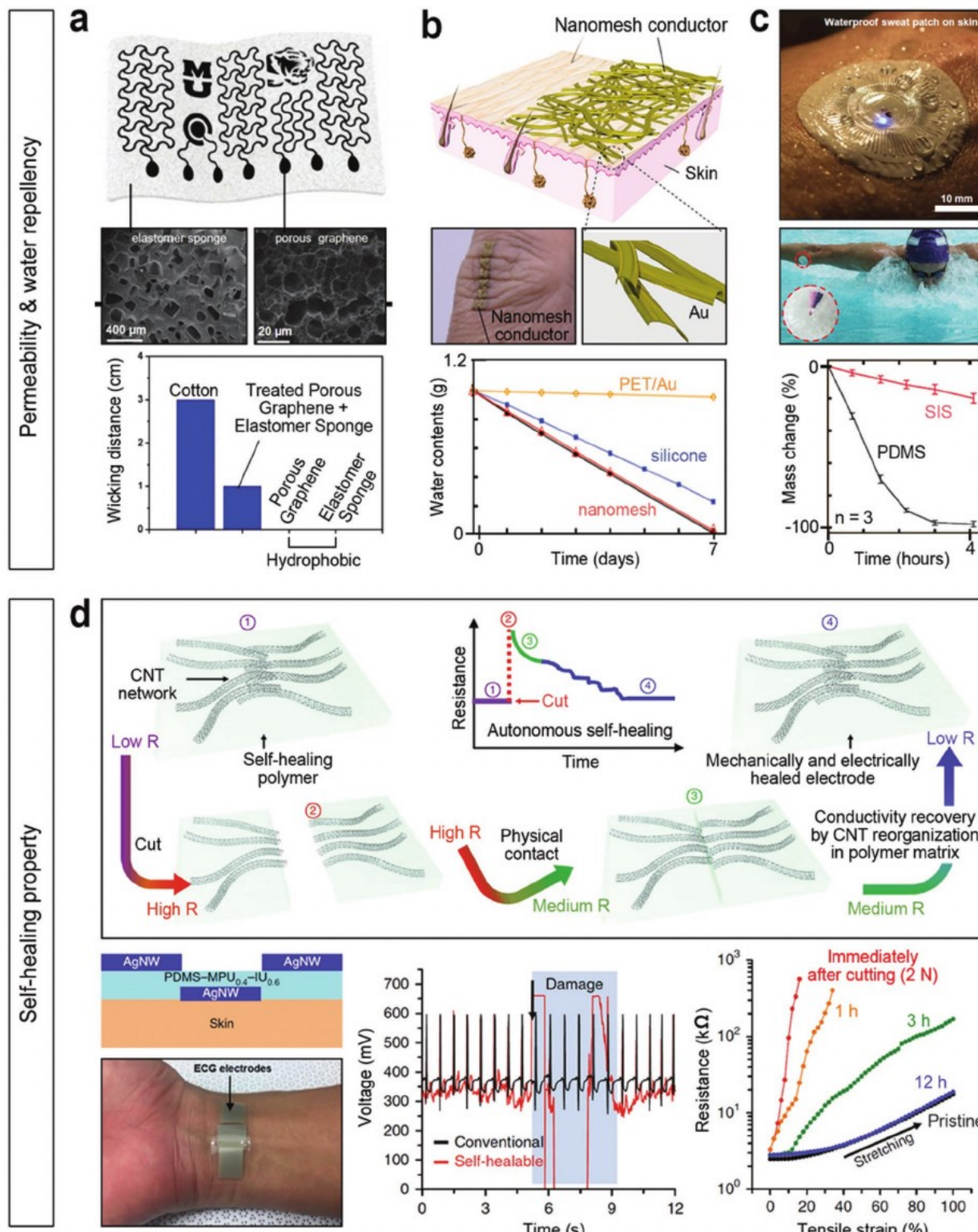


Figure 9. Strategies for enhancing permeability, water repellency, and self-healing capability. a) Strain sensing system using silicone elastomer sponge and porous graphene with low water-wicking distance. Reproduced with permission.^[98] Copyright 2018, Wiley-VCH. b) Au nanomesh electrode mounted on the skin. Reproduced with permission.^[222] Copyright 2017, Nature Publishing Group. c) Waterproof microfluidic sweat sensing system using poly(styrene-isoprene-styrene) and its stable collection and storage of sweat. Reproduced with permission.^[239] Copyright 2019, American Association for the Advancement of Science. d) Proposed recovery mechanism of CNTs embedded in self-healing polymer matrix, self-healable ECG sensor damaged and subsequently recovered in a few seconds, and its resistance after making a cut and self-healing for 12 h. Reproduced with permission.^[132] Copyright 2018, Nature Publishing Group.

of a superhydrophobic and conductive surface by spray coating of multiwalled carbon nanotube (MWCNT) dispersed in a commercial thermoplastic elastomer, which endowed such composites with strain sensing capabilities.^[240] The surface of this MWCNT/elastomer composite ensured its superhydrophobicity (water contact angle >150°) under strain and even after alkali, acid, and UV stresses.

However, making the substrates superhydrophobic inextricably affects the other processes for assembling devices, enhancing sensing performances, especially when WFHE possesses nanocompositing structure. To use hydrophilic nanomaterial as a pillar, the substrates should be treated beforehand to increase the number of hydrophilic functional groups on their surface and this may lead to outer water penetration.^[241,242] Also, the surface charges and hydrophobic property of all the components, such as sensing materials, layouts, and membranes, should be considered in providing the WFHE hybrid functionalities. Specifically, several different areas have deeply discussed such hydrophilic–hydrophobic nature: 1) microfluidic channels, 2) adhesions, 3) newly emerging materials including ionic conductors, and 4) immobilization of biosensors. First, a selective creation of hydrophilic channels has been utilized to flow sweat inside the hydrophobic substrate eliminating the need for external pumps or power supplies. The mechanism is on the basis of not only the capillary action but also the hydrophilicity of particular area. Gao et al. fabricated a flexible 3D nitrocellulose nanopillar array paper that has three different hydrophilic branches used for sweat split-flow microfluidic channels via a stamping–patterning method.^[243] With a view to choosing and engineering materials, the efforts to render the attraction force between two materials have been made to modify their surface affinity either by structure modification,^[244] or chemical treatment. For instance, an extra chemical treatment such as benzophenone treatment can be applied to generate chemical bonds between intrinsically hydrophilic hydrogels and typical flexible surfaces that are hydrophobic.^[14] In adopting fully stretchable electronics, Wang et al. modified the surface of styrene-based block copolymer dielectrics by using octadecyltrimethoxysilane molecules to increase the hydrophobicity, and thereby reduce their interaction with a semiconductor film.^[101] Besides, hydrophobicity of self-healing polymer directly affects the hydrogen bond formation that is responsible for self-healing capabilities.^[102] As for an aerogel, Zhang et al. reported a wearable flexible carbon black aerogel composite that affords its thermal insulation property and thus thermal protection better than cotton fabrics.^[224] This composite showed hydrophobicity and ultrafast oil/water separation capability owing to its abundant methyl groups on the surface and high porosity (93.6%). Furthermore, a recent study showed that the hydrophobic polymer coating method stabilized LM NPs for more than 60 days.^[219] When WFHE are intended to have hybrid functions on drug release, a multilayered film composed of the hydrophilic mesh containing therapeutic agents and hydrophobic encapsulation layers can function to release drugs.^[245] Since the crack propagation is induced by strain due to the mechanical mismatch at the surface, water infiltration and drug release occurred subsequently. In another application, a biochemical sensor exploited a biofouling membrane coated on the surface to limit the accumulation of unwanted materials

on the surface and to pass analyte of interest. In this case, the membrane has a certain degree of hydrophobicity to change interfacial energy,^[229] enable a better orientation of immobilized antibodies,^[246] or prevent the formation of a hydration layer as well as the adhesion of bacteria.^[231,247]

3.2.6. Self-Healing

Autonomous systems, which determine the practical application of WFHE, require great robustness that can last long enough for external environments as well as for the availability of self-powered batteries.^[21] In this regard, certain materials with self-healing effects are of great interest due to their prominent features restoring the original properties, mostly shape, structure, and mechanical/chemical/physical properties, even after damage and cutting.^[248,249] Such effects enhance WFHE durability and reliability, which usually rely on a substrate that makes up the device (>99 wt%), thus maintaining wearable form factors and other functionalities for a longer time.^[96] Based on a representative mechanism, self-healing materials are categorized into two main scopes: dynamic formation of noncovalent (physical) or covalent (chemical) bonding, or utilization of noncovalent bonding of ions.^[250] Since the latter is so soft that it is not enough to have the required mechanical toughness at the processing stage, it mainly utilizes the former, which is mostly based on the hydrogen bonding, hydrophobic interactions, and metal-coordination interactions, dominating the degree of self-healing effect. In this section, we will briefly introduce substrates that have recently been used for self-healing and connected wearable devices. Self-healing efficiency is generally defined as the elongation ratio of the healed and pristine gels. Hydrogels, which are stretchable and conductive because of their inherent large amounts of water and small molecules, have been exploited as substrates for wearable strain sensors by monitoring the changes in resistance.^[103,207] Wang et al. recently demonstrated a ternary polymer composite comprised of polyaniline (PANI), poly(acrylic acid), and phytic acid that shows high stretchability (~500%) without a significant change in the gauge factor between strain sensors, which are the original one and the healed one.^[156] The self-healing efficiency is obtained as ~99% in 24 h, enabled by the dynamic hydrogen bonding and electro-elastic interactions. However, self-healing hydrogel possesses several issues: it relies on conductivity and toughness and suffers from water and low temperature owing to its high water content. To address these problems, efforts to increase toughness,^[153] conductivity,^[197] and water insensitivity^[102,210] have been conducted. In terms of conductivity, compositing graphene oxide (GO) sheets with poly(sodium 4-vinyl-benzenesulfonate-*co*-N-(2-(methacryloyloxy)ethyl)-*N,N*-dimethylbutan-1-aminium bromide) was conducted.^[197] The results showed a high ionic conductivity of 10.5 mS dm⁻¹ with the storage modulus (G') recovered within 80 s after stopping a large strain of 500% (original 2038 Pa; recovered 2042 Pa), which is enabled by multiphysical cross-linking in the hydrogel. Kang et al. reported water-insensitive elastomers with PDMS oligomers (PDMS–MPU_x–IU_{1-x}) linked by MPU as a strong bonding unit and isophorone bisurea units (IU) as weak bonding units. This polymer film is able to have a high

self-healing efficiency of 78% in dry conditions (strain: 1500% after 48 h) while showing a corresponding healing capability in water (strain: 1100% after 24 h), which is unprecedented.^[102] Further research focused on the self-healing chemistry of the reconfigurable electrode part showed a high potential for integrated self-healable electronic skin (Figure 9d).^[132] Compositing conducting nanostructures, CNT, in contact with a dynamically cross-linked polymer network, PDMS–MPU_{0.4}–IU_{0.6}, restored the electrical conductivity after cutting and damage after 12 h. Their stretchable (up to 50% strain without crack propagation) and self-healing features can be used as electrodes in active electronic components, including a fully healable multifunctional electronic skin system with a strain monitor, ECG sensor, and light-emitting capacitor display array by the use of dielectric, AgNW network, and Cu-doped zinc sulfide (ZnS) particles, respectively.

3.3. Biocompatible Properties

3.3.1. Biocompatibility

Considering fully attached WFHE onto the human skin, particular emphasis should be given to nontoxic, nonirritant, and nonallergenic features. The term biocompatibility refers to “the ability of a material to perform with an appropriate host response in a specific situation.”^[251] To date, on the basis for the intuitively obvious fact that WFHE should cause no harm to users by intent or by accidents, researchers have adopted a set of biocompatible materials: passivable alloys (stainless steel, titanium (Ti) alloys), inorganic novel metals (Au, Pt, palladium (Pd)), oxide ceramics (zirconia (ZrO_2), alumina (Al_2O_3)), carbon-based allotropes, stable polymers (silicone elastomer, polyacrylates), etc.^[252] Recently, the more concerns provide several attempts as a means to give hybrid functions above biocompatibility (Figure 10). For instance, Yin et al. used graphene as a soft contact lens due to its biocompatibility, optical transparency, high electrical conductivity, and flexibility (Figure 10a).^[56] These features enabled conformal, full-cornea recording of electroretinography (ERG) from cynomolgus monkeys by using soft graphene as transparent (71.7% at 550 nm) and soft electrodes for ophthalmic diagnostic testing.^[56] These features can allow a uniform illuminance, which is important for high spatial resolution mapping of corneal potential, with more homogeneity compared to the metal-based electrodes used before. When it comes to humans, the meaning of biocompatibility is expanded to the comfortability that users feel. As shown in Figure 10b, Au nanomesh ensures nontoxicity to the body as well as a practical compatibility, providing more possibility of eliminating the inconvenience that participants may feel than conventional silicone and Parylene film, which are considered to be biocompatible.^[222] By contrast, adopting intrinsically nontoxic materials yields the simple processing step and there is no need to cover the device with a multilayered structure, which is usually combined with detachment issues. Using inherent biocompatibility, and also a capability of amplifying received vital signals from the body, organic thin-film transistors bridge the gap between the materials, which cannot be fully biocompatible, and wearable sensors.^[253] In addition,

ionic conducting polymers such as hydrogel and nanofibrils recently attributed to biocompatibility as well as biodegradability (will be discussed in the next section). Wang et al. synthesized tough conductive hydrogels composed of interpenetrating PANI and poly(acrylamide-co-hydroxyethyl methacrylate) networks, which show reliable detection of repeated large strains and subtle vibrations.^[254] The other candidate includes biomimicking nanofibril polymers, such as silk, chitin, and cellulose, which form a hierarchical structure sharing natural biorepetitive sequences.^[107] Recently, biomass material, bacterial cellulose (BC), is reported as flexible, biocompatible, and electrically conductive ($1.0 \times 10^{-3} \text{ S cm}^{-1}$) fibers for wearable health monitor applications (Figure 10c).^[255] The film made a simple structure, called nanochannel, with a 3D interconnected network of 10–30 nm thick BC NFs containing 1–2 nm nanochannels. This biocompatible nanofluidic device was engineered with charge selectivity that was enabled with a large negatively charged surface group (zeta potential = -45 mV) and high ionic conductivity ($1.0 \times 10^{-3} \text{ S cm}^{-1}$) by oxidation with 2,2,6,6-tetramethylpiperidine-1-oxyl radical. After integration of fully cured PDMS, a flexible humidity sensor detected 40–80% relative humidity (RH) by electrochemical impedance spectroscopy measurement at 37 °C on the basis of the change in the ionic resistance of the BC film. The other application includes wearable high-performance piezoelectric generator. A recent study changed the conventionally used lead zirconate titanate, which is undesirable due to the presence of toxic lead (Pb), to a biocompatible group III nitride thin film.^[256] This flexible harvester generates an open-circuit voltage of 50 V and a maximum power of 167 μW, which can charge a commercial battery system to operate an optical pulse sensor. Nonetheless, the regulation including preclinical testing is still only conducted on the materials, not the devices that have many passive and active components.^[252] Above this regulation, encapsulating strategies introduced the concept of covering the whole device with biocompatible materials, so that the device or newly developed material can act as biocompatible and functional electronics. These attempts have continued thus far, and examples include LM/Ecoflex,^[151] LM/PU,^[257] or WFHE/PDMS.^[69] Furthermore, the biocompatible performance follows the rule of not having toxic or injurious effects that trigger the body's immune response, so that the use of gel-free dry adhesives should be concerned as mentioned earlier.^[202]

3.3.2. Bioresorbability

Beyond biocompatibility, bioresorbable electronics, which is classified as a branch of transient electronics, eliminates environmental, chemical, and physical damages in a way that the constituent materials dissolve, disintegrate, or decompose without environmental and toxic residue after using the electronics.^[19] Since this concept was first introduced in 2009, attempts have been made to integrate such biocompatible materials composing substrates, electrodes, dielectrics, and encapsulation layers into wearable and flexible electronics.^[258] Studies to date are mainly applied to implantable electronics while immersing in water or biofluids to hydrate and form harmless by-products in the human body after a biologically relevant

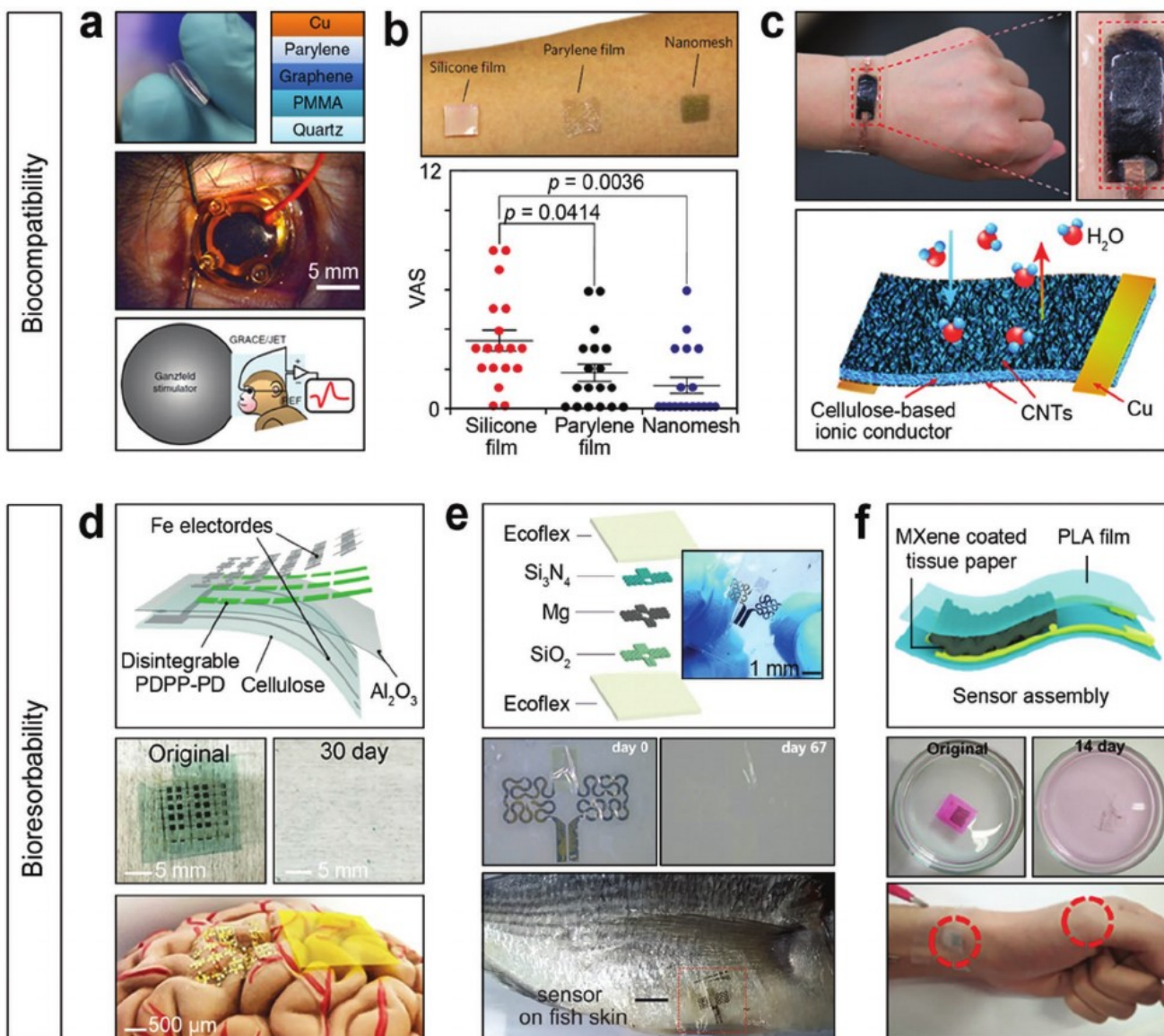


Figure 10. Strategies for enhancing biocompatibility and bioresorbability. a) Soft graphene-based contact lens for recording of ERG from cynomolgus monkeys. Reproduced with permission.^[56] Copyright 2018, Nature Publishing Group. b) Films of silicone, Parylene, and Au nanomesh conductors attached to the forearm and measured discomfort reported by participants. Reproduced with permission.^[222] Copyright 2017, Nature Publishing Group. c) Humidity sensor using bacterial cellulose embedded in PDMS band. Reproduced with permission.^[255] Copyright 2018, American Chemical Society. d) CMOS device mounted on a human brain model. Reproduced with permission.^[263] Copyright 2017, National Academy of Sciences. e) Temperature sensor for the internet of things (fish skin). Reproduced with permission.^[264] Copyright 2017, Wiley-VCH. f) A dissolvable pressure sensor and its application on the human wrist and palm. Reproduced with permission.^[265] Copyright 2019, American Chemical Society.

period. As such, in WFHE, they may circumvent the need to consider long-term complications associated with detachment processes. Recent reviews show a comprehensive understanding of materials and processes.^[19,259] Therefore, in this section, we instead introduce more recent attempts made to provide the ultimate solution associated with biocompatibility as a means to apply in WFHE. Bioresorbable materials can be classified into nanomembrane or porous Si^[262] metals (Mg, Zn, Fe, tungsten (W), Mo, and their alloys), inorganics (SiO₂, SiN_x, magnesium oxide (MgO)), synthetic polymers (PVA, PVP, polycaprolactone, poly(lactic acid), poly(lactic-co-glycolic acid), poly(1,8-octanediol-co-citrate)), and natural/nature-derived

polymers (silk, cellulose, sodium alginate) as the basis for electrode, substrate, and functional features, including dielectric property.^[260,261] The dissolution rate, which refers to the degree of the bioresorbability, is expressed by the unit of $\mu\text{m h}^{-1}$ or mg h^{-1} in a representative biofluid (Hank's solution)^[259] or deionized water at room temperature. The rate is highly dependent on the morphology and chemistry of materials and the composition and temperature of the solution. Lei et al. developed totally disintegrable and biocompatible CMOS flexible circuits by integrating conjugated polymers that consist of reversible imine bonds that were decomposed under mild acidic conditions, biodegradable cellulose substrate, Al₂O₃, and

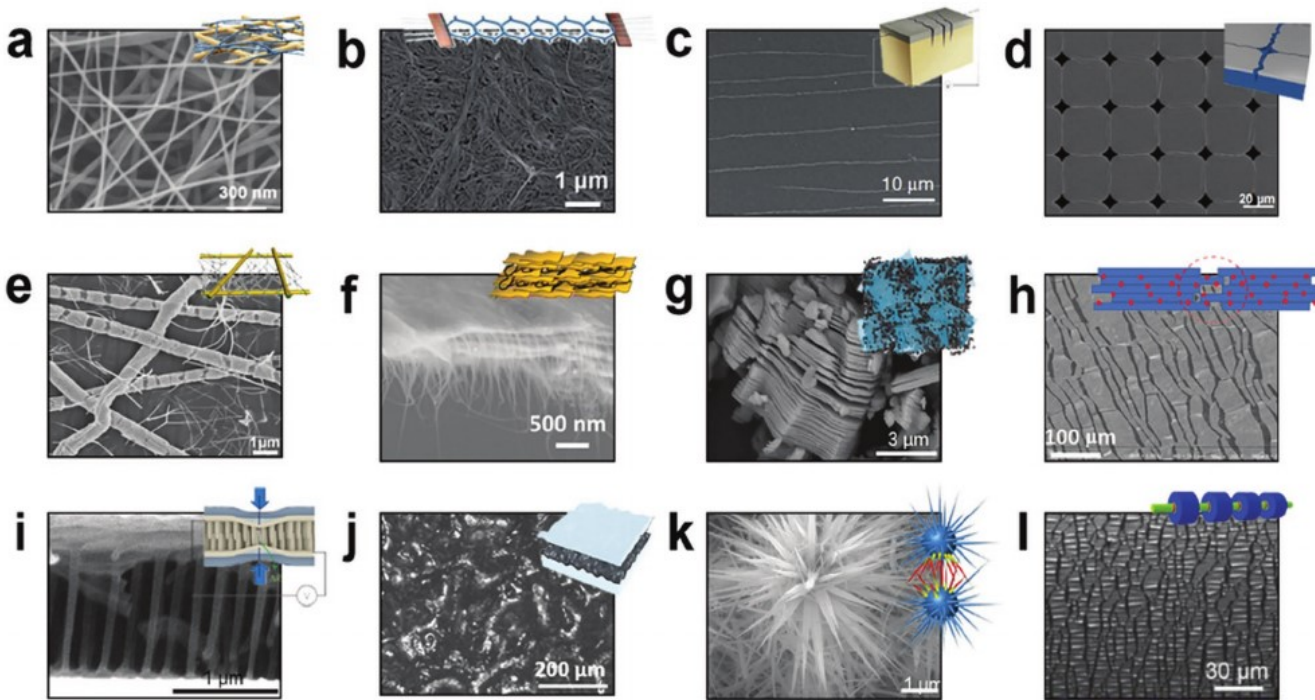


Figure 11. Strategies for improving electrical conductivity under mechanical strains. a) Scaffold-reinforced nanonetwork using AuNWs and PA NFs. Reproduced with permission.^[184] Copyright 2018, American Chemical Society. b) Kirigami-inspired MnO₂ nanowire/CNT composites. Reproduced with permission.^[129] Copyright 2018, Wiley-VCH. c) Spider-sensory-system-inspired Pt on a PUA structure. Reproduced with permission.^[280] Copyright 2014, Nature Publishing Group. d) Hole-patterned C-polyurethane acrylate with uniform guided crack. Reproduced with permission.^[281] Copyright 2017, Nature Publishing Group. e) AuNW–AgNW hybrid networks on a PDMS substrate. Reproduced with permission.^[135] Copyright 2018, Wiley-VCH. f) 1D–2D Ti₃C₂T_x MXene/CNT percolation network composite structure. Reproduced with permission.^[282] Copyright 2018, American Chemical Society. g) 0D–2D Ti₃C₂T_x MXene hybrid network. Reproduced with permission.^[283] Copyright 2018, Wiley-VCH. h) 0D–1D–2D ternary nanocomposite structure using fullerene, GO, and AgNWs. Reproduced with permission.^[139] Copyright 2018, American Chemical Society. i) Pt/PDMS nanohair interlocking structure. Reproduced with permission.^[284] Copyright 2012, Nature Publishing Group. j) Epidermis-microstructure-inspired rGO/PDMS interlocking structure. Reproduced with permission.^[285] Copyright 2018, American Chemical Society. k) Sea-urchin-inspired ZnO NP interlocking structure. Reproduced with permission.^[286] Copyright 2018, Nature Publishing Group. l) Fiber-shaped Au/PDMS with beads. Reproduced with permission.^[165] Copyright 2018, Wiley-VCH.

Fe electrodes (Figure 10d).^[263] The degradation speed was controlled with decomposable encapsulation materials. Salvatore et al. demonstrated a wireless flexible temperature sensor, which was designed for food tracking and composed of a bioresorbable electrode (Mg) encapsulated by thin layers of Si₃N₄, SiO₂, and Ecoflex elastomer (Figure 10e).^[264] The measured resistance showed an accuracy of 0.2% variation at 10% strain for about 1 day, in which the thickness of Ecoflex can change the timescales for use. More recently, a wearable transient pressure sensor made with porous MXene nanosheet paper was fabricated by sandwiching between biodegradable PLA, which functions as a substrate as well as an encapsulation layer (Figure 10f).^[265] Such sensor exhibits a low detection limit (10.2 Pa) and low power consumption (10^{-8} W) over 10 000 cycles. The study for degradable performance demonstrated that the sensor was degraded after 14 days in phosphate-buffered saline solution (23%) and 0.5 M sodium hydroxide (NaOH) solution (68%) at 37 °C, not causing any harm to the environment. Besides wearables, implantable devices are an undoubtedly compelling area that takes advantage of biocompatibility.^[106] Moreover, flexible and biocompatible energy devices can help the practical use of WFHE. For example, the combination of a water-soluble Mo wire, PVA-based biodegradable polymer electrolyte, and a biodegradable elastomer has been used as a supercapacitor

(strain: 50%; dissolution rate: 5.4 mg h⁻² in 2 h; power density: 0.8 mW cm⁻²).^[266] Also, recent papers have utilized a variety of biodegradable power sources from batteries based on Mg/silk fibroin-ionic liquid polymer electrolyte^[267] to radiofrequency energy harvester with a Mg antenna,^[268] Si photovoltaic microcells,^[269] and triboelectric nanogenerator.^[270,271]

3.4. Electrical Properties

3.4.1. Conductivity

The various methods for developing WFHE are mostly aimed at improving their sensing capability and relevant performance. Their electrical conductivity should be reliable under high strain over time while the device detects vital signals seamlessly without any degradation from the effects of external environments and shows programmable change by structural deformation (i.e., a gauge factor). The challenges of functional nanocomposites as strain sensors are undergoing unpredictable changes in mechanical and electrical properties associated with the irrevocable collapse of the structure. In this section (Figure 11), we explore the electrical properties of recently published materials and structures accepted as

a promising electrode with high flexibility, stability, and the like. Ag is the most powerful electrode when it is used as an electrode for wearable electronics because of its high conductivity and processability.^[180,272] Scaffold-reinforced conductive network using AgNWs and PA NFs showed a stable resistance under bending for 3000 cycles at maximum curvature of 300 m⁻¹ ($\Delta R < 0.1\%$) and under saline solution for 2500 cycles ($\Delta R < 1.5\%$) (Figure 11a). Cu, the more cost-effective and conductive metal, was also used as an electrode material. Kwon et al. recently reported a Cu electrode with a high conductivity of 43 478 000 S m⁻¹ via inkjet printing followed by an intense pulsed light sintering method.^[242] These low-cost and highly conductive electrode arrays were mounted on a soft membrane with a PI encapsulation layer, enabling the detection of physiological signals such as electrooculogram (EOG), EMG, and ECG. Currently, an LM is of great interest in terms of its intrinsic liquid-like feature and thus high conductivity over high strain combined with the scalable printing processes. Examples include screen-printed Ga alloys with an electrical conductivity of 3 800 000 S m⁻¹ at a strain of 1000%,^[257] and direct laser written eutectic gallium–indium (GaIn) alloys (564 970 S m⁻¹) with strain limit of >100%.^[152] Composites consisting of diverse functional nanomaterials and stretchable polymers can also have a range of conductivity depending on their architectures. The kirigami-inspired film was used for obtaining electrical or capacitive stability under a high strain (Figure 11b).^[129] In this manner, kirigami-patterned AgNWs/Parylene hybrid electrodes with a sheet resistance of 2.24 Ω sq⁻¹ (stable after 60 days) were used as a wearable stretchable humidity sensor, enabled by a linear correlation between conductance and humidity.^[131] In carbon-based composites, graphene nanosheets served as a highly conductive enhancer, achieving a conductivity of 61 000 S m⁻¹ compared to those from CNT/cross-linked PH1000 film without graphene (9600 S m⁻¹).^[273] Another report achieved a high conductivity of 331 600 S m⁻¹ at 100% tensile strain by incorporating 3.2 μm long CNT into a PDMS substrate.^[189] On the basis of the high electrical conductivity and transparency, graphene exploited itself as a wearable lens with Cu, showing great sheet resistances of 850–1520 Ω sq⁻¹.^[56] To increase the conductivity of composites, novel metal can be additionally added to enhance electrical transport ability mostly at the interfaces. Xu et al. demonstrated the use of a freestanding metal mesh for a foldable supercapacitor electrode with a high conductivity (400 000 S m⁻¹), high areal capacitance (268 mF cm⁻²), and long cycling life (capacitive retention of 90.1%; 10 000 cycles) by forming AuNPs and active manganese dioxide (MnO₂) microstructures on the nickel (Ni) mesh via two-step electrodeposition.^[274] This mesh structure also shows effective features such as ultralight weight, high optical transparency, and high air permeability, providing high potential toward the next wearable electronics. Conducting polymers are flexible but have an intrinsic conductivity lower than 55 000 S m⁻¹. Wen et al. reported that when the conducting polymer poly(3,4-ethylenedioxythiophene):poly(styrene sulfonate) (PEDOT:PSS) was deposited onto the prestrained platform, its wrinkled structure decreased the original resistivity of 22.90 kΩ sq⁻¹ (flat structure; 100% strain) to 1.40–4.63 kΩ sq⁻¹ (0–100% strain), which can be effectively used for wearable triboelectric nanogenerators.^[275] The other report showed that dimethyl sulfoxide doping can

increase the conductivity of PEDOT:PSS film (60 000 S m⁻¹), which partly ensured a high gauge factor, providing the wearable strain sensor with small R_0 .^[276] The other examples of ionic conductors include hydrogels and nanofibrils, whose conductivities are dependent on the concentration of ion charge carrier of ionic conductors. A typical conductivity of hydrogel (100 S m⁻¹) decreased to 10 S m⁻¹ by controlling moles per liter of ions.^[196] When the hydrogel was dispersed with graphene oxide sheets, the ionic conductivity was 0.1 S m⁻¹, which was calculated according to $\sigma = l/RS$, where l is the thickness of the gel, R is the bulk resistance that was obtained from the complex impedance diagram, and S is the contact area between hydrogel and Cu plates.^[197] A biodegradable silk fibroin showed low sheet resistance (10.5 Ω sq⁻¹) and a good extensibility up to 60% strain, yet the value slightly increased to 11 Ω sq⁻¹ with stretching above 80%.^[110]

3.4.2. Gauge Factor (GF)

The use of strain and pressure sensors is likely to be the most prevalent means of monitoring physiological signals. To monitor a user's heart rate, heart pressure, body motion, and other signals produced from the body, such sensors can operate in conjunction with a resistive or capacitive mechanism, regardless of whether the deformation degree is negligible or considerable. Their capabilities are well known to be quantitatively assessed by gauge factor, which refers to the ratio between resistance and the induced strain. GF provides an opportunity for researchers to sense the interconnection between mechanical and electrical properties. This term can help link the two major requirements for such wearable sensors that are in demand: 1) high stretchability that is based on the mechanical property itself and 2) high sensitivity that is derived from the changes in its electrical properties. Nevertheless, the contradictory relationship between stretchability and sensitivity has been clearly proved thus far because they operate in different strain ranges. Specifically, high stretchability requires that the WFHE remain morphologically intact despite large strains, while high sensitivity needs a detectable structural change under even the tiniest of strains.^[277] Indeed, the most urgent concern is to search for new materials, designs, or methodologies to examine some trade-off points between mechanical and electrical properties; at present, the achievement of both high stretchability ($\varepsilon \geq 100\%$) and high sensitivity ($GF \geq 50$) is challenging.^[277] In this section, we organized recent papers by how they improve the stretchability and gauge factor simultaneously (the more sensor-related categorization will be given in Section 4). The GF associated with piezoresistive mechanism can be expressed by the following equation:

$$GF = \frac{\Delta R/R}{\varepsilon} = (1 + 2\nu) + \frac{\Delta\rho/\rho}{\varepsilon} \quad (5)$$

where R and ΔR are the initial resistance and the change in resistance, respectively, ε is the applied strain, ν is the Poisson's ratio, and ρ and $\Delta\rho$ are the initial resistivity and the change in resistivity, respectively. Given that the resistivity effect ($\Delta\rho/\rho$) in semiconductors is much larger than that in metals (up to

100 times), semiconducting materials have more promise than thin-film metals ($GF \approx 2$).^[278] Nonetheless, a crack-driven sensor can enhance the GF of metal films.^[279] Kang et al. demonstrated crack-shaped sensor of 20 nm thick Pt on 10 μm thick poly(urethane acrylate) (PUA) with a GF of over 2000 at strains of 0–2% inspired by the geometry of a spider's slit organ, which senses extremely small variations in mechanical stress using crack-shaped slit organs (Figure 11c).^[280] More recently, such mechanical crack-based sensors were producing free cracks via coating the same material in the same thickness on 100 μm PUA with a guided straight crack, resulting in a programmable resistance against the strain (Figure 11d).^[281] This structure demonstrated high sensitivity to strain ($GF = 20\,00\,000$ at strains of 0–10%). These results, large GFs in the small strain range, can be useful for detecting subtle changes from the body. When the pressure or strain applied from the outside is large, compositing conductive materials within a soft substrate is mainly used. In this case, the change in resistance is more influenced by the carrier conduction between the materials than the intrinsic property of the material. The truly successful examples include a nanomaterial-based sensor. NW-based composites composed of AuNWs and small-sized AgNWs showed high GFs from 12 at 5% to 2360 at 70% with prominent cyclic stability up to 1000 times (Figure 11e).^[135] Note that, unlike the similar structure (AuNWs scaffolded within PA NFs; Figure 11a) showing high electrical conductivity,^[184] small-sized AgNW network demonstrated high sensitivity in a range up to 90% strain with AuNWs, which has a continuous backbone network bridging the detached AgNW regions. Likewise, binary nanocomposites with strain-sensitive materials have been studied widely; among them, the 2D materials are in the spotlight to develop strain sensors with both large strain range and high gauge factor. By adopting MXene, which is highly conductive, mechanically robust, low-cost, and controllable 2D transition metal carbide or carbonitride, nanocomposites comprised of 1D CNTs–2D titanium carbide ($\text{Ti}_3\text{C}_2\text{T}_x$) (a typical MXene material) and 0D $\text{Ti}_3\text{C}_2\text{T}_x$ NPs–2D $\text{Ti}_3\text{C}_2\text{T}_x$ sheet showed high GF of 772.6 with tunable strain range of 30–130% (Figure 11f) and $GF > 178.4$ over the full broad range of 0–53% (Figure 11g), respectively.^[282,283] Shi et al. reported ternary-nanocomposite-based strain sensor composed of 0D fullerene, 1D AgNWs, and 2D GO that offered lubricity, high electrical conductivity, and brittle layered structure, respectively, resulting in GF of 2392.9 at 62% strain (Figure 11h).^[139] Based on micro- and nanoscale dimensions, engineering the sensing materials by designing in interlocked arrays with biomimicked geometries can greatly improve the GF as well as repeatability of the strain sensors. Since Pang et al. presented an architecture of interlocked Pt-coated polymeric NFs with high aspect ratios reversibly showing GF of 11.45 with reproducibility up to 10 000 cycles (Figure 11i),^[284] bioinspired structures such as epidermis–dermis (Figure 11j) and sea-urchin-shaped microparticles (Figure 11k) provided the ultimate solution.^[285,286] One example of such bioinspired bristled microparticles using zinc oxide (ZnO) microparticles that have spherically distributed, high aspect ratio, and high-density nanostructured spines rendered the composite showing a strain GF of >10 000 up to 80% strain and cyclability >2000.^[286] Other than that, fiber-shaped micrometer fiber that can likely be used for stretchable strain

sensors on the human body was also reported (Figure 11l). Liu and coworkers reported a surface strain redistribution strategy by fabricating Ag/PDMS elastic fibers modified with intrinsic microbeads. The resulting structure showed a linear strain range up to 120% with GF of 9–25 that can be modified by changing the bead diameter to 250–550 μm . Furthermore, this sensor showed high scalability up to 5000 strain cycles at 30% strain, enabled by microcracks on the surface of the stretchable Au film rendering the whole fibers still conductive under the large mechanical deformation.^[165]

3.5. Device Properties

3.5.1. Scalability

Ongoing efforts in the field of WFHE now focus on leading to practical implementation in everyday life. However, most of the processes require lithography, vacuum deposition, and high-cost materials. Progress in the processing steps to overcome this challenge is based on solution-synthesized materials and diverse printing methods. In this section (Figure 12), the conversion of methodologies from the conventional processes into the large-scale and cost-effective strategies is explored. As a means to decrease the cost of the conventional system, Kim et al. presented a modularized manufacturing process for solderable sensing systems based on nickel–vanadium and Au pad metal layers and Cu interconnection.^[287] Unlike previous manufacturing methods, the excellent solderability of the sensing systems with large-area adhesives enables manufacturing of stretchable electronics on a large scale. However, the aforementioned challenges to production of these WFHE persisted. Solution-synthesized functional substrates or nanomaterials provide the breakthrough that addresses these issues and also obtains the desired properties.^[68,165] One example is the use of electrodeless deposition, which does not require external power sources or vacuum deposition processes to develop desired electrode system; the active areas, mainly onto the electrodes, were deposited with Cu (conductivity: $1.75\ \Omega\ \text{sq}^{-1}$) and applied for skin-attachable physiological pressure sensor with sensitivity of $2.22\ \text{kPa}^{-1}$.^[288] Wu et al. reported, using a hydro-thermal method, the piezoelectric selenium (t-Se) NWs stacked with PDMS and Ag electrode, integrated into wearable self-powered nanogenerator (maximum power: $0.135\ \text{nW cm}^{-2}$), which withstands tensile strength of 1.78 MPa along with a maximum strain of 200%.^[68] In addition, attempts to form LM on flexible substrates using screen-printing techniques have sped up a real-life application of this quite new area of development. Tang et al. fabricated scalable metal–polymer conductors by providing the basis of Ga alloys LM dispersed with a large quantity (>20 mL) in a polymer solution, and then printed onto the different substrates, such as silicon, PU, and PDMS films. Such remarkable fluidity of solution-based ink helps the metal, carbon, LM electrode,^[152,289,290] inorganic semiconductors,^[24,291] and even etched substrate^[292] to be formed by laser writing, bar coating, inkjet printing, and further roll-to-roll printing method. Recently, a large-area strain sensor with high GF (4000) and great stability (over 4500 cycles) was obtained via an all-inkjet printing method (Figure 12a).^[293] A microcracked Ag film was

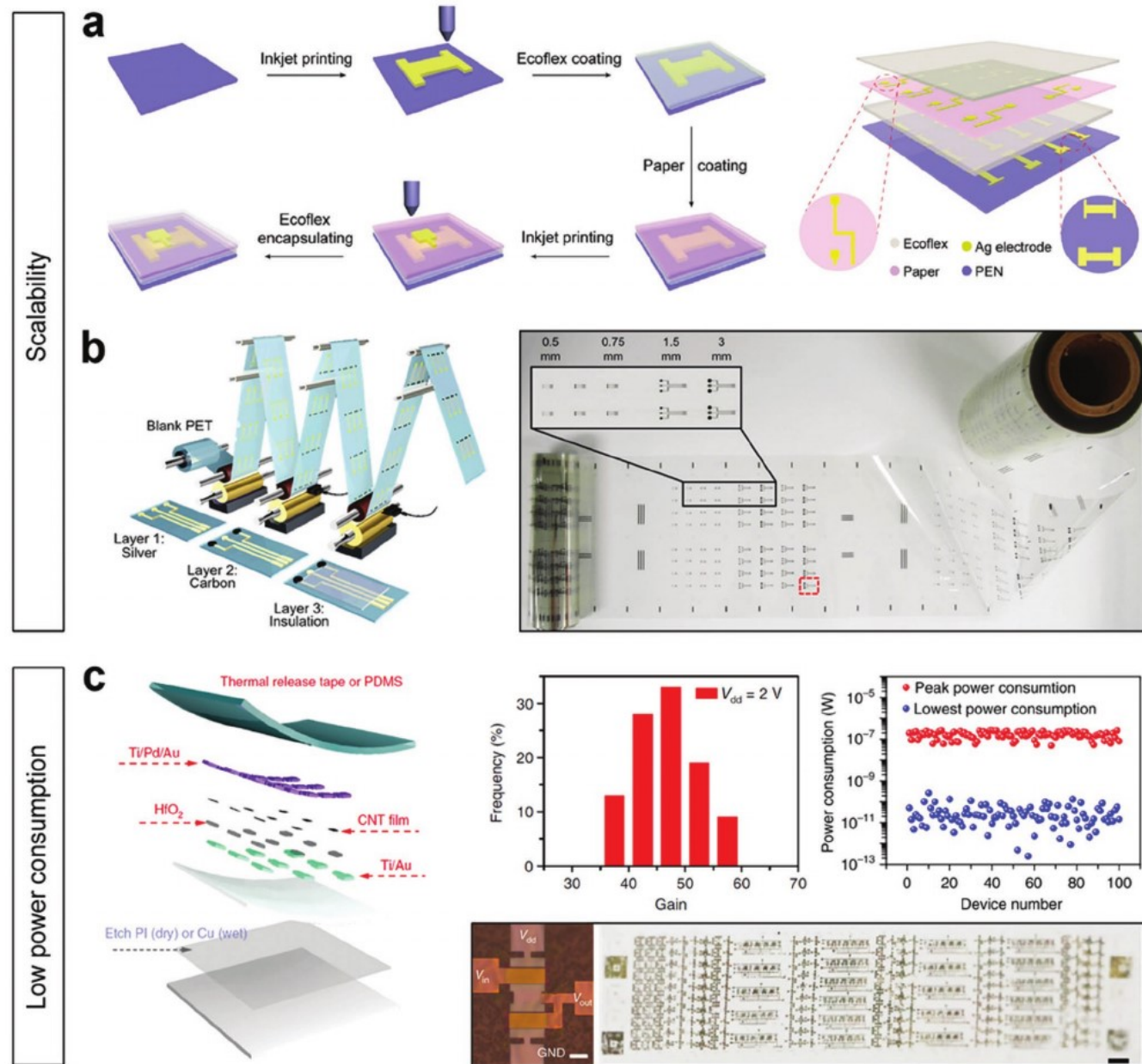


Figure 12. Strategies for enhanced scalability and low-power electronics. a) Schematic diagram of all-inkjet-printed bimodal sensor and circuit for detecting human motion. Reproduced with permission.^[293] Copyright 2019, Wiley-VCH. b) Roll-to-roll gravure printed biocompatible electrodes on a flexible PET substrate. Reproduced with permission.^[289] Copyright 2018, American Chemical Society. c) Low-power CNT-based integrated circuits that can be transferred onto a wrist and driven by a small single supply voltage of 2 V. Reproduced with permission.^[299] Copyright 2018, Nature Publishing Group.

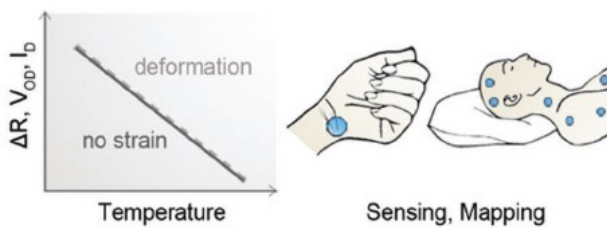
sandwiched by capacitor combined with PEN film, Ecoflex, and paper, as a flexible and hydrophilic substrate, encapsulating layer, and soaking layer, respectively. Consequently, the sensing array containing 4×4 pixels was obtained via maskless inkjet printing, enabling the spatial mapping of strain and pressure distribution. The printing strategy demonstrated an important attribute of large-scale production capabilities, which can go further to roll-to-roll process. The conventional three-electrode system electrochemical sensors can change their process by adopting 150 m flexible PET substrate rolls (width: 250 mm; thickness: 100 μm) (Figure 12b).^[289] Various functionalized

sensors where the working electrodes are Ag and carbon and those with stabilizing or selective layers were evaluated to monitor pH, K^+ , Na^+ , glucose, Cu^{2+} , and caffeine.

3.5.2. Low Power Consumption

Rapid advances in WFHE have improved the efficiency of mechanical, physicochemical, biocompatible, and electrical performance. By adopting a low-cost and large-scale production method, it is likely to integrate the powerful wearable flexible devices

a. Temperature Sensors



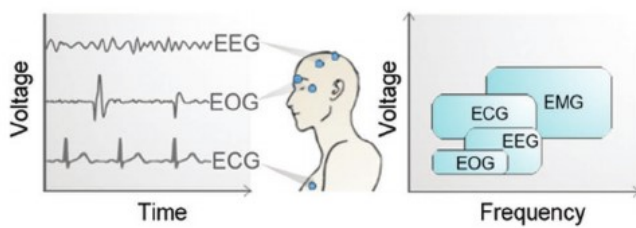
Types

thermoresistive; pyroelectric; thermoelectric, TFTs, etc.

Range at least 25–40 °C (body temperature)

Accuracy down to 0.1 °C; 0.01 °C (clinical consideration)

b. Electrophysiological Sensors

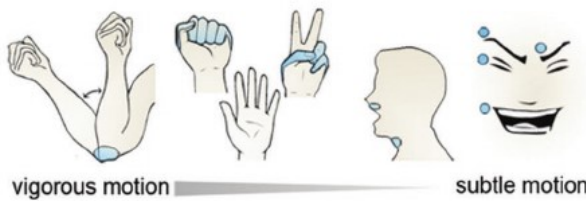
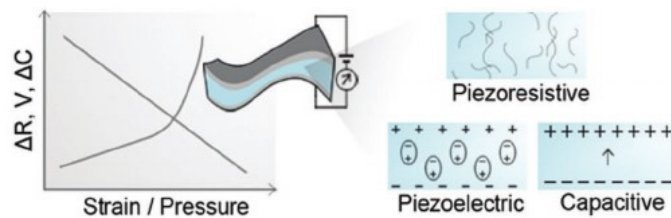


Purpose monitoring bioelectric signals

Types ECG, EOG, EEG, EMG, etc.

Range from 10^{-6} to almost 1 V; from 1 Hz to 10 kHz

c. Strain and Pressure Sensors



Strain Sensor

Purpose monitoring deformation produced by human-body motion

Types piezoresistive, piezoelectric, capacitive, etc.

Range at least 0.1–100 % strain (human body deformation)

Pressure Sensor

Purpose monitoring pressure produced by human-body motion

Types piezoresistive, piezoelectric, capacitive, etc.

Range < 10 kPa (low); < 100 kPa (medium); > 100 kPa (high)

Figure 13. a–c) Summarized description, mechanisms, types, and signal characteristics of temperature sensors (a), electrophysiological sensors (b), and strain and pressure sensors (c) in WFHE.

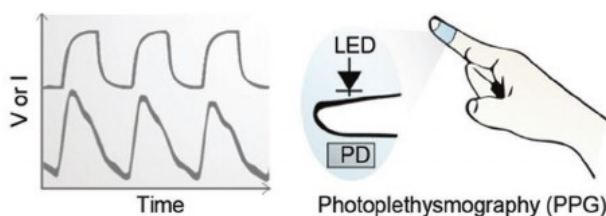
into everyday life. However, the power source that is needed to operate the whole electronics, combined with the sensor, battery, and wireless system, still presents a challenge. The adoption of a fully autonomous system and the related technologies in high-efficiency setting is continually growing, while offering either low power consumption or self-powered energy harvesting. Regarding low-power devices, their performance is dependent on the battery capability, including capacity, flexibility, and so on.^[294] On the other hand, the source of self-powered energy harvesting system is on the body, which includes temperature, strain, and pressure. To maximize the efficiency, these devices are required to have not only high energy capacity but also intimate and conformal contact on the skin.^[130,131] Details of progress and challenges of self-powered systems are described in Section 5.

When conventional batteries are applied in WFHE, the issue of power consumption is a challenge because WFHE require small, thin, and flexible form factors that hardly offer a sufficient area for the large and hard battery system.^[295] Furthermore, high barrier encapsulation is inevitable in materials that are sensitive to air and moisture environments. To solve these problems, two representative materials have recently been applied to WFHE and are being actively studied. One strategy is using organic diodes and transistors,^[296,297] and the other is using

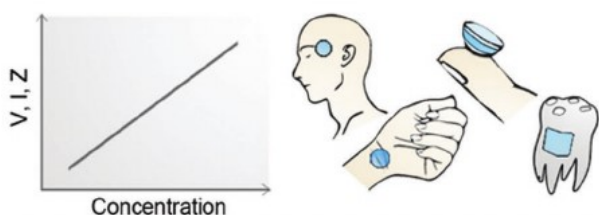
nanomaterials.^[298,299] Xiang et al. reported a flexible substrate driven by a single supply voltage of 2 V by CNT-based TFTs on a biodegradable PVA substrate via the dip-coating method (Figure 12c).^[299] After the formation of gate, source, and drain electrodes (Ti/Au, Ti/Pd/Au), dielectrics (hafnium dioxide (HfO_2)), hexamethyldisilazane (HMDS), and passivation layer (HMDS), the results show a static power consumption of 2.5×10^{-13} W. The development of nanomaterial-based power system is promising in this respect. More recently, MoS₂ has been used for triboiontronic transistors instead of an external gate voltage, which forms electrical double layers in the ion-gel dielectric layer owing to the prompt and strong accumulation of ions and charge carriers at the interface. In this manner, a low-power-consuming performance achieved the desired gain (8.3 V mm^{-1}).^[298]

4. Sensor Capability

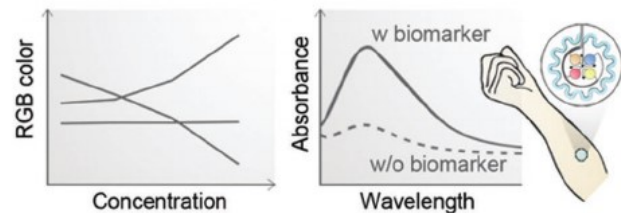
In this section, we summarize various types of wearable sensors that utilize the required properties (described in the previous sections) to develop WFHE (Figures 13 and 14). For those sensors, we describe the details of key applications, sensor types, and required sensitivity and sensing range (Table 2).

a. Optical Sensors

Method	detecting changes in light scattering/absorption through skin [collected by a photodetector (PD)]
Types	photoconductive, photogating, photovoltaic, etc.
Range	from UV into near infrared (depending on penetration depth)

b. Electrochemical Sensors

Method	real-time monitoring of the concentration and its changes of various types of ions, molecules, etc.
Types	potentiometry, amperometry, voltammetry, etc.
Target	sweat, saliva, tear, etc.

c. Colorimetric Chemical Sensors

Purpose/Method	monitoring colorimetric changes of sensitive reagents via direct interactions with the biomarker without localized electronics and detectors
-----------------------	--

Figure 14. a–c) Summarized description, mechanisms, types, and signal characteristics of optical sensors (a), electrochemical sensors (b), and colorimetric chemical sensors (c) in WFHE.

4.1. Temperature Sensors

Body temperature is one of the key indicators to detect abnormal signs in human health monitoring and to provide medical diagnostics and it is frequently measured by thermometers, but the conventional periodic measurement cannot track

acute vital changes. Wearable temperature sensors (Figure 13a), conformally mounted on skins, enable continuous temperature monitoring with capability of real-time mapping applicable from inpatient service to home care, which should provide high sensitivity, fast response, good repeatability, long-term stability, and skin compatibility. The wearable temperature sensor devices should function in the temperature range from 25 to 40 °C in high accuracy with clinically desired resolution of 0.01 °C. Light weight and small form factor are also required. Most wearable temperature sensors are in operation by detecting the change of electrical characteristics of sensor components such as reduced graphene oxide (rGO) as a thermistor. Trung et al. demonstrated a 70% stretchable temperature sensor with sensitivity of $1.34\text{ }\mu\text{V}^{\text{-1}}$ and minute detection resolution ($0.2\text{ }^{\circ}\text{C}$) based on transparent rGO onto PU matrix.^[300] A resistance temperature detector (RTD) integrated into near-field communication (NFC) chip showed fast response with lower thermal mass per unit area ($48.1\text{ }\mu\text{J mm}^{-2}\text{ K}^{-1}$) compared to human skin ($380\text{ }\mu\text{J mm}^{-2}\text{ K}^{-1}$) and measured transient temperature within $\pm 0.2\text{ }^{\circ}\text{C}$.^[13] Zhang et al. incorporated thermoelectric effect to detect temperature stimuli through organic thermoelectric materials generating instantaneous voltage ($3\text{ }\mu\text{V}$ at 0.1 K difference) induced by the difference between sensing surface and base temperatures.^[301] Flexible OFET with pyroelectric polymer/barium titanate (BrTiO_3) nanocomposite has been demonstrated as a precise temperature sensor with standard deviation of $0.006\text{--}0.012\text{ K}$.^[302] Zhu et al. reported a temperature sensor based on stretchable CNT transistors to minimize strain-dependent errors, working within a uniaxial strain range of 0–60% with $\pm 1\text{ }^{\circ}\text{C}$ accuracy by a single temperature point calibration.^[136]

4.2. Electrophysiological Sensors

Biological cells and tissues produce a wide range of voltage signals from single ion channel proteins to whole organs in human body.^[11] Detecting the changes in voltage is useful for medical diagnosis and healthcare monitoring. Wearable electrophysiological sensors (Figure 13b) measure bioelectric signals noninvasively through skins. These biopotentials include ECG providing detailed information on the ventricles and atria for heart activities, electroencephalogram (EEG) monitoring electrical activities in the brain, EMG measuring electric potential generated by electrically or neurologically activated muscle cells, and EOG capturing the corneo-retinal dipole potential changes from eye movements. The biopotentials via various noninvasive wearable sensors show a wide range of frequency scale from 1 Hz to a few kHz and voltage range between 1 μV and 1 V. To detect such weak electrical signals without using conventional sensing techniques, wearable electrophysiological sensors should provide high electrical conductivity resulting in better signal-to-noise ratios, tight self-adhesion, and low motion artifacts for the accurate signal processing through the surface of skins.^[134,235,303] In addition, the wearable electronics based on skin-compatible and liquid (or water)-repellent materials should be expected to offer a long-lasting sensor capability.^[110,236,239] Stauffer et al. reported clinical quality of EEG recordings using soft macropillar polymer electrodes, conductive polymer with

Table 2. Examples of recently published WFHE sensors and their material properties.

Sensor	Material, working principle	Material properties			Sensing capabilities	Refs.
		Mechanical	Physicochemical; biocompatible	Electrical; system		
Temperature sensor	Cr/Au on silicone patch, TCR ^{a)} -based resistometry	Uniaxial strains ≈15%	P ^{b)} encapsulation, size = 1.6 cm, mass = 200 mg, work of adhesion >50 N m ⁻¹ , precise in Δw _{H2O} <5%; N/M ^{c)}	TCR = 0.0027 Ω K ⁻¹ ; NFC ^{d)} -based wireless, battery-free system	Range = 25–45 °C (R ^e = 0.9999), D ^f <2% in ΔT (t = 6 s), wearable for 1 week	[70]
	CNT ^{f)} in SEBS ^{g)} , thin-film FET ^{h)} -based	Uniaxial strains ≈60% (T ± 1 °C)	SEBS as a transparent encapsulation layer; N/M	μ = 6.18 ± 0.31 cm ² V ⁻¹ s ⁻¹ , down to 6 V	S ⁱ⁾ = -24.2 mV °C ⁻¹ (in 15–55 °C); D = 0.5 °C; stable V _{OD} over 100 cycles	[136]
Electrophysiological sensor	Au–Ag NWs ^{k)} in SBS ^{l)} matrix, ECG and EMG ^{A)}	Stretchability ≈840%	1 cm ² , attached using Tegaderm dressing film; Au used as a biocompatible coating layer (~6 months); implantable	σ ^{m)} = 41 850 S cm ⁻¹ (maximum = 72 600 S cm ⁻¹); N/M	Sampling rate ≈1 kHz, pulse duration ≈2 ms, 30–250 Hz, sweep speed ≈200 mm s ⁻¹	[134]
	CNTs or AgNWs in PDMS–MPU _{0.4} –IU _{0.6} ⁿ⁾ , ECG ^{B)}	Modulus = 0.7 MPa (substrate); stretchability ≈1600% (substrate), 250% (device)	Self-healing (after 12 h at room temperature); N/M	R _{AgNWs} = 34.0–65.9 Ω, R _{CNT} = 9 kΩ; Bluetooth-enabled wireless system with a 3.3 V Li-ion battery	Sampled at 500 Hz, heart rate from <60 to >90 bpm with an interval of 10 bpm	[132]
	1–3 composites as a piezoelectric transducer, ECG and blood pulse ^{C)}	Elastic and failure strain ≈30%, 60%	Si elastomer used as a hydrophobic encapsulation layer, ultrathin device ≈240 μm; 100% survival rate after 16 h; implantable	k ₃₃ = 0.81; power consumption = 23.6 mW	S = 32% at -6 dB bandwidth, peak-to-peak voltage of ≈100 mV; working frequency = 7.5 MHz, 400 μm axial resolution	[131]
Pressure/strain sensor	Stretchable and conformable matrix network on PVA ^{o)} or PDMS substrate ^{p)}	Meandering interconnection ≈800% expansion	Original: 16 cm ⁻² , expandable: 400 cm ⁻² , humidity sensing ≈0.07% % ⁻¹ (RH ^p) ≈20–80%; N/M	R ≈ 22 Ω; N/M	GF ^{q)} = 18 (0–2.5% strain); S = 22.4 MPa ⁻¹ (P < 16 kPa); 1.25 MPa ⁻¹ (16 kPa < P < 360 kPa)	[331]
	AgNW/polyamide nanofibers, touch sensor	R increases 2.3 times higher than original (~50% strain)	Almost invisible; T ^{r)} = 84.9% (at 550 nm), tightly adhered, 3 × 2.5 cm ² , air permeable; 6 cm ³ s ⁻¹ cm ⁻² ; N/M	Sheet resistance = 8.2 Ω sq ⁻¹ ; applied V = 0.1 V with an integrated pattern	I ≈ 80 μA (touch 0.25–1.5 Hz)	[184]
	Hierarchical pyramid-shaped SWNT ^{s)} -embedded PDMS ^{E)}	Modulus = 2 MPa (substrate)	Parylene used as a dielectric layer, semitransparent, 1 × 1 cm ² , 30 μm thick; N/M	Sheet resistance = 345 Ω sq ⁻¹ ; temperature-independent dielectric Al ₂ O ₃ layer	S = 0.7 kPa ⁻¹ (0–25 kPa), response =50 ms	[330]
	ZnO ^{t)} sea urchin-shaped microparticles ^{f)}	N/M	PDMS used as an encapsulation layer; 5 × 5 cm ² , 70 μm thick; N/M	N/M; bias voltage = 1–5 V	GF > 10 ⁴ ; S = 75–121 kPa ⁻¹ (0.015–200 Pa), response ≈7 ms, cyclability >2000	[286]
Optical sensor	OLDE ^{u)} - and OPD ^{v)} -based OPOs ^{w)}	Wearable	PET ^{x)} used as a gas barrier, 10 days (27 °C, RH = 47%), 1 cm ² , 50 μm thick (substrate); N/M	EQE ^{y)} (%) = 21.9 (green), 20.8 (red); power efficiency (Im W ⁻¹) = 59.8 (G), 29.3 (R); turn-on voltage = 2.8 (G), 2.1 (R); ultralow-power down to 24 μW	D ^{z)} = 2.3 × 10 ¹⁰ Jones (at 610 nm), 3.2 × 10 ¹⁰ Jones (at 520 nm)	[144]
	QD ^{aa)} LEDs and QD PDs on prestrained PEN ^{ab)} elastomer	Strain ≈70%, bending radius of curvature ≈35 μm	SLG ^{ac)} used as a transparent and flexible electrode; Ecoflex as a passivation layer against oxygen and moisture; N/M	EQE (%) = 12 (at 618 nm); sheet resistance = 78.3 Ω sq ⁻¹ , σ = 2394.1–2504.2 S cm ⁻¹ ; power = 17–31 μW	Responsivity and detectivity (at 0 V, at 633 nm) = 0.13 A W ⁻¹ , 6.05 × 10 ⁹ cm Hz ^{1/2} W ⁻¹	[317]
Electrochemical sensor	MIP ^{ad)} -based membrane between PEDOT:PSS ^{ee)} on SEBS substrate, OECT ^{ff)} -based cortisol sensor	≈40% stretching	SBES used as a flexible and stretchable substrate; 100 μm thick (substrate); N/M	N/M; V _C = 0.2 V vs Ag/AgCl	0.01 × 10 ⁻⁶ to 10.0 × 10 ⁻⁶ M cortisol with sensitivity of 2.68 μA per decade	[63]

Table 2. Continued.

Sensor	Material, working principle	Material properties			Sensing capabilities	Refs.
		Mechanical	Physicochemical; biocompatible	Electrical; system		
Colorimetric chemical sensor	CoCl ₂ ^{ag)} in pHEMA ^{ah)} , PDMS, lactate, sodium, potassium sensor	Wearable	Acrylic film used as an adhesive layer, microfluidic system, device diameter = 3 cm; PDMS used due to its biocompatibility	N/M; flow rates up to 1.0 μL min ⁻¹	300 μL sweat (1.8 μL each from 0.8 min of sweating, 0.60 μL min ⁻¹ sweat rate)	[178]

^{a)}TCR = temperature coefficient of resistance; ^{b)}PI = polyimide; ^{c)}N/M = not mentioned; ^{d)}NFC = near-field communication; ^{e)}D = deviation (related to accuracy); ^{f)}CNT = carbon nanotube; ^{g)}SEBS = styrene–ethylene–butadiene–styrene; ^{h)}FET = field-effect transistor; ⁱ⁾μ = mobility; ^{j)}S = Sensitivity; ^{k)}AgNWs = silver nanowires; ^{l)}SBS = styrene–butadiene–styrene; ^{m)}σ = conductivity; ⁿ⁾PDMS–MPU_{0.4}–IU_{0.6} = strong (4,4'-methylenebis(phenylurea) unit, MPU) and weak (isophorone bisurea unit, IU) dynamic bonding units incorporated into a polydimethylsiloxane (PDMS) backbone; ^{o)}PVA = poly(vinyl alcohol); ^{p)}RH = relative humidity; ^{q)}GF = gauge factor; ^{r)}T = transmittance; ^{s)}SWNT = single-wall nanotube; ^{t)}ZnO = zinc oxide; ^{u)}OLED = organic light-emitting diode; ^{v)}OPD = organic photodiode; ^{w)}OPOs = organic pulse oximeters; ^{x)}PET = poly(ethylene terephthalate); ^{y)}EQE = external quantum efficiency; ^{z)}D* = specific detectivity (typical); ^{ab)}QD = quantum dot; ^{ac)}SLG = single-layered graphene; ^{ad)}MIP = molecularly imprinted polymer; ^{ae)}PEDOT:PSS = poly(3,4-ethylenedioxythiophene):poly(styrene sulfonate); ^{af)}OEET = organic electrochemical transistor; ^{ag)}CoCl₂ = cobalt chloride; ^{ah)}pHEMA = poly(hydroxyethyl methacrylate); Multifunctional sensors: ^{a)}Electrophysiological/temperature sensor; ^{B)}Strain/electrophysiological sensor; ^{C)}Pressure/electrophysiological sensor; ^{D)}Temperature/RH/UV light/magnetic field/in-plane strain/pressure/proximity sensor; ^{E)}Temperature/pressure sensor; ^{F)}Pressure/strain sensor.

25 vol% of Ag with highly conductive porous polymer coating, in 0–20 Hz with potential variation within 50 μV.^[303] These soft porous electrodes also acquired stable swimmer's ECG signals with less movement noise in water during strong movements and muscle activity. Son et al. demonstrated ECG data acquisition through percolated CNT network in PDMS–MPU_{0.4}–IU_{0.6} polymer matrix and the detected signal peaks blinked a light-emitting capacitor display as a heartbeat indicator.^[132]

4.3. Strain and Pressure Sensors

Tactile sensors monitoring strain and/or mechanical pressure are operated by detecting the stimuli with changes in electrical properties of sensing materials based on various principles (Figure 13c): piezoresistivity,^[142,156] piezoelectricity,^[304,305] capacitance,^[158,306] percolation network,^[307] crack propagation,^[280,308] resonant frequency shift,^[309] and triboelectricity.^[310] The strain sensors require large GF in a wide range of deformation from vigorous actions at joint areas to subtle motion on face. High pressure sensitivity with low detection limit is desired for the pressure sensors. Both strain and pressure sensors should be in low temperature coefficient of resistance (TCR) response to minimize temperature effect on sensing materials. A constantan-alloy-based strain sensor shows high GF of 18 (0–2.5% strain) with low TCR (0.03% °C⁻¹ at 22–60 °C).^[136] Fan et al. presented the sensing capability of uniaxial strain (0–50% elongation) and high durability under 3000 bending cycles with 300 m⁻¹ curvature of a scaffold-reinforced conductive nanonetwork sensor based on AgNWs.^[184] Yin et al. reported a dual-mode sensor based on ZnO microparticles, which has spherically distributed, high aspect ratio nanostructured tapering spines resembling a sea urchin.^[286] The bristles collected both resistive changes of interspine contacts and piezoresistive changes from spine bending for local signal amplifications of pressure and strain. The bioinspired bristle sensor featured high pressure sensitivity of 121 kPa⁻¹, large strain GF of over 10⁴, and rapid response time of 7 ms.

4.4. Optical Sensors

Optoelectronic devices (Figure 14a) convert signal changes in light by scattering and absorbing into electrical signal changes captured by a photodetector and provide a key clinical information like photoplethysmogram (PPG) and peripheral oxygen saturation signals.^[311,312] Wearable photodetectors have been developed based on various nanostructured materials,^[313–316] such as quantum dots (QDs),^[317] nanocrystals, NWs, 2D layered materials, organic semiconductors, and perovskite materials. The photodetectors require high photoresponse sensitivity with thick sensing materials for high absorption coefficient and high temperature processing to form high-quality contacts between sensing materials and electrodes, which is required in some photodetector fabrication to ensure efficient transport of photogenerated carriers, but it conflicts excellent mechanical flexibility. Moreover, low power consumption, minimized motion artifacts, and low noise from ambient light sources should be desired. Lee et al.^[297] presented organic pulse oximeters driven by very low power consumption (17–31 μW) that were composed of an organic photodetector and two light sources, a green OLED and a red OLED and the organic photodetector. The photodetector showed external quantum efficiency (EQE) of 15–20% with responsivity of 0.21 A W⁻¹ at 610 nm for the red OLED and 0.29 A W⁻¹ at 520 nm for the green OLED, where the responsivity is proportional to EQE and higher EQE represents that a light absorbing material has high absorption coefficient and large thickness.

4.5. Electrochemical Sensors

The aforementioned wearable sensors track human body's physical activities in dry conditions by detecting changes in electrical signals, which provide the variety of physiological information, but do not include the body's biomolecular state. Noninvasive wearable electrochemical sensors have been developed (Figure 14b) to detect target analytes in accessible

biofluids such as saliva,^[55,318] tears,^[174,319] sweat,^[179,320] and skin ISF,^[321,322] while the use of blood is challenging to access in vitro wearable platform.^[32] Electrochemical sensors are placed close to the fluid origination, local stimulation, and on-demand or ideal sites for continuous monitoring, tracking the concentration and its changes for various types of analytes such as ions, biomolecules, and proteins, and then converting to electrical signal changes through various techniques such as potentiometry, voltammetry, chronoamperometry, and electrochemical impedance spectroscopy.^[50,323–325] In addition to reliability, high sensitivity, and fast responsibility required in common for wearable biosensors, electrochemical sensors desire excellent selectivity and wide detection range among enormous but subtle biomolecules with high precision. Lee et al. reported real-time ion-selective sodium monitoring using a low-profile sensor mounted in the oral cavity with high selectivity and sensitivity in food intake.^[55] Lipani et al. presented noninvasive transdermal glucose monitoring from the ISF through follicular pathways in the skin using electroosmotic extraction.^[322] A wearable theranostic contact lens to detect a pathogenic attack was demonstrated using tear fluid as the diagnostic medium with good surface wettability (43°), optical transparency (91.5%), and bioaffinity to human corneal epithelial cells.^[174] Emaminejad et al. developed an autonomous platform that extracts sweat (100 nL min⁻¹ cm⁻²) on demand or periodically without skin damage, evaluates contents of sodium and chloride ions in the cystic fibrosis patients, and establishes blood/sweat glucose correlation.^[323]

4.6. Colorimetric Chemical Sensors

Another type of chemical sensors is based on colorimetric response (Figure 14c) in functionalized porous microfluidic substrates.^[326,327] A closed epidermal microfluidic (epifluidic) system can harvest sweat from pores on the surface of the skin, route to different channels and microreservoirs containing a colorimetric chemical reagent for a targeted biomarker of interest, and quantitatively measure pH, lactate, chloride, and glucose concentrations by colorimetric detection.^[328] The measurement includes sweat rate and instantaneous total sweat loss through additional serpentine microchannel. As sweat entered the channel, each microreservoir detected the target biomarker through chemical reaction and its color change was observed by analyzing the absorbance. Digital image processing via smart devices allowed assessment of the color change along with the concentration. Such epifluidic devices can monitor human biomolecules without localized electronic components.

4.7. Recent Advances in Sensor Capabilities

Figure 15 shows a wide spectrum of sensor capabilities of advanced WFHE. Typical wearable temperature sensors characterized by a TCR are relatively strong function of strain,^[91,300,329] and it is difficult to specify the exact degree of strain in actual operations, which gives rise to difficulty of accurate measurements and calibrations. Figure 15a shows a strain-independent temperature sensor, mounted on the surface of the epidermis at

joint areas such as a wrist or knuckle, composed of multiple TFTs based on single-walled carbon nanotubes (SWCNTs).^[136] The temperature sensor with a dynamic differential circuit demonstrated high sensitivity of $-24.2 \text{ mV } ^\circ\text{C}^{-1}$ in the temperature range of 12–55 °C, strain suppression with negligible temperature variation under repeated bending motion (up to 15% uniaxial strain), and low hysteresis. Electrophysiological signals such as ECG and EMG are acquired by detecting biopotentials through wearable electrodes tightly adhering to human skins. As shown in Figure 15b, Choi et al. showed that Au–Ag nanocomposites consisting of ultralong Au-coated AgNWs dispersed in poly(styrene–butadiene–styrene) (SBS) elastomer improved biocompatibility by preventing Ag ion leaching and Ag oxidation and showed dual sensing technology.^[134] The sensor has high stretchability (up to 840% strain) and lower electrode–skin interface impedance resulting in a lower threshold current than conventional electrodes. The Ag–Au core–sheath biosensor measured ECG showing high signal-to-noise ratio from the right forearm with an ankle ground electrode (Figure 15b, right upper) and EMG detecting rapid response of a degree of contractions from the right forearm (Figure 15b, right lower). Wang et al. also showed electrophysiological sensors based on wearable ultrasonic device for continuous monitoring of blood pressure in three different sites—brachial artery (case 1), radial artery (case 2), and pedal artery (case 3), where central blood pressure is measured in carotid artery on neck as shown in Figure 15c.^[131] It clearly demonstrated that the amplification effect increases as the measurement site moves from the large and highly elastic carotid artery to the small and stiff peripheral arteries (radial artery and pedal artery) depending on the travel distance of the reflected pulses. Owing to the strong relationship between arterial pulse propagation and vascular stiffness, the ultrasonic sensor presented ECG correlation with blood pressure by characterizing pulse wave velocity (PWV) from pulse arrival times (PAT) at the sensor locations and the distance (D) between ECG sensor mounted on the chest and the ultrasonic sensors using $\text{PWV} = D/\text{PAT}$, where PWV in case 2 (ECG and radial artery) is 5.8 m s⁻¹ (band in gray, Figure 15c, bottom left). Compared to the commercial tonometer, the wearable ultrasonic blood pressure sensors showed stable blood pressure waveform measurements with various angles without distortion, operator-independent measurement results, and high precision within 2 mmHg. Figure 15d illustrates a wearable optoelectronic sensor composed of uniformly wavy structural QDs as a photodetector and self-emissive materials for light-emitting diodes (LEDs) with a graphene electrode were mounted around the tip of a forefinger.^[144] The wearable biosensor, stretchable up to 70% and foldable to a radius of curvature of 35 μm, can measure PPG signal pulses by illuminating the skin with the LED located on the back and absorbing the light transmitted through the skin with the photodetector placed on the front. The red light emitted from the QD LED passed through the tip of the forefinger and was detected by the photodetector. The measurement of the changes in light absorption helps to determine the pressure pulse of the cardiac cycles (Figure 15d, right) and real-time analysis of the peak ratio and time ratio of a pulse can monitor any abnormalities. The firmly mountable sensor also demonstrated waterproof capability up to 2 h immersion in water. There are multifunctional sensors

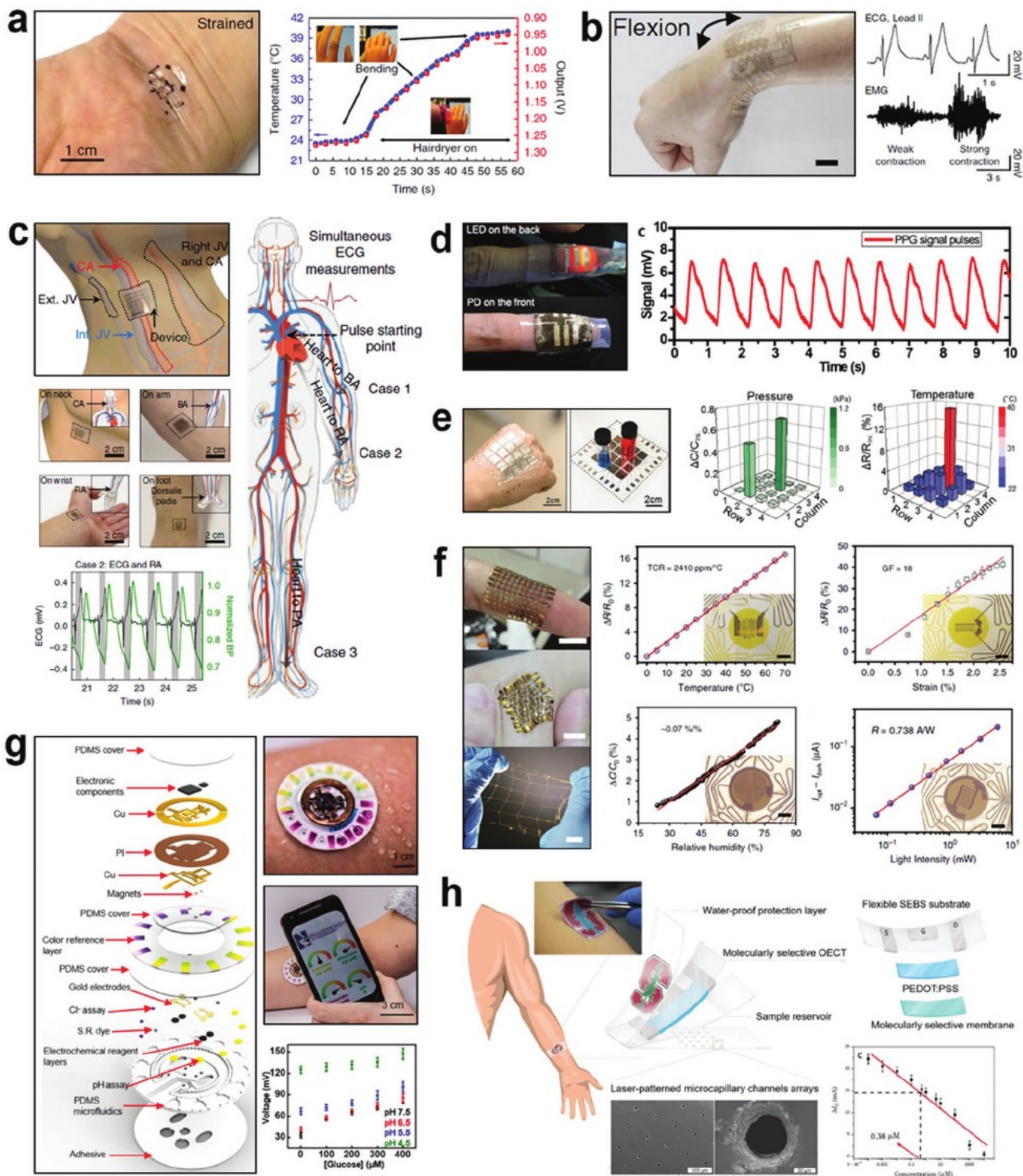


Figure 15. Various types of WFHE for recording of noninvasive physiological signals. a) Skin-wearable temperature sensor. Reproduced with permission.^[136] Copyright 2018, Nature Publishing Group. b) Electrophysiological sensor for ECG and EMG recording. Reproduced with permission.^[134] Copyright 2018, Nature Publishing Group. c) Electrophysiological blood pressure sensors. Reproduced with permission.^[131] Copyright 2018, Nature Publishing Group. d) Optical sensor for pulse detection. Reproduced with permission.^[144] Copyright 2017, American Chemical Society. e) Temperature-pressure monitoring sensor. Reproduced with permission.^[330] Copyright 2018, Wiley-VCH. f) Multifunctional sensor system. Reproduced with permission.^[331] Copyright 2018, Nature Publishing Group. g) Colorimetric chemical sensor system. Reproduced with permission.^[332] Copyright 2018, Nature Publishing Group. h) Electrochemical sensor system. Reproduced with permission.^[63] Copyright 2018, American Association for the Advancement of Science.

capable of measuring two or more properties simultaneously (Figure 15e) or through separate units in a single device (Figure 15f). Bae et al. reported bimodal electronic skins consisting of spray-coated rGO thermistor for the temperature sensing and conductive truncated pyramidal microstructures with SWCNTs and Ni/Ti electrodes on pressure sensing surface, which can simultaneously detect and discriminate pressure and temperature stimuli in real time.^[330] Figure 15e shows the device mounted on the back of the hand and sensing locations of the cold (blue bottle, room temperature) stimulus with lighter pressure and hot (red bottle, 40 °C) stimulus with heavier pressure. The sensor shows linear sensitivity of 0.83% °C⁻¹ and fast response (<100 ms) and high pressure sensitivity of 0.7 kPa⁻¹ in the pressure range up to 25 kPa compared to the conventional sensitivity of 0.2 kPa⁻¹. This is because of the larger relative change in the contact area of the sensing surface than the relative change in height of parallel dielectric layers. Also, linear sensitivity over the pressure range and high durability under 10 000 cycles with loading pressure of 14 kPa were exhibited. Figure 15f shows a stretchable and conformable matrix network composed of 100 sensory nodes to achieve multifunctional sensing performance such as temperature, in-plane strain, RH, and UV light.^[331] Resistive metals of Pt and constantan alloy were used as an RTD, operating from 0 to 70 °C with linear sensitivity of 0.24% °C⁻¹. For the strain sensor unit, constantan alloy with low TCR (0.03% °C⁻¹ at 22–60 °C) was used to minimize thermal effect on strain sensing and it has high GF of 18 in the range of 0–2.5% strain. The capacitor-based humidity sensor unit detected ambient RH, in which the absorption of water molecules changed the permittivity of the PI and this yielded a linear correlation between relative changes in capacitance. The sensor based on ZnO as a UV photodetector measured UV illumination with rapid response time of 14 ms and the photocurrent induced by UV light showed fast, linear photoresponsivity of 0.738 A W⁻¹. External disturbance between the different sensing units has a negligible effect. Figure 15g shows that a circular epifluidic sweat sensor located in the microfluidic structure with 32 mm diameter, ≈1 mm thickness, and 18 mm diameter biofluid harvesting and wireless networking area at the center was mounted on the forearm for quantitative colorimetric analysis of sweat loss and the concentration of chloride, lactate, glucose, and pH in the sweat.^[332] The colorimetric indicator of biofuel cell-based sensors and the color with yellow and purple along with the orbicular channel was changed, which yields quantitative information on the sweat rate and volume by characterizing the color changed area of the channel. According to a previous report from the same group,^[328] the concentration of glucose could be analyzed by an enzymatic reaction that showed a change in color from yellow to brown. Colorimetric detection of chloride through chemical binding reaction induced a change in color from transparent to blue. Lactate concentration variation induced a change in color of a chromogenic reagent such as formazan dyes. The quantitative colorimetric detection was analyzed through digital image processing by using a white dot in the middle of the device and four black crosses distributed near the center as 100% and 0% in RGB coordinates, respectively. Figure 15h shows a patch-type molecularly selective organic electrochemical transistor (OEET) as a cortisol biosensor

consisting of four layers: microcapillary channel arrays for sweat acquisition, reservoir layer for sample delivery, molecularly selective OEET layer as a sensor component, and waterproof protection layer.^[63] This electrochemical biosensor absorbed 10–50 µL of sweat through the passive capillary effect and accommodated more than 100 µL in a sample reservoir. For the on-body measurements, the sensor patch was mounted on forearm to assess cortisol concentration after 20 min outdoor running exercise. In Figure 15h, the cortisol concentration change in the range of 0.001 × 10⁻³ to 1 × 10⁻³ M was recorded by measuring the change of drain current (ΔI_D), where the red line is the cortisol concentration– ΔI_D relation as a control device without molecularly selective membrane in the sensing layer.

5. Applications of WFHE

Recent advancements in WFHE have enabled noninvasive and conformal class of sensors by stacking multifunctional electronic layers on soft, ultrathin platforms. This approach not only reduces their sensitivity to mechanical stress caused by body movements, but also improves tissue comfortability for long-term integration with the skin. Here, we introduce some of the representative examples (Figure 16) of WFHE for promising real-world applications in health monitoring, environmental sensing, and energy harvesting. These concepts drive the field of healthcare further from early diagnosis to access the well-being and athletic performances (Figure 16a). High sensitivity of nanomaterial is beneficial to detection of toxic species in air because their resistance changes that a given surface can reduce or oxidize by the interaction with gaseous species (Figure 16b). This effect is pertinent to systems with a multiplexed sensor. The approach to overcoming such challenge is to exploit human body motion, temperature, or external sunlight by integrating energy harvesting devices into skin-attached wearables (Figure 16c).

5.1. Healthcare

Healthcare and other biomedical applications^[55,333–335] of WFHE exploit their ability to make intimate, conformal integration on soft, stretchable, and curvilinear human tissue to provide wearing comfort as well as high-quality monitoring of biopotentials. However, their potential to replace existing technology truly hinges on their ability to reduce healthcare costs and to offer continuous monitoring of physiological data as well as appropriate therapeutics. Below are a few representative technologies that solve unique challenges to enhance utility and implementation of WFHE for various healthcare and medical applications.

5.1.1. Recyclable Paper-Based WFHE

One of the emerging markets for wearable technology is in the healthcare industry where continuous physiological monitoring of the body vitals is deemed necessary to predict health wellness (fitness industry) or to anticipate diseased abnormalities so

a. Detection of health factors

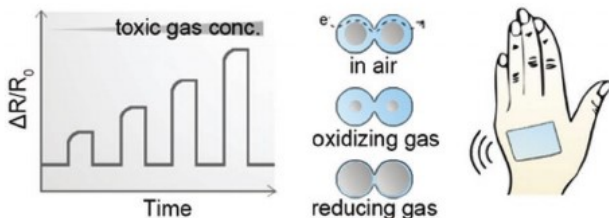

Purpose/Method

early diagnosis, management of chronic diseases, timely response to life-threatening situations, access to the well-being and athletic performances

Types

all types of sensors detecting vital biosignals

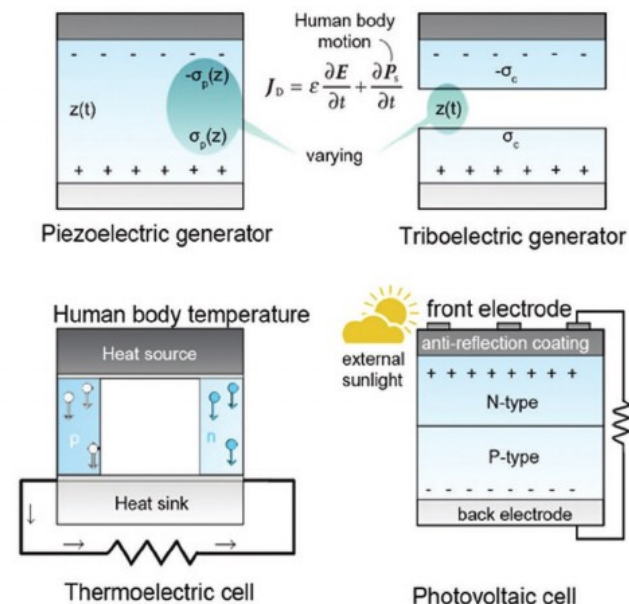
b. Detection of environmental exposure


One example: gas sensor

tracking environmental gas concentration for personal wellness and security surveillance

Types chemiresistive, optical, electrochemical, etc.

c. Development of self-powered systems


Purpose

to solve the high consumption problem of multifunctional WFHE for the convenience of consumers

Method

developing a self-sufficient power system by integrating energy-harvesting devices with energy storage devices

Types

energy-harvesting devices such as piezoelectric, triboelectric, thermoelectric generators, solar, radio-frequency (RF) cells, etc.

Figure 16. a–c) Description, types, and methods of key factors, including detection of health factors (a), detection of environmental exposure (b), and development of self-powered systems (c), for WFHE applications in healthcare, environment, and energy.

that they can be diagnosed on time (in hospitals). Conventional health monitoring devices are not cost-effective and have rigid structures, making them uncomfortable to wear over a long period. In a recent development, a low-cost, wearable health monitoring device called “paper watch” (Figure 17a) was created by using recyclable, flexible, and readily available “Post-It” papers.^[336] This device integrates flexible electronics within the paper substrates to enable a highly deformable and conformable form factor. The 3D stackable architecture highlights its unique scalability for vertical integration of multiple functional layers in between the insulating papers. The multisensory layer was placed in the bottommost layer to make direct contact with the skin for monitoring of multiple vital signs such as heart rate, arterial stiffness, sweat levels, and blood pressure. Overall, the device was built using facile fabrication techniques and low-cost materials such as aluminum foil for electrodes, micro-fiber tissue for a dielectric layer for capacitive pressure sensors, and Ag ink for drawing conductive elements. This ultralow-cost paper electronics was integrated inside a lightweight, 3D

printed wristband to allow effortless monitoring of various vital signs by wearing it on the wrist. Even with its low-cost and easy manufacturing process, the paper watch showed excellent reliability for monitoring of physiological signals such as heart rate, which were comparable to the readings recorded by a commercial smartphone application (Samsung S5, S Health).

5.1.2. Wireless Intraoral WFHE

In another application, wireless intraoral electronics was developed by conformally laminating a miniaturized (1.5 g), soft (68 kPa), and flexible electronics onto an oral retainer. This novel class of intraoral electronics can provide real-time quantified monitoring of the sodium intake during food consumption for hypertension management (Figure 17b).^[55] The device consists of off-the-shelf chip components (such as a tiny Bluetooth IC, a rechargeable battery, and other signal processing units) and stretchable interconnects encapsulated in a

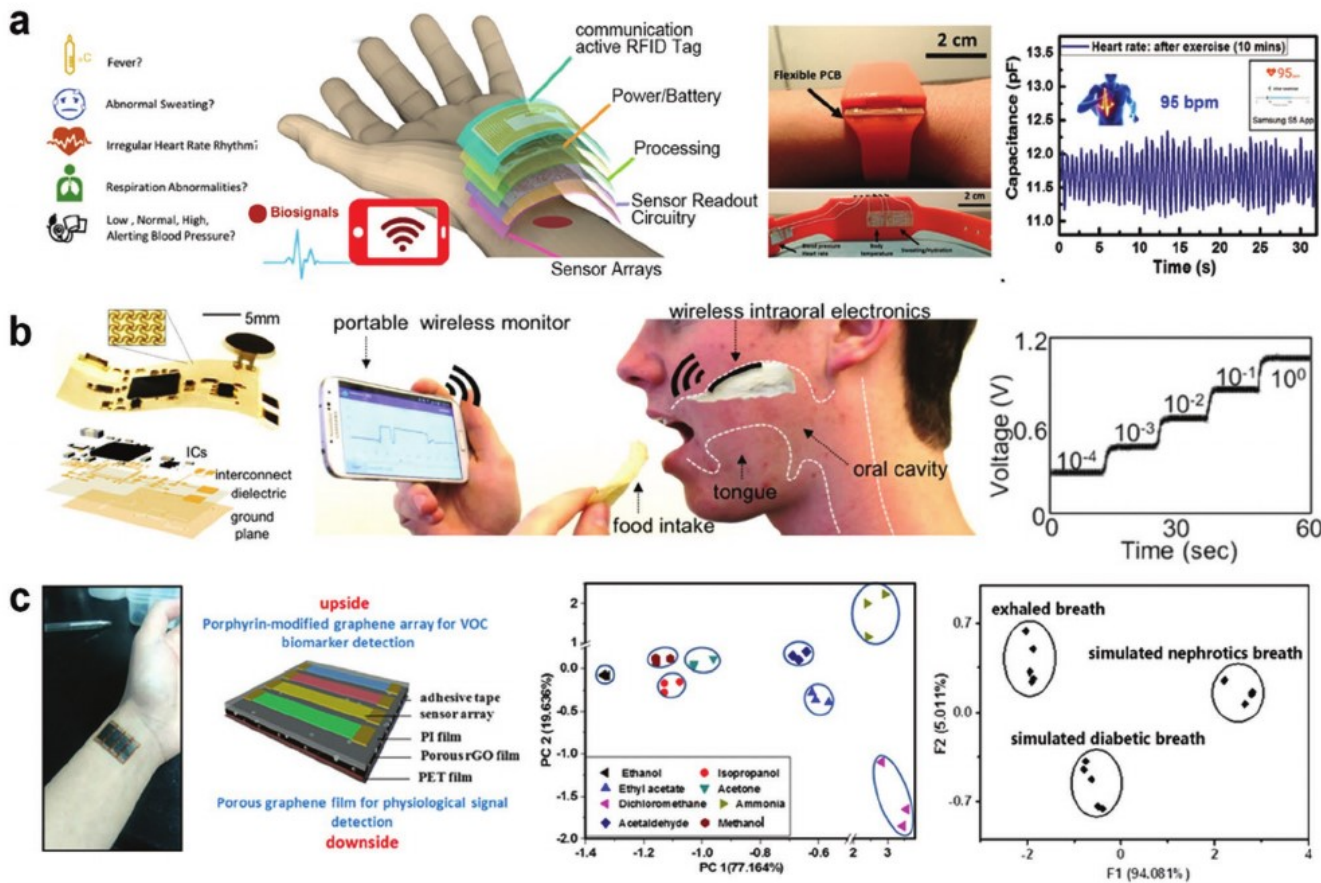


Figure 17. Examples of WFHE applications in healthcare and environment. a) Paper-based autonomous healthcare monitoring system. Reproduced with permission.^[336] Copyright 2017, Wiley-VCH. b) Wireless intraoral hybrid electronics for measuring sodium intake via real-time monitoring. Reproduced with permission.^[55] Copyright 2018, National Academy of Sciences. c) Wearable sensory system enabling simultaneous detection of physiological signals and volatile organic compound biomarkers. Reproduced with permission.^[337] Copyright 2018, American Chemical Society.

soft elastomeric shell (0.2–0.5 mm thick Ecoflex), which passivates the whole electronics from intraoral fluids except the sodium sensing electrodes. The flexible, low-profile device was mounted on a microporous retainer to enable breathability and low thermal loading when interfaced with the intraoral tissue. The inexpensive and fast responsive ion-selective sodium electrodes (ISEs) consisting of electroplated Pd (working) and Ag/AgCl (reference) electrodes are key for accurate measurement of sodium intake. The ISE sensors combined with wireless data transmission capability showed highly reliable and fast linear voltage response to the sodium concentration change of the food intake, demonstrating its potential as a wearable hypertension management device. The device also showcased high selectivity to sodium ions in comparison to other normal food constituents such as K⁺, Ca²⁺, and Mg²⁺, thus validating its utility in real-life scenarios.

5.2. Environment

Wearable electronics that can simultaneously monitor both physiological status and environmental conditions can significantly improve health and wellness management. Here, we introduce an example of a wearable sensor with such symbiotic

functions. Multiplexed sensory layers in WFHE can help evaluate both physiological and environmental conditions on a single platform. Researchers developed a mass manufacturable gas sensor (Figure 17c), which is capable of sensing both volatile organic compound (VOC) vapors and physiological signals simultaneously without any crosstalk.^[337] The device consists of two distinct graphene films, including 1) the upper layer: four different types of porphyrin-modified rGO films with distinct electron transfer characteristics for gas sensing; and 2) the bottom layer: porous rGO film (with 10–20% mixture of soft P(BA-co-MMA) NPs to increase resistive sensitivity) for measuring pulse and breath rates through resistive changes caused by momentary strains in the film. The two layers were physically separated by a flexible PI substrate for electrical insulation. The graphene gas sensor detects VOC vapors by linearly increasing sheet resistance of the graphene electrodes with increasing vapor concentrations. Principal component analysis in Figure 17c shows that this wearable gas sensor can detect eight distinct VOC vapors (i.e., ethanol, propanol, ethyl acetate, acetone, dichloromethane, ammonia, acetaldehyde, and methanol), each with its own unique footprint with reproducibility. Its functional demonstration as a wearable device to simultaneously quantify pulse rate as well as ammonia and acetone gases in exhaled breaths (which are important biomarkers for

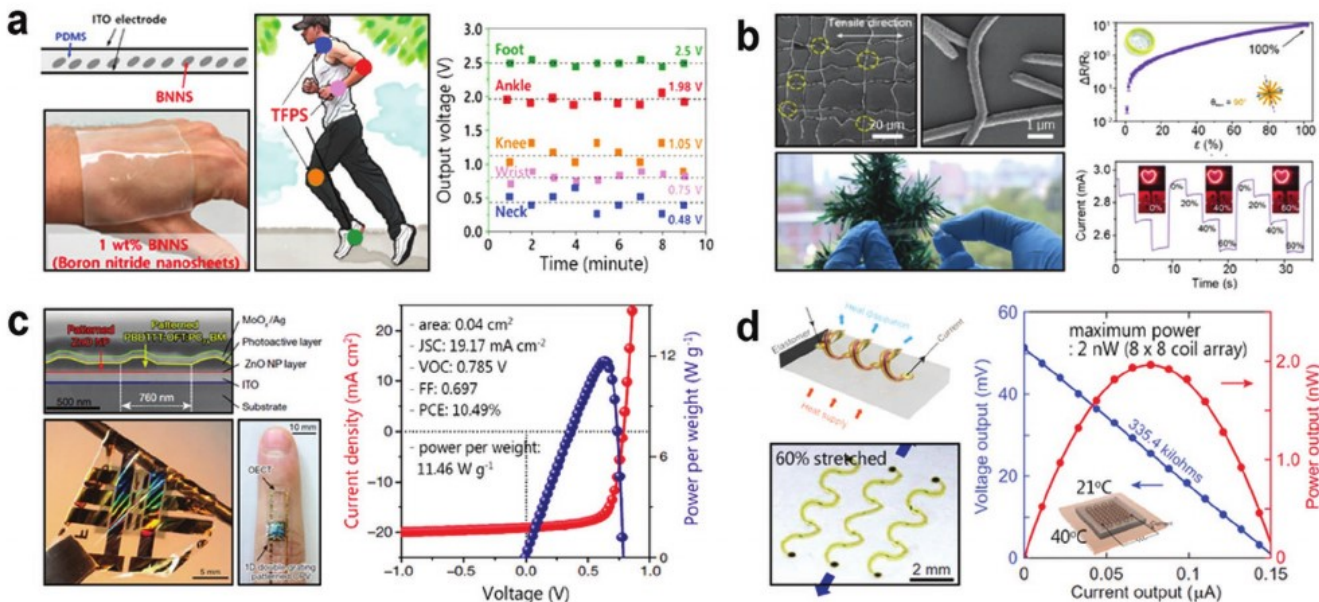


Figure 18. Examples of WFHE applications in energy. a) Piezoelectric energy harvesting system. Reproduced with permission.^[338] Copyright 2018, Elsevier. b) Triboelectric energy harvesting structure. Reproduced with permission.^[183] Copyright 2018, Wiley-VCH. c) Solar energy harvesting system. Reproduced with permission.^[341] Copyright 2018, Nature Publishing Group. d) Highly stretchable thermoelectric generator. Reproduced with permission.^[130] Copyright 2018, Nature Publishing Group.

nephrotic and diabetic patients, respectively) highlighted its distinctive ability to obtain multiplexed measurements of both gaseous biomarkers and vital signs.

5.3. Energy

One of challenges for wearable electronics is to power electronic components long enough for prolonged use of WFHE. Unlike battery-powered wearable devices, which require intermittent replacement or recharging of batteries, battery-free approach can maximize the full potential of wearable electronics. This section summarizes some of the latest development of flexible, self-powered technologies, which can truly leverage the utility of WFHE.

5.3.1. Transparent Piezoelectric Energy Harvester

Converting mechanical energy from physical motions into electrical energy through soft, flexible piezoelectric harvesters holds promising applications for self-powered WFHE (Figure 18). To demonstrate its utility, a transparent, flexible, and wearable piezoelectric device was fabricated (Figure 18a) by creating a PDMS–boron nitride nanosheet composite that was sandwiched with indium tin oxide (ITO) electrodes.^[338] To ensure uniform dispersion of BNNS within PDMS, it was functionalized with oleylamine. The resulting device was not only highly flexible, allowing conformal lamination on the skin surface, but also transparent (transmission rate of 65–81% in visible light wavelengths when BNNS concentrations did not exceed 1 wt%). Compressive and tensile pressures on the device surface accumulate positive and negative charges, respectively, thus generating voltage signals that were found to be proportional

to BNNS concentrations used and the stress experienced. The experimental study shows that the device mounted on the various parts of the body can generate electricity through normal body movements (e.g., 2.5 V (foot), 1.98 V (ankle), 1.05 V (knee), 0.75 V (wrist), and 0.48 V (neck)). Its capacity to generate a peak power of 40 μW with a power density of 0.106 mW cm⁻³ shows the capability for powering small electronic components and wearable sensors (e.g., voltage supervisors^[339] or ECG monitoring system-on-chips^[340]).

5.3.2. Triboelectric Tactile Electronics

Tactile sensing offers a unique approach to generate voltages through touch interaction with WFHE. A low-cost stretchable triboelectric tactile sensor with fast response time (70 ms) was fabricated by encapsulating 600 nm thick Ag-coated PVA NFs with a thin PDMS layer.^[183] This triboelectric tactile sensor harvests energy through currents that are generated to balance the electrostatic charges created by touching the PDMS surface. The fabricated tactile sensor was highly transparent (70% transmission rate in the UV-vis light spectra with a density of AgNFs <0.5 μm⁻¹) and stretchable (up to 100%). The stretchable nature of the sensor was found to be heavily influenced by the orientation of AgNFs. When AgNFs were oriented in multiple directions (Figure 18b), it demonstrated reduced fracture sensitivity in the direction perpendicular to the tensile stress (only 10% resistance increase at 100% strain), thus limiting decrease in generated currents (in comparison to unidirectional AgNFs). The device reliability was further validated through multiple stretching tests repeated at various strains (up to 60%). This feature to harvest energy upon stretching makes this technology a promising option for use in future self-powered wearables.

5.3.3. Organic Photovoltaic Device

Another study developed an ultraflexible WFHE (Figure 18c), where OECTs were self-powered through an ultrathin (3 µm), ultralight (36.6 µg), and nanograting-patterned (760 nm pitch) photovoltaic device (OPV).^[341] It consists of a ZnO NP layer for electron transport and a heterojunction layer (composed of poly[4,8-bis(5-(2-ethylhexyl)thiophen-2-yl)benzo[1,2-*b*;4,5-*b'*]dithiophene-2,6-diyl-*alt*-(4-octyl-3-fluorothieno[3,4-*b*]thiophene)-2-carboxylate-2,6-diyl] polymer with [6,6]-phenyl-C₇-butyric acid methyl ester as a photoactive layer, sandwiched with Ag and ITO electrodes. The whole device was mounted on a Parylene substrate (1 µm thick) to facilitate handling. With a power conversion efficiency of 10.49%, this OPV was found to be superior to other flexible OPVs,^[162,164] due to its reduced sensitivity to high strains and illumination angles. The device demonstrated robust functionality even under 200% compression strain with no effect on open-circuit voltage (V_{oc}) and little effect on short-circuit current (I_{sc}). The nanograted OPV showed increased values for I_{sc} and power efficiency compared to nonpatterned OPVs regardless of the illumination angle. Application of a self-powered cardiac sensor on a human fingertip presented its promise for various biomedical applications.

5.3.4. Stretchable Thermoelectric Coils

Wearable thermoelectric generator (TEG) is a promising technology for self-powered electronics, which can harvest energy by using the temperature difference between the skin and the ambient environment. Figure 18d shows a stretchable class of wearable TEG based on the design utilizing interconnected functional 3D helical coil array transformed from microfabricated 2D structures (p/n-type 0.2 µm thick Si ribbons encapsulated with 4 µm thick PI sheaths on both sides for mechanical support) on an elastomeric substrate.^[130] Using a thermoelectric leg design, which is a 1.57 mm long buckled structure, this 3D device allows heat to flow naturally from the bottom side of the device in contact with the skin (hot side) to the side away from the skin surface (cold side). Thus, it greatly improves its thermoelectric conversion efficiency by maximizing the temperature difference. In addition, each thermoelectric leg was designed to have tapered geometry with PI sheath on the cold side being twice as wide compared to the hot side in order to further enhance the temperature difference across each leg. Based on this design, an 8 × 8 coil array was able to generate 2 nW of peak power at a temperature difference of 19 °C. The stretchable nature also enabled 60% in-plane stretching and 30% vertical compression with minimal degradation in its functionality, thus ensuring its reliable utility in conformal wearable applications involving dynamic tissue deformation.

6. Conclusions and Outlook

Recent progress in functional hybrid materials, manufacturing, and packaging technologies has enabled significant advances in the development of WFHE. Herein, key requirements of material properties, sensor capabilities, electronics

performance, and skin integrations, along with a few wearable applications, have been summarized. Assorted properties in WFHE, summarized here, have boosted the development of wearable functional devices, accompanying a concurrent improved yield of integrated skin-like artificial sensory system, autonomous energy harvester, and personal healthcare on demand. Advances in material foundations and hybrid integration strategies offer enhanced mechanical compliance, and physicochemical and/or biological properties that are suitable for direct integration with the human skin. One common and representative example summarized here, in which the programmed functionalities were enabled by a structural modification in molecular,^[155,191] nano/microdimensional,^[81,139,184,203,212,222] and device group levels,^[130] already plays a key part in managing multiple interface-related conditions and suitable methodologies. Parallel efforts in the development of intrinsically stretchable, transparent, or self-healable electronics are focusing on the successful integration of multimodal materials exhibiting liquid-like,^[151] ionic conducting,^[224] and biomimetic behaviors^[192] as electrodes, substrates, dielectrics, and transistors. These devices are promising for next-generation biomedical systems and persistent human-machine interfaces. The elevation of such newly developed materials is persuaded to apply into the WFHE for help with vexing problems such as ensuring long-term tight contact in an elbow,^[342] beyond abstruse functionalities.

Nevertheless, there are still many aspects of WFHE that must be further developed for the realization of multisensors in everyday life in terms of sensor usability and opportunities for noninvasive health monitoring beyond laboratory-scale applications. Currently, the bottleneck is the device reliability, long-term use, and readily available data set. Unlike single-point detection or single-function sensor, multiplexed setting in a way that is seamless and redundant requires deep and varied consideration of the correlation between two or more sensing features that could be attributed to altering each other.^[177,343] For the further growth, the efficient extraction of important physiological information from WFHE would be enabled by either the isolation of the body movement and environmental conditions or the detection of multiple signals on the basis of comprehensive signal processing and machine learning algorithms.^[344] In addition to the consideration of multifunctional sensors, wireless systems that are ultralight, low profile, highly flexible, and battery-free should be integrated with WFHE in a conformal manner for a portable, onsite monitoring of health at home settings.^[345]

We believe that consideration of these challenges will provide great opportunities to further develop WFHE for practical applications, which will eventually reach the ultimate goal of enabling wireless, noninvasive, continuous, personalized, and predictive monitoring of physiological signals for advanced, smart healthcare and wellness.

Acknowledgements

W.-H.Y. gratefully acknowledges financial support from the Samsung Global Research Outreach Award, the Imlay Innovation Fund, and funds from the Marcus Foundation, the Georgia Research Alliance, and the Georgia Tech Foundation through their support of the Marcus

Center for Therapeutic Cell Characterization and Manufacturing at Georgia Tech. J.-W.J. acknowledges support from the National Research Foundation of Korea funded by the Ministry of Science and ICT (NRF-2018R1C1B6001706 and 2018R1A4A1025230).

Conflict of Interest

The authors declare no conflict of interest.

Keywords

energy harvesting, environmental exposure, healthcare devices, sensor integration, soft materials, wearable flexible hybrid electronics (WFHE)

Received: March 27, 2019

Revised: April 18, 2019

Published online: July 8, 2019

- [1] S. Wang, K. Chen, M. Wang, H. Li, G. Chen, J. Liu, L. Xu, Y. Jian, C. Meng, X. Zheng, S. Liu, C. Yin, Z. Wang, P. Du, S. Qu, C. W. Leung, *J. Mater. Chem. C* **2018**, *6*, 4737.
- [2] S. Wang, P. Xiao, Y. Liang, J. Zhang, Y. Huang, S. Wu, S.-W. Kuo, T. Chen, *J. Mater. Chem. C* **2018**, *6*, 5140.
- [3] S. Majumder, T. Mondal, M. J. Deen, *Sensors* **2017**, *17*, 130.
- [4] S. S. Kwak, H.-J. Yoon, S.-W. Kim, *Adv. Funct. Mater.* **2019**, *29*, 1804533.
- [5] M. Parrilla, M. Cuartero, G. A. Crespo, *TrAC, Trends Anal. Chem.* **2019**, *110*, 303.
- [6] X. Zhou, L. Zhu, L. Fan, H. Deng, Q. Fu, *ACS Appl. Mater. Interfaces* **2018**, *10*, 31655.
- [7] C. M. Boutry, Y. Kaizawa, B. C. Schroeder, A. Chortos, A. Legrand, Z. Wang, J. Chang, P. Fox, Z. Bao, *Nat. Electron.* **2018**, *1*, 314.
- [8] B. W. An, S. Heo, S. Ji, F. Bien, J.-U. Park, *Nat. Commun.* **2018**, *9*, 2458.
- [9] J. Heikenfeld, A. Jajack, J. Rogers, P. Gutruf, L. Tian, T. Pan, R. Li, M. Khine, J. Kim, J. Wang, J. Kim, *Lab Chip* **2018**, *18*, 217.
- [10] R. Herbert, J.-H. Kim, Y. Kim, H. Lee, W.-H. Yeo, *Materials* **2018**, *11*, 187.
- [11] Y. Liu, M. Pharr, G. A. Salvatore, *ACS Nano* **2017**, *11*, 9614.
- [12] C. Wang, K. Xia, H. Wang, X. Liang, Z. Yin, Y. Zhang, *Adv. Mater.* **2019**, *31*, e1801072.
- [13] Y. Zhang, L. Zhang, K. Cui, S. Ge, X. Cheng, M. Yan, J. Yu, H. Liu, *Adv. Mater.* **2018**, *30*, 1801588.
- [14] H.-R. Lee, C.-C. Kim, J.-Y. Sun, *Adv. Mater.* **2018**, *30*, 1704403.
- [15] J. Kim, I. Jeerapan, J. R. Sempionatto, A. Barfidokht, R. K. Mishra, A. S. Campbell, L. J. Hubble, J. Wang, *Acc. Chem. Res.* **2018**, *51*, 2820.
- [16] C. Wang, C. Wang, Z. Huang, S. Xu, *Adv. Mater.* **2018**, *30*, 1801368.
- [17] S. Huang, Y. Liu, Y. Zhao, Z. Ren, C. F. Guo, *Adv. Funct. Mater.* **2019**, *29*, 1805924.
- [18] T. Q. Trung, N.-E. Lee, *Adv. Mater.* **2017**, *29*, 1603167.
- [19] X. Yu, W. Shou, B. K. Mahajan, X. Huang, H. Pan, *Adv. Mater.* **2018**, *30*, 1707624.
- [20] W. Wu, H. Haick, *Adv. Mater.* **2018**, *30*, 1705024.
- [21] T.-P. Huynh, H. Haick, *Adv. Mater.* **2018**, *30*, 1802337.
- [22] S. Yao, P. Swetha, Y. Zhu, *Adv. Healthcare Mater.* **2018**, *7*, 1700889.
- [23] S. Gong, W. L. Cheng, *Adv. Electron. Mater.* **2017**, *3*, 1600314.
- [24] S. K. Garlapati, M. Divya, B. Breitung, R. Kruk, H. Hahn, S. Dasgupta, *Adv. Mater.* **2018**, *30*, 1707600.
- [25] I. Hwang, H. N. Kim, M. Seong, S.-H. Lee, M. Kang, H. Yi, W. G. Bae, M. K. Kwak, H. E. Jeong, *Adv. Healthcare Mater.* **2018**, *7*, 1800275.
- [26] T. R. Ray, J. Choi, A. J. Bandodkar, S. Krishnan, P. Gutruf, L. Tian, R. Ghaffari, J. A. Rogers, *Chem. Rev.* **2019**, *119*, 5461.
- [27] Q. Li, L.-N. Zhang, X.-M. Tao, X. Ding, *Adv. Healthcare Mater.* **2017**, *6*, 1601371.
- [28] R.-C. Qian, Y.-T. Long, *ChemistryOpen* **2018**, *7*, 118.
- [29] M. Y. Lee, H. R. Lee, C. H. Park, S. G. Han, J. H. Oh, *Acc. Chem. Res.* **2018**, *51*, 2829.
- [30] S. F. Zhao, J. H. Li, D. X. Cao, G. P. Zhang, J. Li, K. Li, Y. Yang, W. Wang, Y. F. Jin, R. Sun, C. P. Wong, *ACS Appl. Mater. Interfaces* **2017**, *9*, 12147.
- [31] T. T. Yang, D. Xie, Z. H. Li, H. W. Zhu, *Mater. Sci. Eng., R* **2017**, *115*, 1.
- [32] M. Bariya, H. Y. Y. Nyein, A. Javey, *Nat. Electron.* **2018**, *1*, 160.
- [33] J. Li, R. Bao, J. Tao, Y. Peng, C. Pan, *J. Mater. Chem. C* **2018**, *6*, 11878.
- [34] E. Rovini, C. Maremmani, F. Cavallo, *Front. Neurosci.* **2017**, *11*, 555.
- [35] M. M. Baig, H. Gholamhosseini, A. A. Moqeeem, F. Mirza, M. Lindén, *J. Med. Syst.* **2017**, *41*, 115.
- [36] T. Q. Trung, N. E. Lee, *Adv. Mater.* **2016**, *28*, 4338.
- [37] Z. Pang, G. Yang, R. Khedri, Y. Zhang, *IEEE Rev. Biomed. Eng.* **2018**, *11*, 249.
- [38] H. Jin, Y. S. Abu-Raya, H. Haick, *Adv. Healthcare Mater.* **2017**, *6*, 1700024.
- [39] A. K. Yetisen, J. L. Martinez-Hurtado, B. Ünal, A. Khademhosseini, H. Butt, *Adv. Mater.* **2018**, *30*, 1706910.
- [40] J. H. Koo, D. C. Kim, H. J. Shim, T. H. Kim, D. H. Kim, *Adv. Funct. Mater.* **2018**, *28*, 1801834.
- [41] W. Liu, M. S. Song, B. Kong, Y. Cui, *Adv. Mater.* **2017**, *29*, 1603436.
- [42] X. Pu, W. Hu, Z. L. Wang, *Small* **2018**, *14*, 1702817.
- [43] D. P. Dubal, N. R. Chodankar, D.-H. Kim, P. Gomez-Romero, *Chem. Soc. Rev.* **2018**, *47*, 2065.
- [44] C. Xie, F. Yan, *Small* **2017**, *13*, 1701822.
- [45] C. Wan, G. Chen, Y. Fu, M. Wang, N. Matsuhisa, S. Pan, L. Pan, H. Yang, Q. Wan, L. Zhu, X. Chen, *Adv. Mater.* **2018**, *30*, 1801291.
- [46] K. K. Kim, S. Hong, H. M. Cho, J. Lee, Y. D. Suh, J. Ham, S. H. Ko, *Nano Lett.* **2015**, *15*, 5240.
- [47] D.-H. Kim, J. Song, W. M. Choi, H.-S. Kim, R.-H. Kim, Z. Liu, Y. Y. Huang, K.-C. Hwang, Y.-W. Zhang, J. A. Rogers, *Proc. Natl. Acad. Sci. USA* **2008**, *105*, 18675.
- [48] J. C. K. Tham, *J. Tech. Writing Commun.* **2016**, *47*, 22.
- [49] S. A. Wood, *Comput. Compos.* **2018**, *50*, 66.
- [50] W. Gao, S. Emaminejad, H. Y. Y. Nyein, S. Challal, K. Chen, A. Peck, H. M. Fahad, H. Ota, H. Shiraki, D. Kiriyama, D.-H. Lien, G. A. Brooks, R. W. Davis, A. Javey, *Nature* **2016**, *529*, 509.
- [51] S. Mishra, J. J. S. Norton, Y. Lee, D. S. Lee, N. Agee, Y. Chen, Y. Chun, W.-H. Yeo, *Biosens. Bioelectron.* **2017**, *91*, 796.
- [52] C. Howe, S. Mishra, Y.-S. Kim, Y. Chen, S.-H. Ye, W. R. Wagner, J.-W. Jeong, H.-S. Byun, J.-H. Kim, Y. Chun, W.-H. Yeo, *ACS Nano* **2018**, *12*, 8706.
- [53] D.-H. Kim, N. Lu, R. Ma, Y.-S. Kim, R.-H. Kim, S. Wang, J. Wu, S. M. Won, H. Tao, A. Islam, K. J. Yu, T.-I. Kim, R. Chowdhury, M. Ying, L. Xu, M. Li, H.-J. Chung, H. Keum, M. McCormick, P. Liu, Y.-W. Zhang, F. G. Omenetto, Y. Huang, T. Coleman, J. A. Rogers, *Science* **2011**, *333*, 838.
- [54] W.-H. Yeo, Y.-S. Kim, J. Lee, A. Ameen, L. Shi, M. Li, S. Wang, R. Ma, S. H. Jin, Z. Kang, Y. Huang, J. A. Rogers, *Adv. Mater.* **2013**, *25*, 2773.
- [55] Y. Lee, C. Howe, S. Mishra, D. S. Lee, M. Mahmood, M. Piper, Y. Kim, K. Tieu, H.-S. Byun, J. P. Coffey, M. Shayan, Y. Chun, R. M. Costanzo, W.-H. Yeo, *Proc. Natl. Acad. Sci. USA* **2018**, *115*, 5377.
- [56] R. Yin, Z. Xu, M. Mei, Z. Chen, K. Wang, Y. Liu, T. Tang, M. K. Priydarshi, X. Meng, S. Zhao, B. Deng, H. Peng, Z. Liu, X. Duan, *Nat. Commun.* **2018**, *9*, 2334.
- [57] R. Feiner, T. Dvir, *Nat. Rev. Mater.* **2018**, *3*, 17076.

- [58] B. Shi, Z. Li, Y. Fan, *Adv. Mater.* **2018**, *30*, 1801511.
- [59] Y.-H. Joung, *Int. Neurorol. J.* **2013**, *17*, 98.
- [60] M. Liu, X. Pu, C. Jiang, T. Liu, X. Huang, L. Chen, C. Du, J. Sun, W. Hu, Z. L. Wang, *Adv. Mater.* **2017**, *29*, 1703700.
- [61] D.-H. Kim, J.-H. Ahn, W. M. Choi, H.-S. Kim, T.-H. Kim, J. Song, Y. Y. Huang, Z. Liu, C. Lu, J. A. Rogers, *Science* **2008**, *320*, 507.
- [62] R. C. Webb, A. P. Bonifas, A. Behnaz, Y. Zhang, K. J. Yu, H. Cheng, M. Shi, Z. Bian, Z. Liu, Y.-S. Kim, *Nat. Mater.* **2013**, *12*, 938.
- [63] O. Parlak, S. T. Keene, A. Marais, V. F. Curto, A. Salleo, *Sci. Adv.* **2018**, *4*, eaar2904.
- [64] N. Kalid, A. A. Zaidan, B. B. Zaidan, O. H. Salman, M. Hashim, H. Muzammil, *J. Med. Syst.* **2018**, *42*, 30.
- [65] P. Kumari, L. Mathew, P. Syal, *Biosens. Bioelectron.* **2017**, *90*, 298.
- [66] Y. Lu, K. Jiang, D. Chen, G. Shen, *Nano Energy* **2019**, *58*, 624.
- [67] Z. Liu, J. Nie, B. Miao, J. Li, Y. Cui, S. Wang, X. Zhang, G. Zhao, Y. Deng, Y. Wu, Z. Li, L. Li, Z. L. Wang, *Adv. Mater.* **2019**, *31*, 1807795.
- [68] M. Wu, Y. Wang, S. Gao, R. Wang, C. Ma, Z. Tang, N. Bao, W. Wu, F. Fan, W. Wu, *Nano Energy* **2019**, *56*, 693.
- [69] G. Xu, C. Cheng, Z. Liu, W. Yuan, X. Wu, Y. Lu, S. S. Low, J. Liu, L. Zhu, D. Ji, S. Li, Z. Chen, L. Wang, Q. Yang, Z. Cui, Q. Liu, *Adv. Mater. Technol.* **2019**, *1800658*, <https://doi.org/10.1002/admt.201800658>.
- [70] S. R. Krishnan, C.-J. Su, Z. Xie, M. Patel, S. R. Madhvapathy, Y. Xu, J. Freudman, B. Ng, S. Y. Heo, H. Wang, T. R. Ray, J. Leshock, I. Stankiewicz, X. Feng, Y. Huang, P. Gutruf, J. A. Rogers, *Small* **2018**, *14*, 1803192.
- [71] M. Ferrari, V. Quaresima, *NeuroImage* **2012**, *63*, 921.
- [72] Y. Khan, D. Han, A. Pierre, J. Ting, X. Wang, C. M. Lochner, G. Bovo, N. Yaacobi-Gross, C. Newsome, R. Wilson, A. C. Arias, *Proc. Natl. Acad. Sci. USA* **2018**, *115*, E11015.
- [73] N. Kazem, T. Hellebrekers, C. Majidi, *Adv. Mater.* **2017**, *29*, 1605985.
- [74] D. J. Lipomi, *Adv. Mater.* **2016**, *28*, 4180.
- [75] A. F. Jankowski, T. Tsakalakos, *J. Phys. F: Met. Phys.* **1985**, *15*, 1279.
- [76] R. J. Roberts, R. C. Rowe, *Int. J. Pharm.* **1987**, *37*, 15.
- [77] A. I. Fedorchenko, A.-B. Wang, H. H. Cheng, *Appl. Phys. Lett.* **2009**, *94*, 152111.
- [78] M. P. Wolf, G. B. Salieb-Beugelaar, P. Hunziker, *Prog. Polym. Sci.* **2018**, *83*, 97.
- [79] R. A. Hardin, C. Beckermann, *Metall. Mater. Trans. A* **2013**, *44*, 5316.
- [80] T. J. Wallin, J. Pikul, R. F. Shepherd, *Nat. Rev. Mater.* **2018**, *3*, 84.
- [81] R. A. Nawrocki, H. Jin, S. Lee, T. Yokota, M. Sekino, T. Someya, *Adv. Funct. Mater.* **2018**, *28*, 1803279.
- [82] N. S. Lu, Z. G. Suo, J. J. Vlassak, *Acta Mater.* **2010**, *58*, 1679.
- [83] S. Gupta, W. T. Navaraj, L. Lorenzelli, R. Dahiya, *npj Flexible Electron.* **2018**, *2*, 8.
- [84] D. Yin, J. Feng, R. Ma, Y.-F. Liu, Y.-L. Zhang, X.-L. Zhang, Y.-G. Bi, Q.-D. Chen, H.-B. Sun, *Nat. Commun.* **2016**, *7*, 11573.
- [85] S. I. Park, D. S. Brenner, G. Shin, C. D. Morgan, B. A. Copits, H. U. Chung, M. Y. Pullen, K. N. Noh, S. Davidson, S. J. Oh, J. Yoon, K.-I. Jang, V. K. Samineni, M. Norman, J. G. Grajales-Reyes, S. K. Vogt, S. S. Sundaram, K. M. Wilson, J. S. Ha, R. Xu, T. Pan, T.-I. Kim, Y. Huang, M. C. Montana, J. P. Golden, M. R. Bruchas, R. W. GereauIV, J. A. Rogers, *Nat. Biotechnol.* **2015**, *33*, 1280.
- [86] Y. Zhang, S. Wang, X. Li, J. A. Fan, S. Xu, Y. M. Song, K. J. Choi, W. H. Yeo, W. Lee, S. N. Nazaar, *Adv. Funct. Mater.* **2014**, *24*, 2028.
- [87] I. W. Frank, D. M. Tanenbaum, A. M. Van der Zande, P. L. McEuen, *J. Vac. Sci. Technol. B* **2007**, *25*, 2558.
- [88] C. Lee, X. Wei, J. W. Kysar, J. Hone, *Science* **2008**, *321*, 385.
- [89] V. Georgakilas, J. A. Perman, J. Tucek, R. Zboril, *Chem. Rev.* **2015**, *115*, 4744.
- [90] B.-J. Wen, S.-A. Huang, *IEEE Sens. J.* **2019**, *19*, 1701.
- [91] Y. Khan, A. E. Ostfeld, C. M. Lochner, A. Pierre, A. C. Arias, *Adv. Mater.* **2016**, *28*, 4373.
- [92] M. Ha, S. Lim, H. Ko, *J. Mater. Chem. B* **2018**, *6*, 4043.
- [93] J. Rivnay, S. Inal, A. Salleo, R. M. Owens, M. Berggren, G. G. Malliaras, *Nat. Rev. Mater.* **2018**, *3*, 17086.
- [94] W. G. Bae, D. Kim, M. K. Kwak, L. Ha, S. M. Kang, K. Y. Suh, *Adv. Healthcare Mater.* **2013**, *2*, 109.
- [95] J. Chen, J. Zheng, Q. Gao, J. Zhang, J. Zhang, O. Ormisore, L. Wang, H. Li, *Appl. Sci.* **2018**, *8*, 345.
- [96] T. Someya, Z. N. Bao, G. G. Malliaras, *Nature* **2016**, *540*, 379.
- [97] N. Adly, S. Weidlich, S. Seyock, F. Brings, A. Yakushenko, A. Offenhäusser, B. Wolfrum, *npj Flexible Electron.* **2018**, *2*, 15.
- [98] B. Sun, R. N. McCay, S. Goswami, Y. Xu, C. Zhang, Y. Ling, J. Lin, Z. Yan, *Adv. Mater.* **2018**, *30*, 1804327.
- [99] X. Zheng, H. Lee, T. H. Weisgraber, M. Shusteff, J. DeOtte, E. B. Duoss, J. D. Kuntz, M. M. Biener, Q. Ge, J. A. Jackson, S. O. Kucheyev, N. X. Fang, C. M. Spadaccini, *Science* **2014**, *344*, 1373.
- [100] M. Ha, S. Lim, S. Cho, Y. Lee, S. Na, C. Baig, H. Ko, *ACS Nano* **2018**, *12*, 3964.
- [101] S. Wang, J. Xu, W. Wang, G.-J. N. Wang, R. Rastak, F. Molina-Lopez, J. W. Chung, S. Niu, V. R. Feig, J. Lopez, T. Lei, S.-K. Kwon, Y. Kim, A. M. Foudeh, A. Ehrlich, A. Gasperini, Y. Yun, B. Murmann, J. B. H. Tok, Z. Bao, *Nature* **2018**, *555*, 83.
- [102] J. Kang, D. Son, G.-J. N. Wang, Y. Liu, J. Lopez, Y. Kim, J. Y. Oh, T. Katsumata, J. Mun, Y. Lee, L. Jin, J. B. H. Tok, Z. Bao, *Adv. Mater.* **2018**, *30*, 1706846.
- [103] R. Li, K. Zhang, L. Cai, G. Chen, M. He, *Polymer* **2019**, *167*, 154.
- [104] H. Qiao, P. Qi, X. Zhang, L. Wang, Y. Tan, Z. Luan, Y. Xia, Y. Li, K. Sui, *ACS Appl. Mater. Interfaces* **2019**, *11*, 7755.
- [105] Q. Zhang, X. Liu, L. Duan, G. Gao, *Chem. Eng. J.* **2019**, *365*, 10.
- [106] Y. Du, J. Ge, Y. Li, P. X. Ma, B. Lei, *Biomaterials* **2018**, *157*, 40.
- [107] S. Ling, D. L. Kaplan, M. J. Buehler, *Nat. Rev. Mater.* **2018**, *3*, 18016.
- [108] P. Beri, B. F. Matte, L. Fattet, D. Kim, J. Yang, A. J. Engler, *Nat. Rev. Mater.* **2018**, *3*, 418.
- [109] G. Chen, N. Matsuhisa, Z. Liu, D. Qi, P. Cai, Y. Jiang, C. Wan, Y. Cui, W. R. Leow, Z. Liu, S. Gong, K.-Q. Zhang, Y. Cheng, X. Chen, *Adv. Mater.* **2018**, *30*, 1800129.
- [110] C. Hou, Z. Xu, W. Qiu, R. Wu, Y. Wang, Q. Xu, X. Y. Liu, W. Guo, *Small* **2019**, *15*, 1805084.
- [111] R. Xiong, A. M. Grant, R. Ma, S. Zhang, V. V. Tsukruk, *Mater. Sci. Eng., R* **2018**, *125*, 1.
- [112] R. Liu, X. Kuang, J. Deng, Y.-C. Wang, A. C. Wang, W. Ding, Y.-C. Lai, J. Chen, P. Wang, Z. Lin, H. J. Qi, B. Sun, Z. L. Wang, *Adv. Mater.* **2018**, *30*, 1705195.
- [113] G. Ico, A. Showalter, W. Bosze, S. C. Gott, B. S. Kim, M. P. Rao, N. V. Myung, J. Nam, *J. Mater. Chem. A* **2016**, *4*, 2293.
- [114] S. K. Ghosh, D. Mandal, *Nano Energy* **2018**, *53*, 245.
- [115] D. Rus, M. T. Tolley, *Nature* **2015**, *521*, 467.
- [116] J. Shintake, V. Cacucciolo, D. Floreano, H. Shea, *Adv. Mater.* **2018**, *30*, 1707035.
- [117] S. Kim, C. Laschi, B. Trimmer, *Trends Biotechnol.* **2013**, *31*, 287.
- [118] L. V. Kayser, D. J. Lipomi, *Adv. Mater.* **2019**, *31*, 1806133.
- [119] J. A. Fan, W.-H. Yeo, Y. Su, Y. Hattori, W. Lee, S.-Y. Jung, Y. Zhang, Z. Liu, H. Cheng, L. Falgout, *Nat. Commun.* **2014**, *5*, 3266.
- [120] S. Xu, Y. Zhang, J. Cho, J. Lee, X. Huang, L. Jia, J. A. Fan, Y. Su, J. Su, H. Zhang, H. Cheng, B. Lu, C. Yu, C. Chuang, T.-I. Kim, T. Song, K. Shigeta, S. Kang, C. Dagdeviren, I. Petrov, P. V. Braun, Y. Huang, U. Paik, J. A. Rogers, *Nat. Commun.* **2013**, *4*, 1543.
- [121] Z. Wang, L. Zhang, J. Liu, C. Li, *ACS Appl. Mater. Interfaces* **2019**, *11*, 5316.
- [122] H.-B. Lee, C.-W. Bae, L. T. Duy, I.-Y. Sohn, D.-I. Kim, Y.-J. Song, Y.-J. Kim, N.-E. Lee, *Adv. Mater.* **2016**, *28*, 3069.

- [123] E. Roh, H.-B. Lee, D.-I. Kim, N.-E. Lee, *Adv. Mater.* **2017**, *29*, 1703004.
- [124] T. C. Shyu, P. F. Damasceno, P. M. Dodd, A. Lamoureux, L. Xu, M. Shlian, M. Shtain, S. C. Glotzer, N. A. Kotov, *Nat. Mater.* **2015**, *14*, 785.
- [125] S. J. P. Callens, A. A. Zadpoor, *Mater. Today* **2018**, *21*, 241.
- [126] Y. Morikawa, S. Yamagiwa, H. Sawahata, R. Numano, K. Koida, M. Ishida, T. Kawano, *Adv. Healthcare Mater.* **2018**, *7*, 1701100.
- [127] Y.-S. Guan, Z. Zhang, Y. Tang, J. Yin, S. Ren, *Adv. Mater.* **2018**, *30*, 1706390.
- [128] W. Zheng, W. Huang, F. Gao, H. Yang, M. Dai, G. Liu, B. Yang, J. Zhang, Y. Q. Fu, X. Chen, Y. Qiu, D. Jia, Y. Zhou, P. Hu, *Chem. Mater.* **2018**, *30*, 6063.
- [129] Z. Lv, Y. Luo, Y. Tang, J. Wei, Z. Zhu, X. Zhou, W. Li, Y. Zeng, W. Zhang, Y. Zhang, D. Qi, S. Pan, X. J. Loh, X. Chen, *Adv. Mater.* **2018**, *30*, 1704531.
- [130] K. Nan, S. D. Kang, K. Li, K. J. Yu, F. Zhu, J. Wang, A. C. Dunn, C. Zhou, Z. Xie, M. T. Agne, H. Wang, H. Luan, Y. Zhang, Y. Huang, G. J. Snyder, J. A. Rogers, *Sci. Adv.* **2018**, *4*, eaau5849.
- [131] C. Wang, X. Li, H. Hu, L. Zhang, Z. Huang, M. Lin, Z. Zhang, Z. Yin, B. Huang, H. Gong, S. Bhaskaran, Y. Gu, M. Makihata, Y. Guo, Y. Lei, Y. Chen, C. Wang, Y. Li, T. Zhang, Z. Chen, A. P. Pisano, L. Zhang, Q. Zhou, S. Xu, *Nat. Biomed. Eng.* **2018**, *2*, 687.
- [132] D. Son, J. Kang, O. Vardoulis, Y. Kim, N. Matsuhisa, J. Y. Oh, J. W. F. To, J. Mun, T. Katsumata, Y. Liu, A. F. McGuire, M. Krason, F. Molina-Lopez, J. Ham, U. Kraft, Y. Lee, Y. Yun, J. B. H. Tok, Z. Bao, *Nat. Nanotechnol.* **2018**, *13*, 1057.
- [133] K. Qi, J. He, H. Wang, Y. Zhou, X. You, N. Nan, W. Shao, L. Wang, B. Ding, S. Cui, *ACS Appl. Mater. Interfaces* **2017**, *9*, 42951.
- [134] S. Choi, S. I. Han, D. Jung, H. J. Hwang, C. Lim, S. Bae, O. K. Park, C. M. Tschabrunn, M. Lee, S. Y. Bae, J. W. Yu, J. H. Ryu, S.-W. Lee, K. Park, P. M. Kang, W. B. Lee, R. Nezafat, T. Hyeon, D.-H. Kim, *Nat. Nanotechnol.* **2018**, *13*, 1048.
- [135] S. Duan, Z. Wang, L. Zhang, J. Liu, C. Li, *Adv. Mater. Technol.* **2018**, *3*, 1800020.
- [136] C. Zhu, A. Chortos, Y. Wang, R. Pfattner, T. Lei, A. C. Hinckley, I. Pochorovski, X. Yan, J. W. F. To, J. Y. Oh, J. B. H. Tok, Z. Bao, B. Murmann, *Nat. Electron.* **2018**, *1*, 183.
- [137] K. Dong, Z. Wu, J. Deng, A. C. Wang, H. Zou, C. Chen, D. Hu, B. Gu, B. Sun, Z. L. Wang, *Adv. Mater.* **2018**, *30*, 1804944.
- [138] W. Guo, P. Zheng, X. Huang, H. Zhuo, Y. Wu, Z. Yin, Z. Li, H. Wu, *ACS Appl. Mater. Interfaces* **2019**, *11*, 8567.
- [139] X. Shi, S. Liu, Y. Sun, J. Liang, Y. Chen, *Adv. Funct. Mater.* **2018**, *28*, 1800850.
- [140] J.-E. Lim, S. Yoon, B.-U. Hwang, N.-E. Lee, H.-K. Kim, *Adv. Mater. Interfaces* **2019**, *6*, 1801936.
- [141] C. Choi, Y. Lee, K. W. Cho, J. H. Koo, D.-H. Kim, *Acc. Chem. Res.* **2019**, *52*, 73.
- [142] Y. Ma, N. Liu, L. Li, X. Hu, Z. Zou, J. Wang, S. Luo, Y. Gao, *Nat. Commun.* **2017**, *8*, 1207.
- [143] X. Shi, H. Wang, X. Xie, Q. Xue, J. Zhang, S. Kang, C. Wang, J. Liang, Y. Chen, *ACS Nano* **2018**, *13*, 649.
- [144] T.-H. Kim, C.-S. Lee, S. Kim, J. Hur, S. Lee, K. W. Shin, Y.-Z. Yoon, M. K. Choi, J. Yang, D.-H. Kim, T. Hyeon, S. Park, S. Hwang, *ACS Nano* **2017**, *11*, 5992.
- [145] R. Nur, N. Matsuhisa, Z. Jiang, M. O. G. Nayem, T. Yokota, T. Someya, *Nano Lett.* **2018**, *18*, 5610.
- [146] Y. Yu, C. Yan, Z. Zheng, *Adv. Mater.* **2014**, *26*, 5508.
- [147] N. Li, S. Bedell, H. Hu, S.-J. Han, X. H. Liu, K. Saenger, D. Sadana, *Adv. Mater.* **2017**, *29*, 1606638.
- [148] Z. Huang, Y. Hao, Y. Li, H. Hu, C. Wang, A. Nomoto, T. Pan, Y. Gu, Y. Chen, T. Zhang, W. Li, Y. Lei, N. Kim, C. Wang, L. Zhang, J. W. Ward, A. Maralani, X. Li, M. F. Durstock, A. Pisano, Y. Lin, S. Xu, *Nat. Electron.* **2018**, *1*, 473.
- [149] A. Hirsch, H. O. Michaud, A. P. Gerratt, S. de Mulatier, S. P. Lacour, *Adv. Mater.* **2016**, *28*, 4507.
- [150] Y. Yang, N. Sun, Z. Wen, P. Cheng, H. Zheng, H. Shao, Y. Xia, C. Chen, H. Lan, X. Xie, C. Zhou, J. Zhong, X. Sun, S.-T. Lee, *ACS Nano* **2018**, *12*, 2027.
- [151] Y. Yoon, S. Kim, D. Kim, S. K. Kauh, J. Lee, *Adv. Mater. Technol.* **2019**, *4*, 1800379.
- [152] C. Pan, K. Kumar, J. Li, E. J. Markvicka, P. R. Herman, C. Majidi, *Adv. Mater.* **2018**, *30*, 1706937.
- [153] C. Shao, M. Wang, L. Meng, H. Chang, B. Wang, F. Xu, J. Yang, P. Wan, *Chem. Mater.* **2018**, *30*, 3110.
- [154] G. Zhang, M. McBride, N. Persson, S. Lee, T. J. Dunn, M. F. Toney, Z. Yuan, Y.-H. Kwon, P.-H. Chu, B. Ristein, E. Reichmanis, *Chem. Mater.* **2017**, *29*, 7645.
- [155] C.-H. Li, C. Wang, C. Keplinger, J.-L. Zuo, L. Jin, Y. Sun, P. Zheng, Y. Cao, F. Lissel, C. Linder, X.-Z. You, Z. Bao, *Nat. Chem.* **2016**, *8*, 618.
- [156] T. Wang, Y. Zhang, Q. C. Liu, W. Cheng, X. R. Wang, L. J. Pan, B. X. Xu, H. X. Xu, *Adv. Funct. Mater.* **2018**, *28*, 1705551.
- [157] L. Shi, T. Zhu, G. Gao, X. Zhang, W. Wei, W. Liu, S. Ding, *Nat. Commun.* **2018**, *9*, 2630.
- [158] M. S. Sarwar, Y. Dobashi, C. Preston, J. K. Wyss, S. Mirabbasi, J. D. Madden, *Sci. Adv.* **2017**, *3*, e1602200.
- [159] C. Narayanaswami, M. T. Raghunath, presented at *Defense, Security, and Cockpit Displays*, **2004**.
- [160] A. Tinka, Q. Wu, K. Weekly, C. A. Oroza, J. Beard, A. M. Bayen, *J. Field Robotics* **2016**, *33*, 618.
- [161] Y. Yu, D. Yu, B. Sadighi, C. A. Orme, *Nat. Comm.* **2018**, *9*, 4211.
- [162] M. Kaltenbrunner, G. Adam, E. D. Glowacki, M. Drack, R. Schwodrauer, L. Leonat, D. H. Apaydin, H. Groiss, M. C. Scharber, M. S. White, N. S. Sariciftci, S. Bauer, *Nat. Mater.* **2015**, *14*, 1032.
- [163] M. Kaltenbrunner, T. Sekitani, J. Reeder, T. Yokota, K. Kuribara, T. Tokuhara, M. Drack, R. Schwodrauer, I. Graz, S. Bauer-Gogonea, S. Bauer, T. Someya, *Nature* **2013**, *499*, 458.
- [164] M. Kaltenbrunner, M. S. White, E. D. Glowacki, T. Sekitani, T. Someya, N. S. Sariciftci, S. Bauer, *Nat. Commun.* **2012**, *3*, 770.
- [165] H. Ren, N. Cui, Q. Tang, Y. Tong, X. Zhao, Y. Liu, *Small* **2018**, *14*, 1801020.
- [166] Y. Liang, P. Xiao, S. Wang, J. Shi, J. He, J. Zhang, Y. Huang, T. Chen, *J. Mater. Chem. C* **2018**, *6*, 6666.
- [167] C. Yan, W. Deng, L. Jin, T. Yang, Z. Wang, X. Chu, H. Su, J. Chen, W. Yang, *ACS Appl. Mater. Interfaces* **2018**, *10*, 41070.
- [168] Y. Ding, T. Xu, O. Onyilagha, H. Fong, Z. Zhu, *ACS Appl. Mater. Interfaces* **2019**, *11*, 6685.
- [169] S. Y. Oh, S. Y. Hong, Y. R. Jeong, J. Yun, H. Park, S. W. Jin, G. Lee, J. H. Oh, H. Lee, S.-S. Lee, J. S. Ha, *ACS Appl. Mater. Interfaces* **2018**, *10*, 13729.
- [170] J. Kim, J. R. Sempionatto, S. Imani, M. C. Hartel, A. Barfodokht, G. Tang, A. S. Campbell, P. P. Mercier, J. Wang, *Adv. Sci.* **2018**, *5*, 1800880.
- [171] S. Kabiri Ameri, R. Ho, H. Jang, L. Tao, Y. Wang, L. Wang, D. M. Schnyer, D. Akinwande, N. Lu, *ACS Nano* **2017**, *11*, 7634.
- [172] P. A. Lopes, H. Paisana, A. T. De Almeida, C. Majidi, M. Tavakoli, *ACS Appl. Mater. Interfaces* **2018**, *10*, 38760.
- [173] T. An, Y. Ling, S. Gong, B. Zhu, Y. Zhao, D. Dong, L. W. Yap, Y. Wang, W. Cheng, *Adv. Mater. Technol.* **2019**, *4*, 1800473.
- [174] W. C. Mak, K. Y. Cheung, J. Orban, C. J. Lee, A. P. F. Turner, M. Griffith, *ACS Appl. Mater. Interfaces* **2015**, *7*, 25487.
- [175] H. Lee, S. Kim, K.-B. Kim, J.-W. Choi, *Nano Energy* **2018**, *53*, 225.
- [176] A. M. Zamarayeva, A. E. Ostfeld, M. Wang, J. K. Duey, I. Deckman, B. P. Lechene, G. Davies, D. A. Steingart, A. C. Arias, *Sci. Adv.* **2017**, *3*, e1602051.
- [177] M. C. Brothers, M. DeBrosse, C. C. Grigsby, R. R. Naik, S. M. Hussain, J. Heikenfeld, S. S. Kim, *Acc. Chem. Res.* **2019**, *52*, 297.

- [178] J. Choi, R. Ghaffari, L. B. Baker, J. A. Rogers, *Sci. Adv.* **2018**, *4*, eaar3921.
- [179] J. Choi, D. Kang, S. Han, S. B. Kim, J. A. Rogers, *Adv. Healthcare Mater.* **2017**, *6*, 1601355.
- [180] M. Mehrali, S. Bagherifard, M. Akbari, A. Thakur, B. Mirani, M. Mehrali, M. Hasany, G. Orive, P. Das, J. Emneus, T. L. Andresen, A. Dolatshahi-Pirouz, *Adv. Sci.* **2018**, *5*, 1700931.
- [181] B. Zhang, A. Korolj, B. F. L. Lai, M. Radisic, *Nat. Rev. Mater.* **2018**, *3*, 257.
- [182] N. Wongkaew, M. Simsek, C. Griesche, A. J. Baeumner, *Chem. Rev.* **2019**, *119*, 120.
- [183] X. Wang, Y. Zhang, X. Zhang, Z. Huo, X. Li, M. Que, Z. Peng, H. Wang, C. Pan, *Adv. Mater.* **2018**, *30*, 1706738.
- [184] Y. J. Fan, X. Li, S. Y. Kuang, L. Zhang, Y. H. Chen, L. Liu, K. Zhang, S. W. Ma, F. Liang, T. Wu, Z. L. Wang, G. Zhu, *ACS Nano* **2018**, *12*, 9326.
- [185] D. Lee, J. Kim, H. Kim, H. Heo, K. Park, Y. Lee, *Nanoscale* **2018**, *10*, 18812.
- [186] F. Pengdong, J. Hongjun, Z. Ling, L. Xuan, L. Xuesong, H. Peng, F. Huanghuang, Z. Jiaheng, M. Xing, Z. Weiwei, *Nanotechnology* **2019**, *30*, 185501.
- [187] K. B. Kim, W. Jang, J. Y. Cho, S. B. Woo, D. H. Jeon, J. H. Ahn, S. Do Hong, H. Y. Koo, T. H. Sung, *Nano Energy* **2018**, *54*, 91.
- [188] D. J. Liporni, M. Vosgueritchian, B. C. K. Tee, S. L. Hellstrom, J. A. Lee, C. H. Fox, Z. Bao, *Nat. Nanotechnol.* **2011**, *6*, 788.
- [189] P. Wang, Z. Peng, M. Li, Y. Wang, *Small* **2018**, *14*, 1802625.
- [190] D.-W. Shin, M. D. Barnes, K. Walsh, D. Dimov, P. Tian, A. I. S. Neves, C. D. Wright, S. M. Yu, J.-B. Yoo, S. Russo, M. F. Craciun, *Adv. Mater.* **2018**, *30*, 1802953.
- [191] J.-H. Kim, S.-R. Kim, H.-J. Kil, Y.-C. Kim, J.-W. Park, *Nano Lett.* **2018**, *18*, 4531.
- [192] M.-S. Hong, G.-M. Choi, J. Kim, J. Jang, B. Choi, J.-K. Kim, S. Jeong, S. Leem, H.-Y. Kwon, H.-B. Hwang, H.-G. Im, J.-U. Park, B.-S. Bae, J. Jin, *Adv. Funct. Mater.* **2018**, *28*, 1705480.
- [193] L.-D. Koh, J. Yeo, Y. Y. Lee, Q. Ong, M. Han, B. C. K. Tee, *Mater. Sci. Eng., C* **2018**, *86*, 151.
- [194] J. Huang, H. Zhu, Y. Chen, C. Preston, K. Rohrbach, J. Cumings, L. Hu, *ACS Nano* **2013**, *7*, 2106.
- [195] Z. Zhu, R. Li, T. Pan, *Adv. Mater.* **2018**, *30*, 1705122.
- [196] C. Yang, Z. Suo, *Nat. Rev. Mater.* **2018**, *3*, 125.
- [197] Y. Wang, F. Huang, X. Chen, X.-W. Wang, W.-B. Zhang, J. Peng, J. Li, M. Zhai, *Chem. Mater.* **2018**, *30*, 4289.
- [198] K. Kim, Y.-G. Park, B. G. Hyun, M. Choi, J.-U. Park, *Adv. Mater.* **2019**, *31*, 1804690.
- [199] L. Mestach, S. Huygens, A. Goossens, L. Gilissen, *Contact Dermatitis* **2018**, *79*, 81.
- [200] K. Zulkowski, *Adv. Skin Wound Care* **2017**, *30*, 372.
- [201] C. L. Laurie McNichol, T. Rosen, M. Gray, J. Wound Ostomy Continence Nurs. **2013**, *40*, E1.
- [202] J. M. Karp, R. Langer, *Nature* **2011**, *477*, 42.
- [203] S. Chun, D. W. Kim, S. Baik, H. J. Lee, J. H. Lee, S. H. Bhang, C. Pang, *Adv. Funct. Mater.* **2018**, *28*, 1805224.
- [204] D.-M. Drotlef, M. Amjadi, M. Yunusa, M. Sitti, *Adv. Mater.* **2017**, *29*, 1701353.
- [205] D.-G. Hwang, K. Trent, M. D. Bartlett, *ACS Appl. Mater. Interfaces* **2018**, *10*, 6747.
- [206] L. Han, K. Liu, M. Wang, K. Wang, L. Fang, H. Chen, J. Zhou, X. Lu, *Adv. Funct. Mater.* **2018**, *28*, 1704195.
- [207] X. Jing, H.-Y. Mi, Y.-J. Lin, E. Enriquez, X.-F. Peng, L.-S. Turng, *ACS Appl. Mater. Interfaces* **2018**, *10*, 20897.
- [208] Z. Tang, Q. Chen, F. Chen, L. Zhu, S. Lu, B. Ren, Y. Zhang, J. Yang, J. Zheng, *Chem. Mater.* **2019**, *31*, 179.
- [209] Z. Wang, J. Chen, L. Wang, G. Gao, Y. Zhou, R. Wang, T. Xu, J. Yin, J. Fu, *J. Mater. Chem. B* **2019**, *7*, 24.
- [210] Y. Yang, L. Guan, X. Li, Z. Gao, X. Ren, G. Gao, *ACS Appl. Mater. Interfaces* **2019**, *11*, 3428.
- [211] L. Han, L. Yan, M. Wang, K. Wang, L. Fang, J. Zhou, J. Fang, F. Ren, X. Lu, *Chem. Mater.* **2018**, *30*, 5561.
- [212] J. H. Oh, S. Y. Hong, H. Park, S. W. Jin, Y. R. Jeong, S. Y. Oh, J. Yun, H. Lee, J. W. Kim, J. S. Ha, *ACS Appl. Mater. Interfaces* **2018**, *10*, 7263.
- [213] A. Koh, D. Kang, Y. Xue, S. Lee, R. M. Pielak, J. Kim, T. Hwang, S. Min, A. Banks, P. Bastien, *Sci. Transl. Med.* **2016**, *8*, 366ra165.
- [214] Y. S. Shin, K. Cho, S. H. Lim, S. Chung, S.-J. Park, C. Chung, D.-C. Han, J. K. Chang, *J. Micromech. Microeng.* **2003**, *13*, 768.
- [215] J. Lewis, *Mater. Today* **2006**, *9*, 38.
- [216] T. Kim, T. Lee, G. Lee, Y. Choi, S. Kim, D. Kang, M. Choi, *Appl. Sci.* **2018**, *8*, 367.
- [217] E. Song, H. Fang, X. Jin, J. Zhao, C. Jiang, K. J. Yu, Y. Zhong, D. Xu, J. Li, G. Fang, H. Du, J. Zhang, J. M. Park, Y. Huang, M. A. Alam, Y. Mei, J. A. Rogers, *Adv. Electron. Mater.* **2017**, *3*, 1700077.
- [218] M. R. Khan, C. Trlica, J.-H. So, M. Valeri, M. D. Dickey, *ACS Appl. Mater. Interfaces* **2014**, *6*, 22467.
- [219] A. Hirsch, L. Dejace, H. O. Michaud, S. P. Lacour, *Acc. Chem. Res.* **2019**, *52*, 534.
- [220] X. Wang, W. Yao, R. Guo, X. Yang, J. Tang, J. Zhang, W. Gao, V. Timchenko, J. Liu, *Adv. Healthcare Mater.* **2018**, *7*, 1800318.
- [221] H. Liu, H. Qing, Z. Li, Y. L. Han, M. Lin, H. Yang, A. Li, T. J. Lu, F. Li, F. Xu, *Mater. Sci. Eng., R* **2017**, *112*, 1.
- [222] A. Miyamoto, S. Lee, N. F. Cooray, S. Lee, M. Mori, N. Matsuhisa, H. Jin, L. Yoda, T. Yokota, A. Itoh, M. Sekino, H. Kawasaki, T. Ebihara, M. Amagai, T. Someya, *Nat. Nanotechnol.* **2017**, *12*, 907.
- [223] M. Wang, J. M. Gorham, J. P. Killgore, M. Omidvar, H. Lin, F. W. DelRio, L. M. Cox, Z. Zhang, Y. Ding, *ACS Appl. Mater. Interfaces* **2017**, *9*, 28100.
- [224] J. Zhang, Y. Cheng, M. Tebyetekerwa, S. Meng, M. Zhu, Y. Lu, *Adv. Funct. Mater.* **2019**, *29*, 1806407.
- [225] H. Chang, Z. Sun, Q. Yuan, F. Ding, X. Tao, F. Yan, Z. Zheng, *Adv. Mater.* **2010**, *22*, 4872.
- [226] V. Berry, *Carbon* **2013**, *62*, 1.
- [227] W. Du, J. Nie, Z. Ren, T. Jiang, L. Xu, S. Dong, L. Zheng, X. Chen, H. Li, *Nano Energy* **2018**, *51*, 260.
- [228] K.-I. Jang, S. Y. Han, S. Xu, K. E. Mathewson, Y. Zhang, J.-W. Jeong, G.-T. Kim, R. C. Webb, J. W. Lee, T. J. Dawidczyk, R. H. Kim, Y. M. Song, W.-H. Yeo, S. Kim, H. Cheng, S. I. Rhee, J. Chung, B. Kim, H. U. Chung, D. Lee, Y. Yang, M. Cho, J. G. Gaspar, R. Carbonari, M. Fabiani, G. Gratton, Y. Huang, J. A. Rogers, *Nat. Commun.* **2014**, *5*, 4779.
- [229] T. A. Desai, D. J. Hansford, L. Leoni, M. Essenpreis, M. Ferrari, *Biosens. Bioelectron.* **2000**, *15*, 453.
- [230] C. Zhao, L.-Y. Li, M.-M. Guo, J. Zheng, *Chem. Pap.* **2012**, *66*, 323.
- [231] S. Campuzano, M. Pedrero, P. Yáñez-Sedeño, J. M. Pingarrón, *Int. J. Mol. Sci.* **2019**, *20*, 423.
- [232] P. Cai, B. Hu, W. R. Leow, X. Wang, X. J. Loh, Y. L. Wu, X. Chen, *Adv. Mater.* **2018**, *30*, 1800572.
- [233] T. S. Anirudhan, S. S. Nair, *Bioconjugate Chem.* **2018**, *29*, 3262.
- [234] T. S. Anirudhan, S. S. Nair, A. V. Sasidharan, *ACS Appl. Mater. Interfaces* **2017**, *9*, 44377.
- [235] S. M. Lee, H. J. Byeon, J. H. Lee, D. H. Baek, K. H. Lee, J. S. Hong, S. H. Lee, *Sci. Rep.* **2015**, *4*, 6074.
- [236] F. Yi, J. Wang, X. Wang, S. Niu, S. Li, Q. Liao, Y. Xu, Z. You, Y. Zhang, Z. L. Wang, *ACS Nano* **2016**, *10*, 6519.
- [237] H. Zhang, M. Chiao, *J. Med. Biol. Eng.* **2015**, *35*, 143.
- [238] *Chem. Eng. News* **1967**, *45*, 24.
- [239] J. T. Reeder, J. Choi, Y. Xue, P. Gutruf, J. Hanson, M. Liu, T. Ray, A. J. Bandodkar, R. Avila, W. Xia, S. Krishnan, S. Xu, K. Barnes, M. Pahnke, R. Ghaffari, Y. Huang, J. A. Rogers, *Sci. Adv.* **2019**, *5*, eaau6356.

- [240] L. Li, Y. Bai, L. Li, S. Wang, T. Zhang, *Adv. Mater.* **2017**, *29*, 1702517.
- [241] Y. Jin, L. Li, Y. Cheng, L. Kong, Q. Pei, F. Xiao, *Adv. Funct. Mater.* **2015**, *25*, 1581.
- [242] Y.-T. Kwon, Y.-S. Kim, Y. Lee, S. Kwon, M. Lim, Y. Song, Y.-H. Choa, W.-H. Yeo, *ACS Appl. Mater. Interfaces* **2018**, *10*, 44071.
- [243] B. Gao, X. Wang, T. Li, Z. Feng, C. Wang, Z. Gu, *Adv. Mater. Technol.* **2019**, *4*, 1800392.
- [244] T. Kim, J. Park, J. Sohn, D. Cho, S. Jeon, *ACS Nano* **2016**, *10*, 4770.
- [245] J. Wang, J. A. Kaplan, Y. L. Colson, M. W. Grinstaff, *Angew. Chem., Int. Ed.* **2016**, *55*, 2796.
- [246] X. Wu, J. Zhou, J. Huang, *Macromol. Rapid Commun.* **2018**, *39*, 1800084.
- [247] L. R. Freschauf, J. McLane, H. Sharma, M. Khine, *PLoS One* **2012**, *7*, e40987.
- [248] M. D. Hager, in *Handbook of Solid State Chemistry* (Eds: R. Dronskowski, S. Kikkawa, A. Stein), Wiley, New York **2017**, p. 201.
- [249] V. K. Thakur, M. R. Kessler, *Polymer* **2015**, *69*, 369.
- [250] J. Li, L. Geng, G. Wang, H. Chu, H. Wei, *Chem. Mater.* **2017**, *29*, 8932.
- [251] J. Black, *Biological Performance of Materials: Fundamentals of Biocompatibility*, 4th ed., Taylor & Francis, London **2005**.
- [252] D. F. Williams, in *Handbook of Biomaterial Properties*, (Eds: J. Black, G. Hastings), Springer, Boston, MA **1998**, 481.
- [253] N. Wang, A. Yang, Y. Fu, Y. Li, F. Yan, *Acc. Chem. Res.* **2019**, *52*, 277.
- [254] Z. Wang, J. Chen, Y. Cong, H. Zhang, T. Xu, L. Nie, J. Fu, *Chem. Mater.* **2018**, *30*, 8062.
- [255] C. Wang, S. Wang, G. Chen, W. Kong, W. Ping, J. Dai, G. Pastel, H. Xie, S. He, S. Das, L. Hu, *Chem. Mater.* **2018**, *30*, 7707.
- [256] J. Chen, S. K. Oh, N. Nabulsi, H. Johnson, W. Wang, J.-H. Ryou, *Nano Energy* **2019**, *57*, 670.
- [257] L. Tang, L. Mou, W. Zhang, X. Jiang, *ACS Appl. Mater. Interfaces* **2019**, *11*, 7138.
- [258] D.-H. Kim, Y.-S. Kim, J. Amsden, B. Panilaitis, D. L. Kaplan, F. G. Omenetto, M. R. Zakin, J. A. Rogers, *Appl. Phys. Lett.* **2009**, *95*, 133701.
- [259] S.-K. Kang, J. Koo, Y. K. Lee, J. A. Rogers, *Acc. Chem. Res.* **2018**, *51*, 988.
- [260] D.-H. Kim, R. Ghaffari, N. Lu, S. Wang, S. P. Lee, H. Keum, R. D'Angelo, L. Klinker, Y. Su, C. Lu, Y.-S. Kim, A. Armeen, Y. Li, Y. Zhang, B. de Graff, Y.-Y. Hsu, Z. Liu, J. Ruskin, L. Xu, C. Lu, F. G. Omenetto, Y. Huang, M. Mansour, M. J. Slepian, J. A. Rogers, *Proc. Natl. Acad. Sci. USA* **2012**, *109*, 19910.
- [261] S.-K. Kang, R. K. J. Murphy, S.-W. Hwang, S. M. Lee, D. V. Harburg, N. A. Krueger, J. Shin, P. Gamble, H. Cheng, S. Yu, Z. Liu, J. G. McCall, M. Stephen, H. Ying, J. Kim, G. Park, R. C. Webb, C. H. Lee, S. Chung, D. S. Wie, A. D. Gujar, B. Vemulapalli, A. H. Kim, K.-M. Lee, J. Cheng, Y. Huang, S. H. Lee, P. V. Braun, W. Z. Ray, J. A. Rogers, *Nature* **2016**, *530*, 71.
- [262] C. Chiappini, E. De Rosa, J. O. Martinez, X. Liu, J. Steele, M. M. Stevens, E. Tasciotti, *Nat. Mater.* **2015**, *14*, 532.
- [263] T. Lei, M. Guan, J. Liu, H.-C. Lin, R. Pfattner, L. Shaw, A. F. McGuire, T.-C. Huang, L. Shao, K.-T. Cheng, J. B. H. Tok, Z. Bao, *Proc. Natl. Acad. Sci. USA* **2017**, *114*, 5107.
- [264] G. A. Salvatore, J. Sülzle, F. Dalla Valle, G. Cantarella, F. Robotti, P. Jokic, S. Knobelspies, A. Daus, L. Büthe, L. Petti, N. Kirchgessner, R. Hopf, M. Magno, G. Tröster, *Adv. Funct. Mater.* **2017**, *27*, 1702390.
- [265] Y. Guo, M. Zhong, Z. Fang, P. Wan, G. Yu, *Nano Lett.* **2019**, *19*, 1143.
- [266] H. Lee, G. Lee, J. Yun, K. Keum, S. Y. Hong, C. Song, J. W. Kim, J. H. Lee, S. Y. Oh, D. S. Kim, M. S. Kim, J. S. Ha, *Chem. Eng. J.* **2019**, *366*, 62.
- [267] X. Jia, C. Wang, V. Ranganathan, B. Napier, C. Yu, Y. Chao, M. Forsyth, F. G. Omenetto, D. R. MacFarlane, G. G. Wallace, *ACS Energy Lett.* **2017**, *2*, 831.
- [268] S. W. Hwang, X. Huang, J. H. Seo, J. K. Song, S. Kim, S. Hage-Ali, H. J. Chung, H. Tao, F. G. Omenetto, Z. Ma, *Adv. Mater.* **2013**, *25*, 3526.
- [269] L. Lu, Z. Yang, K. Meacham, C. Cvetkovic, E. A. Corbin, A. Vázquez-Guardado, M. Xue, L. Yin, J. Boroumand, G. Pakeltis, T. Sang, K. J. Yu, D. Chanda, R. Bashir, R. W. Gereau IV, X. Sheng, J. A. Rogers, *Adv. Energy Mater.* **2018**, *8*, 1703035.
- [270] Q. Liang, Q. Zhang, X. Yan, X. Liao, L. Han, F. Yi, M. Ma, Y. Zhang, *Adv. Mater.* **2017**, *29*, 1604961.
- [271] S. Chen, T. Huang, H. Zuo, S. Qian, Y. Guo, L. Sun, D. Lei, Q. Wu, B. Zhu, C. He, X. Mo, E. Jeffries, H. Yu, Z. You, *Adv. Funct. Mater.* **2018**, *28*, 1805108.
- [272] Y. Ahn, Y. Jeong, Y. Lee, *ACS Appl. Mater. Interfaces* **2012**, *4*, 6410.
- [273] H. Xiao, Z.-S. Wu, F. Zhou, S. Zheng, D. Sui, Y. Chen, X. Bao, *Energy Storage Mater.* **2018**, *13*, 233.
- [274] J.-L. Xu, Y.-H. Liu, X. Gao, S. Shen, S.-D. Wang, *Energy Storage Mater.* **2019**, <https://doi.org/10.1016/j.ensm.2019.02.013>.
- [275] Z. Wen, Y. Yang, N. Sun, G. Li, Y. Liu, C. Chen, J. Shi, L. Xie, H. Jiang, D. Bao, Q. Zhuo, X. Sun, *Adv. Funct. Mater.* **2018**, *28*, 1803684.
- [276] H. Wu, Q. Liu, W. Du, C. Li, G. Shi, *ACS Appl. Mater. Interfaces* **2018**, *10*, 3895.
- [277] M. Amjadi, K.-U. Kyung, I. Park, M. Sitti, *Adv. Funct. Mater.* **2016**, *26*, 1678.
- [278] Y. S. Rim, S. H. Bae, H. J. Chen, N. De Marco, Y. Yang, *Adv. Mater.* **2016**, *28*, 4415.
- [279] B. Park, J. Kim, D. Kang, C. Jeong, K. S. Kim, J. U. Kim, P. J. Yoo, T.-I. Kim, *Adv. Mater.* **2016**, *28*, 8130.
- [280] D. Kang, P. V. Pikhitsa, Y. W. Choi, C. Lee, S. S. Shin, L. Piao, B. Park, K. Y. Suh, T. I. Kim, M. Choi, *Nature* **2014**, *516*, 222.
- [281] Y. W. Choi, D. Kang, P. V. Pikhitsa, T. Lee, S. M. Kim, G. Lee, D. Tahk, M. Choi, *Sci. Rep.* **2017**, *7*, 40116.
- [282] Y. Cai, J. Shen, G. Ge, Y. Zhang, W. Jin, W. Huang, J. Shao, J. Yang, X. Dong, *ACS Nano* **2018**, *12*, 56.
- [283] Y. Yang, L. Shi, Z. Cao, R. Wang, J. Sun, *Adv. Funct. Mater.* **2019**, *29*, 1807882.
- [284] C. Pang, G.-Y. Lee, T.-I. Kim, S. M. Kim, H. N. Kim, S.-H. Ahn, K.-Y. Suh, *Nat. Mater.* **2012**, *11*, 795.
- [285] Y. Pang, K. Zhang, Z. Yang, S. Jiang, Z. Ju, Y. Li, X. Wang, D. Wang, M. Jian, Y. Zhang, R. Liang, H. Tian, Y. Yang, T.-L. Ren, *ACS Nano* **2018**, *12*, 2346.
- [286] B. Yin, X. Liu, H. Gao, T. Fu, J. Yao, *Nat. Commun.* **2018**, *9*, 5161.
- [287] Y.-S. Kim, J. Lu, B. Shih, A. Gharibans, Z. Zou, K. Matsuno, R. Aguilera, Y. Han, A. Meek, J. Xiao, M. T. Tolley, T. P. Coleman, *Adv. Mater.* **2017**, *29*, 1701312.
- [288] Z. Shi, X. Wu, H. Zhang, H. Chai, C. M. Li, Z. Lu, L. Yu, *J. Colloid Interface Sci.* **2019**, *534*, 618.
- [289] M. Bariya, Z. Shahpar, H. Park, J. Sun, Y. Jung, W. Gao, H. Y. Y. Nyein, T. S. Liaw, L. C. Tai, Q. P. Ngo, M. Chao, Y. Zhao, M. Hettick, G. Cho, A. Jaye, *ACS Nano* **2018**, *12*, 6978.
- [290] F. Torrisi, T. Carey, *Nano Today* **2018**, *23*, 73.
- [291] F. Ge, Z. Liu, S. B. Lee, X. Wang, G. Zhang, H. Lu, K. Cho, L. Qiu, *ACS Appl. Mater. Interfaces* **2018**, *10*, 21510.
- [292] J. Sun, C. Yun, B. Cui, P. Li, G. Liu, X. Wang, F. Chu, *Polymers* **2018**, *10*, 1209.
- [293] S. Fu, J. Tao, W. Wu, J. Sun, F. Li, J. Li, Z. Huo, Z. Xia, R. Bao, C. Pan, *Adv. Mater. Technol.* **2019**, *4*, 1800703.
- [294] B. He, Q. Zhang, L. Li, J. Sun, P. Man, Z. Zhou, Q. Li, J. Guo, L. Xie, C. Li, X. Wang, J. Zhao, T. Zhang, Y. Yao, *J. Mater. Chem. A* **2018**, *6*, 14594.
- [295] A. Manthiram, *ACS Cent. Sci.* **2017**, *3*, 1063.

- [296] K. Torikai, R. Furlan de Oliveira, D. H. Starnini de Camargo, C. C. Bof Bufon, *Nano Lett.* **2018**, *18*, 5552.
- [297] H. Lee, E. Kim, Y. Lee, H. Kim, J. Lee, M. Kim, H. J. Yoo, S. Yoo, *Sci. Adv.* **2018**, *4*, eaas9530.
- [298] G. Gao, J. Yu, X. Yang, Y. Pang, J. Zhao, C. Pan, Q. Sun, Z. L. Wang, *Adv. Mater.* **2019**, *31*, 1806905.
- [299] L. Xiang, H. Zhang, G. Dong, D. Zhong, J. Han, X. Liang, Z. Zhang, L.-M. Peng, Y. Hu, *Nat. Electron.* **2018**, *1*, 237.
- [300] T. Q. Trung, S. Ramasundaram, B.-U. Hwang, N.-E. Lee, *Adv. Mater.* **2016**, *28*, 502.
- [301] F. Zhang, Y. Zang, D. Huang, C.-A. Di, D. Zhu, *Nat. Commun.* **2015**, *6*, 8356.
- [302] N. T. Tien, S. Jeon, D. I. Kim, T. Q. Trung, M. Jang, B. U. Hwang, K. E. Byun, J. Bae, E. Lee, J. B. Tok, Z. Bao, N. E. Lee, J. J. Park, *Adv. Mater.* **2014**, *26*, 796.
- [303] F. Stauffer, M. Thielen, C. Sauter, S. Chardonnens, S. Bachmann, K. Tybrandt, C. Peters, C. Hierold, J. Voros, *Adv. Healthcare Mater.* **2018**, *7*, 1700994.
- [304] J. Shi, L. Wang, Z. Dai, L. Zhao, M. Du, H. Li, Y. Fang, *Small* **2018**, *14*, 1800819.
- [305] W. Wu, X. Wen, Z. L. Wang, *Science* **2013**, *340*, 952.
- [306] B. Nie, R. Li, J. Cao, J. D. Brandt, T. Pan, *Adv. Mater.* **2015**, *27*, 6055.
- [307] S. Gong, D. T. Lai, Y. Wang, L. W. Yap, K. J. Si, Q. Shi, N. N. Jason, T. Sridhar, H. Uddin, W. Cheng, *ACS Appl. Mater. Interfaces* **2015**, *7*, 19700.
- [308] J. J. Park, W. J. Hyun, S. C. Mun, Y. T. Park, O. O. Park, *ACS Appl. Mater. Interfaces* **2015**, *7*, 6317.
- [309] L. Y. Chen, B. C. Tee, A. L. Chortos, G. Schwartz, V. Tse, D. J. Lipomi, H. S. Wong, M. V. McConnell, Z. Bao, *Nat. Commun.* **2014**, *5*, 5028.
- [310] S. H. Wang, L. Lin, Z. L. Wang, *Nano Energy* **2015**, *11*, 436.
- [311] J. Allen, *Physiol. Meas.* **2007**, *28*, R1.
- [312] Y. Mendelson, *Clin. Chem.* **1992**, *38*, 1601.
- [313] S. Park, S. J. Kim, J. H. Nam, G. Pitner, T. H. Lee, A. L. Ayzner, H. Wang, S. W. Fong, M. Vosgueritchian, Y. J. Park, *Adv. Mater.* **2015**, *27*, 759.
- [314] D. B. Velusamy, M. A. Haque, M. R. Parida, F. Zhang, T. Wu, O. F. Mohammed, H. N. Alshareef, *Adv. Funct. Mater.* **2017**, *27*, 1605554.
- [315] J. Huang, J. Du, Z. Cevher, Y. H. Ren, X. H. Wu, Y. L. Chu, *Adv. Funct. Mater.* **2017**, *27*, 1604163.
- [316] X. M. Li, D. J. Yu, J. Chen, Y. Wang, F. Cao, Y. Wei, Y. Wu, L. Wang, Y. Zhu, Z. G. Sun, J. P. Ji, Y. L. Shen, H. D. Sun, H. B. Zeng, *ACS Nano* **2017**, *11*, 2015.
- [317] H. Lee, E. Kim, Y. Lee, H. Kim, J. Lee, M. Kim, H.-J. Yoo, S. Yoo, *Sci. Adv.* **2018**, *4*, eaas9530.
- [318] M. S. Mannoor, H. Tao, J. D. Clayton, A. Sengupta, D. L. Kaplan, R. R. Naik, N. Verma, F. G. Omenetto, M. C. McAlpine, *Nat. Commun.* **2012**, *3*, 763.
- [319] R. C. Reid, S. R. Jones, D. P. Hickey, S. D. Minteer, B. K. Gale, *Electrochim. Acta* **2016**, *203*, 30.
- [320] H. Lee, C. Song, Y. S. Hong, M. S. Kim, H. R. Cho, T. Kang, K. Shin, S. H. Choi, T. Hyeyon, D. H. Kim, *Sci. Adv.* **2017**, *3*, e1601314.
- [321] M. J. Tierney, J. A. Tamada, R. O. Potts, L. Jovanovic, S. Garg, C. R. Team, *Biosens. Bioelectron.* **2001**, *16*, 621.
- [322] L. Lipani, B. G. R. Dupont, F. Doungmene, F. Marken, R. M. Tyrrell, R. H. Guy, A. Ilie, *Nat. Nanotechnol.* **2018**, *13*, 504.
- [323] S. Emaminejad, W. Gao, E. Wu, Z. A. Davies, H. Y. Y. Nyein, S. Challa, S. P. Ryan, H. M. Fahad, K. Chen, Z. Shahpar, S. Talebi, C. Milla, A. Javey, R. W. Davis, *Proc. Natl. Acad. Sci. USA* **2017**, *114*, 4625.
- [324] J. Kim, W. R. de Araujo, I. A. Samek, A. J. Bandodkar, W. Z. Jia, B. Brunetti, T. R. L. C. Paixao, J. Wang, *Electrochem. Commun.* **2015**, *51*, 41.
- [325] D. Kinnamon, R. Ghanta, K. C. Lin, S. Muthukumar, S. Prasad, *Sci. Rep.* **2017**, *7*, 13312.
- [326] V. F. Curto, C. Fay, S. Coyle, R. Byrne, C. O'Toole, C. Barry, S. Hughes, N. Moyna, D. Diamond, F. Benito-Lopez, *Sens. Actuators, B* **2012**, *171–172*, 1327.
- [327] V. Oncescu, D. O'Dell, D. Erickson, *Lab Chip* **2013**, *13*, 3232.
- [328] A. Koh, D. Kang, Y. Xue, S. Lee, R. M. Pielak, J. Kim, T. Hwang, S. Min, A. Banks, P. Bastien, M. C. Manco, L. Wang, K. R. Ammann, K.-I. Jang, P. Won, S. Han, R. Ghaffari, U. Paik, M. J. Slepian, G. Balooch, Y. Huang, J. A. Rogers, *Sci. Transl. Med.* **2016**, *8*, 366ra165.
- [329] C. Yan, J. Wang, P. S. Lee, *ACS Nano* **2015**, *9*, 2130.
- [330] G. Y. Bae, J. T. Han, G. Lee, S. Lee, S. W. Kim, S. Park, J. Kwon, S. Jung, K. Cho, *Adv. Mater.* **2018**, *30*, 1803388.
- [331] Q. Hua, J. Sun, H. Liu, R. Bao, R. Yu, J. Zhai, C. Pan, Z. L. Wang, *Nat. Commun.* **2018**, *9*, 244.
- [332] A. J. Bandodkar, P. Gutruf, J. Choi, K. Lee, Y. Sekine, J. T. Reeder, W. J. Jeang, A. J. Aranyosi, S. P. Lee, J. B. Model, R. Ghaffari, C.-J. Su, J. P. Leshock, T. Ray, A. Verrillo, K. Thomas, V. Krishnamurthi, S. Han, J. Kim, S. Krishnan, T. Hang, J. A. Rogers, *Sci. Adv.* **2019**, *5*, eaav3294.
- [333] S. Mishra, J. J. Norton, Y. Lee, D. S. Lee, N. Agee, Y. Chen, Y. Chun, W.-H. Yeo, *Biosens. Bioelectron.* **2017**, *91*, 796.
- [334] Y. Lee, B. Nicholls, D. S. Lee, Y. Chen, Y. Chun, C. S. Ang, W.-H. Yeo, *Sci. Rep.* **2017**, *7*, 46697.
- [335] C. Howe, S. Mishra, Y.-S. Kim, Y. Chen, S.-H. Ye, W. R. Wagner, J.-W. Jeong, H.-S. Byun, J.-H. Kim, Y. Chun, *ACS Nano* **2018**, *12*, 8706.
- [336] J. M. Nassar, K. Mishra, K. Lau, A. A. Aguirre-Pablo, M. M. Hussain, *Adv. Mater. Technol.* **2017**, *2*, 1600228.
- [337] H. Xu, J. X. Xiang, Y. F. Lu, M. K. Zhang, J. J. Li, B. B. Gao, Y. J. Zhao, Z. Z. Gu, *ACS Appl. Mater. Interfaces* **2018**, *10*, 11785.
- [338] K.-B. Kim, W. Jang, J. Y. Cho, S. B. Woo, D. H. Jeon, J. H. Ahn, S. D. Hong, H. Y. Koo, T. H. Sung, *Nano Energy* **2018**, *54*, 91.
- [339] M. Gotz, O. Kanoun, *IEEE Trans. Ind. Electron.* **2019**, *66*, 3843.
- [340] C. J. Lukas, F. Yahya, J. Breiholz, A. Roy, X. Chen, H. Patel, N. Liu, A. Kosari, S. Li, D. Akella, *IEEE Trans. Biomed. Circuits Syst.* **2019**, *13*, 271.
- [341] S. Park, S. W. Heo, W. Lee, D. Inoue, Z. Jiang, K. Yu, H. Jinno, D. Hashizume, M. Sekino, T. Yokota, K. Fukuda, K. Tajima, T. Someya, *Nature* **2018**, *561*, 516.
- [342] C. Yang, H. Zhang, Y. Liu, Z. Yu, X. Wei, Y. Hu, *Adv. Sci.* **2018**, *5*, 1801070.
- [343] N. X. Viet, S. Kishimoto, Y. Ohno, *ACS Appl. Mater. Interfaces* **2019**, *11*, 6389.
- [344] M. Prsa, K. Morandell, G. Cuenu, D. Huber, *Nature* **2019**, *567*, 384.
- [345] A. D. Mickle, S. M. Won, K. N. Noh, J. Yoon, K. W. Meacham, Y. Xue, L. A. McIlvried, B. A. Copits, V. K. Samineni, K. E. Crawford, D. H. Kim, P. Srivastava, B. H. Kim, S. Min, Y. Shiuan, Y. Yun, M. A. Payne, J. Zhang, H. Jang, Y. Li, H. H. Lai, Y. Huang, S.-I. Park, R. W. Gereau, J. A. Rogers, *Nature* **2019**, *565*, 361.